Title

Intelligent Transportation System Strategies to Mitigate Human Exposure to Mobile-Source Pollutants

Author

Luo, Ji

Publication Date

2015

Peer reviewed|Thesis/dissertation

UNIVERSITY OF CALIFORNIA
RIVERSIDE

Intelligent Transportation System Strategies to Mitigate Human Exposure to Mobile-Source Pollutants

A Dissertation submitted in partial satisfaction
of the requirements for the degree of

Doctor of Philosophy

in

Chemical and Environmental Engineering

by

Ji Luo

December 2015

Dissertation Committee:
Dr. Matthew J. Barth, Co-Chairperson
Dr. David R Cocker III, Co-Chairperson
Dr. Akula Venkatram

The Dissertation of Ji Luo is approved:

Committee Co-Chairperson

Committee Co-Chairperson

University of California, Riverside

Acknowledgements

This is a special moment for me. At the completion of my doctoral degree, I would love to acknowledge my mentors, colleagues, families and friends.

I would like to thank Prof. Matthew Barth, Prof. David Cocker, and Prof. Akula Venkatram - the three top experts in their own research fields. I am truly fortunate to have them as my mentors.

At the first year of my Ph.D. study, Prof. Cocker introduced me to aerosol research and advanced air pollution control engineering. He is always patient answering all of our questions, including different emission research branches, photocatalytic chemistry, and how to cook mashed potatoes. Every Thanksgiving he invites international students to his home and shares the holiday joy with us. One significant incident for me is that, Prof. Cocker introduced me to meet Prof. Barth.

Prof. Barth opened my eyes to a new research field - environmental ITS applications. This picture clicked with my interests almost perfectly that I immediately decided to join the Transportation Systems Research (TSR) group. Prof. Barth generously granted me time to learn brand new subjects. He is such a positive leader that he can always direct me to find best resources. In the early year of my stay in TSR, I needed to get a hold of dispersion model, but the models look like Greek to me. Prof. Barth encouraged me to take Prof. Venkatram's class.

In Prof. Venkatram's class, I learned about boundary layer theories which forms a critical connection for my research topics. He is extremely strict in class yet surprisingly friendly after class, and tries to teach us all his expertise, which made my learning curve peak during that time. Also in his class I met Dr. Si Tan and to-be Dr. Nico Schulte, who become my great friends and help me build my modeling skills.

I thank Dr. Guoyuan Wu, who always offers his personal time to help me to improve my methods and writing skills. I am grateful to Dr. Rashid Shaikh from Health Effects Institute for his detailed instructions on exposure study. Many thanks to Dr. Kanok Boriboonsomsin, who engages me in the Riverside Walkability Project and SCAG Project, which form major parts of my dissertation. I thank Dr. George Scora for teaching me how to make the best use of CMEM. I have received tremendous technical help from Junior Engineer Alexander Vu, who can always solve my programming problems in a matter of minutes.

I cannot say how much I appreciate my fellow graduate friends, who cannot be all named here. Dr. Aaron Lin, Dr. Fu Jia, Dr. Tanfeng Cao, Dr. Nick Gysel and Dr. Chia-Li Chen helped me go through the tough first year with many happy memories. Dr. Qichi Yang, Dr. Haiyu Zhang, Dr. Qiu Jin, Dr. Haitao Xia, and To-be Dr. Xuewei Qi, thank you for helping me to improve my scripting skills and all the great time discussing various topics together. Specific efforts are acknowledged in Chapter Three to Six.

Equally important, I appreciate my family and friends for their love and support. My father, Xinhui Luo and my mother, Zhimin Huang, have been inspiring me to work hard and travel far. My dear friends Saudia Casper's family, Mr. and Mrs. Espinoza, and Mr. Jeffrey Ho's family, give me best accompany and make this journey an amazingly enjoyable one.

This research is partially sponsored by the UC MRPI Program in Sustainable Transportation.

Parts of the dissertation appear in the following papers with the permission of all co-authors:

Luo, J., A. Vu, and M. J. Barth. Vehicle road navigation to minimize pollutant exposure. In *Intelligent Vehicles Symposium (IV), 2013 IEEE*, IEEE, 2013. pp. 847-852.

Luo, J., K. Boriboonsomsin, and M. J. Barth. Reducing Pedestrian's Traffic-Related Air Pollution Exposure through Intelligent Route Choice Decisions. In *Transportation Research Record: Journal of the Transportation Research Board.* Manuscript.

ABSTRACT OF THE DISSERTATION

Intelligent Transportation System Strategies to Mitigate Human Exposure to Mobile-Source Pollutants

by

Ji Luo

Doctor of Philosophy, Graduate Program in Chemical and Environmental Engineering
University of California, Riverside, December 2015
Dr. Matthew J. Barth, Co-Chairperson
Dr. David R. Cocker, Co-Chairperson

Traditional Intelligent Transportation System (ITS) applications aim at improving safety and mobility for roadway transportation. With increasing concern about energy consumption and pollutant emission of transportation sector, a number of environmental-ITS applications have emerged to improve fuel economy and reduce overall emissions. Further, mobile emissions disperse into the atmosphere and impose health risks to public population who are exposed to the contaminated air. To date however, environmental-ITS applications haven't considered emissions from a pollutant exposure point-of-view. This dissertation proposes two environmental-ITS applications and a high-resolution screening method to mitigate human exposure to mobile pollutants. The key contributions are:

- This dissertation develops a vehicle road navigation method to mitigate mobile-source exposure to a localized susceptible population. Routing experiments show that 50% of 400 experiment trips achieve 30% *inhaled mass* reduction for both mobile-source $PM_{2.5}$ and Reactive Organic Gases. Also, the low exposure routes can be more fuel efficient than conventional least duration routes.
- This dissertation defines a state-of-practice digital sidewalk system and proposes a pedestrian navigation tool with the goal of minimizing pedestrians' *inhaled mass* of on-road traffic emissions. Pedestrian routing experiments demonstrate that the navigation tool is able to

advise walking trips that significantly reduce pedestrians' $PM_{2.5}$ exposure up to 90%. As a result, pedestrians can be protected from excessive pollutant exposure.

- This dissertation also develops modeling techniques for large-scale pollutant exposure assessment for Southern California Association of Governments (SCAG) residents, with spatial analysis resolution fifty times higher than previous research. In conjunction with socioeconomic parameter analysis, results reveal that in the SCAG region, low-income and minority population are subject to high-level vehicular emission exposure. This study makes it possible for community outreach and mitigation planning targeted at disadvantaged residential communities.

The frameworks in this dissertation provide valuable implications for environmental transportation and justice research. Future improvements can be focused on real-time population activity collection, exposure assessment, and navigation implementation in the real world.

Keywords: mobile-source, emissions, pollutants, ITS, exposure assessment, exposure mitigation, vehicle navigation, pedestrian navigation, environmental inequality

Table of Contents

List of Tables

Table Page

List of Figures

1 Introduction

Highly developed roadway transportation systems contribute to economic development and social well-being. To improve the safety and mobility of road transportation, Intelligent Transportation System (ITS) technologies have been developed to aid individual drivers and the system as a whole.

With ever-growing vehicle activities, mobile source emissions account for a significant portion of today's air quality degradation, leading to adverse public health problems around the globe. Lately, an increasing number of environmental ITS applications have emerged, aimed at reducing fuel consumption, greenhouse gases (GHG), and airborne pollutants emissions. From a pollutant exposure point-of-view, the vehicles' detrimental emissions, such as fine particles, volatile organic compounds (VOC), and oxides of nitrogen (NO_x), are released from the vehicles and dispersed into the atmosphere. When humans are present in the contaminated ambient environment and undergoing daily activities, they breathe in the contaminated air along with the pollutants. Extensive health studies show that even healthy adults experience adverse reactions to short-term exposure of primary vehicle emission mixtures [*1*, *2*, *3*, *4*]. Long-term exposure, further, lead to an array of health problems, such as cardiovascular, respiratory and reproductive system impairment for various age groups [*5*, *6*, *7*]. Susceptible populations, for example, young children, older adults, patients with respiratory problems, are subject to higher health risks compared with healthy adults.

To date, environmental ITS applications haven't considered emissions from a pollutant exposure point-of-view. This dissertation applies exposure assessment models to develop ITS applications that mitigate human exposure to mobile source pollutants.

1.1 Problem Statement

Typical environmental-ITS applications aim at reducing fuel consumption and overall emissions mass. However, the public population who are exposed to traffic emissions are not specifically considered in any environmental-ITS applications. Mobile-source pollutants degrade ambient air quality on a wide range of spatial scales, from local roadways (a few hundred meters) and urban scales (tens of kilometers) to broad regional background (hundreds of kilometers). The highest exposure is likely to occur at the local scale. To date, concurrent environmental-ITS applications do not account for population exposure to vehicle emissions.

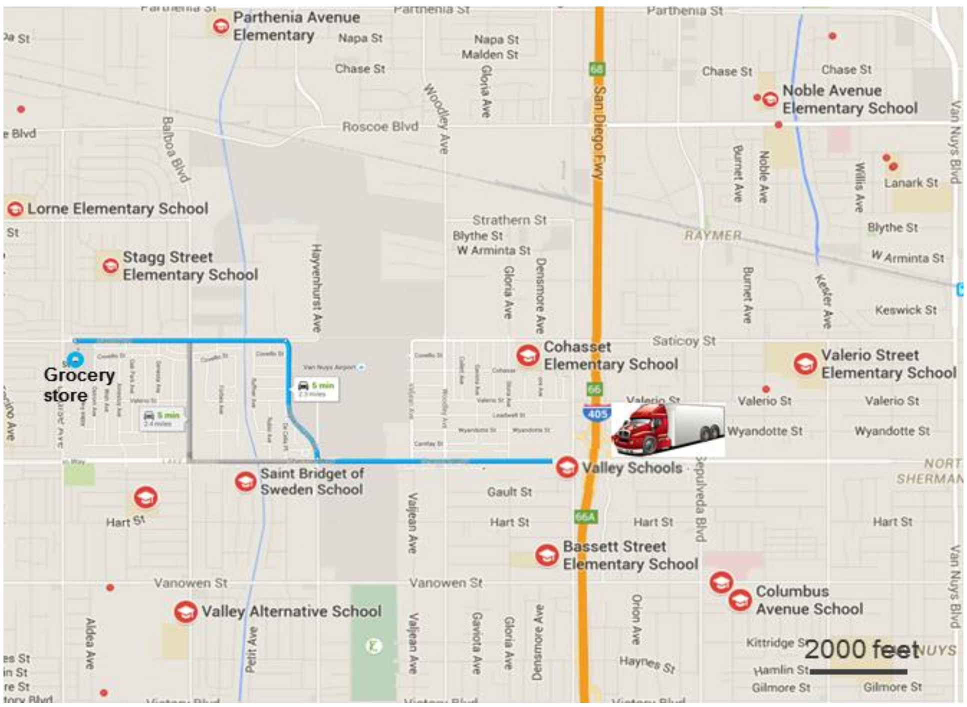

Figure 1-1 An example map of problem statement

Figure 1-1 pictures a common scenario seen in daily life: a heavy-duty freight truck exits the freeway and plans to unload goods to local grocery stores on a normal workday. There are elementary schools located in close proximity to the roadways and young children will likely be inhaling the air contaminated by truck exhaust, if the truck chooses a fastest route (blue and grey lines in Figure 1-1) and drive by the schools. In addition, there are many other population groups who are susceptible to mobile-source emissions, for example, senior adults who live close to busy roadways, and 3-year-old children who attend daycare centers by congested streets. So the question is, is there alternative routes that the truck can take so that the exposure impacts can be minimized to the locally sensitive populations?

The first problem that this dissertation attempts to resolve is heavy-emitting vehicle routing scenarios in a populated local street network, as the question states above. Traditional routing aims at finding a route that has the minimum distance or duration. However, without information of pollutant dispersion and population distribution, a least-duration trip is likely to traverse populated areas and impose excessive health risks to a larger amount of the public population. This study links vehicle activity to population exposure, and optimizes alternative routes for heavy-emitters so that pollutant exposure of selected population groups in the local area can be minimized.

As a second issue, which can also be pictured in Figure 1-1, is for pedestrians. Walking is advocated as a healthy exercise. However, pedestrians walking by busy streets (e.g. from Valley School to grocery store) are directly exposed to a high degree of traffic emissions. This dissertation models pedestrian exposure from traffic activities and advise alternative walking trips so that pedestrians' exposure can be greatly reduced.

The third project focuses on large-scale pollutant exposure modeling, socioeconomic status (SES) analysis, and disadvantaged community screening. For example, in Figure 1-1, primary school clusters indicate that this area is a residential zone. However it is in such a close proximity to major freeways, that we wonder what the average mobile-source pollutant exposure level is for the residents in this community. What are their race, age and income distribution, and how do their exposure and SES compare with other communities? In similar research of relationships between pollutant exposure and SES, the analysis spatial resolution is usually low and mobile source pollutants are not separated from other sources, which makes it inapplicable for community outreach and mitigation planning. This study utilizes regional traffic activities, weather data, and U.S. Census geological units to model high-resolution and large-scale vehicular fine particle exposure for Southern California residents. In addition, U.S. Census SES data is used to screen disadvantaged communities.

To achieve these goals, spatial and temporal variation of emission concentration and population are required. Currently, there are extensive air quality monitoring programs in the U.S., which can be utilized to assess overall exposure to local populations. However, monitoring stations are spatially sparse and expensive to maintain. Also, regular ambient monitoring is not able to differentiate primary traffic emissions from other sources. To actively mitigate transportation pollutant exposure and protect public health, robust exposure modeling methods and environmental ITS applications are in urgent need.

In this dissertation, unless otherwise mentioned, pollutants and exposure refer to those localized primary out-of-tailpipe emissions; in short, mobile-source emissions. For example, in terms of mobile-source $PM_{2.5}$ (fine particles whose equivalent aerodynamic diameter are less than 2.5 μm), it refers to primary out-of-tailpipe $PM_{2.5}$ from on-road traffic, which does not include secondary or brake wear $PM_{2.5}$. Localized emission refers to traffic sources within 2000 meters of receptors. According to measurement studies [*8*, *9*, *21*] and dispersion calculations, mobile-source pollutants' concentration decline to background levels within a few hundred meters. Hence the concentration contribution from mobile-source beyond 2000 meters are considered negligible.

1.2 Research Roadmap

Developing environmental-ITS applications to mitigate exposure are research topics spanning a wide range of research disciplines. Figure 1-2 presents the general research road map of this study. To estimate human exposure to mobile source emissions, there are several factors at play, including vehicle activity (e.g., Vehicle Miles Travelled, traffic speed, traffic volume, *etc*.), vehicle emission rates, and pollutant dispersion. In the fourth component, exposure is quantified based on the previous metrics. With an exposure assessment, environmental ITS applications can be developed targeting at reducing exposure. Generally, this dissertation focuses on intelligent navigation applications that reduce local populations' exposure to transportation pollutants.

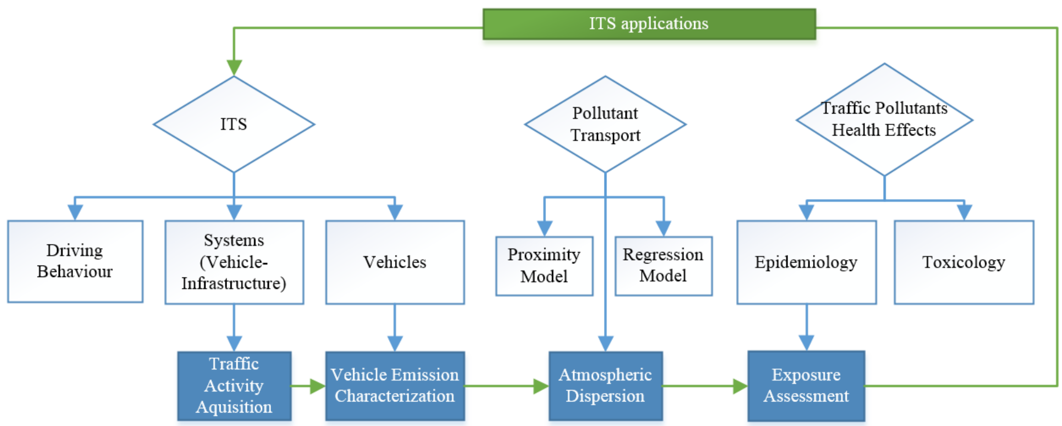

Note: Blue blocks are models applied in this study. Green arrows refer to the interface efforts (e.g. spatial analysis) that connect all the models. The green block is the focus and contribution of this dissertation

Figure 1-2 Research roadmap of this dissertation

This dissertation explores several strategies to mitigate human exposure to mobile source pollutants, which are presented in six chapters.

Chapter Two organizes background research on the related topics. First, it presents the modeling suites to assess human exposure to mobile source emissions, with peer studies on each model component. Then, it introduces frontier environmental ITS research at a global scale.

Chapter Three proposes a vehicle navigation method that minimizes local population's exposure to roadway emissions. First, a unique modeling suite is developed in order to assess human exposure to mobile source emissions. The exposure assessment provides critical inputs for roadway network evaluation and routing implementation. Routing experiments for heavy-emitting trucks show that the vehicle navigation method generally reduces sensitive population's exposure to heavy-duty vehicles' emissions. 50% of 400 experiment trips achieve 30% *inhaled mass* reduction for both mobile-source $PM_{2.5}$ and Reactive Organic Compound.

Chapter Four defines a state-of-practice digital sidewalk system, and proposes a pedestrian navigation tool with the goal of minimizing pedestrians' *inhaled mass* of mobile-source pollutant. Pedestrian routing experiments demonstrate that the navigation tool is able to advise walking trips that significantly reduce pedestrians' $PM_{2.5}$ exposure up to 90% for a typical area. As a result, pedestrians can be protected from excessive pollutant exposure.

Chapter Five develops modeling tools for large-scale mobile-source $PM_{2.5}$ exposure assessment for Southern California Association of Governments (SCAG) residents, with spatial analysis resolution more than fifty times higher than previous research. In conjunction with socioeconomic parameter analysis, results reveal that in SCAG region, low-income and minority population are subject to high-level vehicular emission exposure. This study makes it possible for community outreach and mitigation planning targeted at disadvantaged residential communities.

Chapter Three to Five are unique contributions of this dissertation. Chapter Six concludes the previous chapters and discusses possible future development of the studies presented in this dissertation.

2 Background

Evaluating human exposure to mobile emissions and developing mitigation environmental-ITS applications are research topics which span a wide variety of research disciplines, including transportation engineering, electrical engineering, analytical emission modeling, analytical air quality monitoring, atmospheric dispersion modeling, epidemiology and a portion of social sciences. Published studies are mostly combinations of several aforementioned subjects, covering an array of conferences and journals.

According to the problem framed in Chapter One and research roadmap as Figure 1-2, there are five major branches: traffic activity data acquisition, vehicle emission characterization, atmospheric dispersion, exposure quantification, and ITS applications. Because this dissertation mostly applies pre-calculated traffic activity datasets, the data acquisition is only briefly introduced in Section 3.2. This chapter summarizes published research on four topics. Section 2.1 introduces vehicle emission models. Section 2.2 summarizes various methods to predict mobile emissions' concentration dispersed into atmosphere. Section 2.3 discusses formulations of exposure assessment based on pollutant measurements and concentration modeling. Section 2.4 introduces latest environmental-ITS applications along with their benefits and limitations.

2.1 Mobile-Source Emission Modeling

Roadways carry mixed flow of motor vehicles and are viewed as continuous line-source of traffic pollutants. Vehicle emission models build the relationship between transportation activities and transportation emissions. An emission model is required to estimate the emission factors (mass per unit time, which is also the input to dispersion models), or an emission inventory (mass) given on-road traffic activities, including vehicle fleet composition (e.g. vehicle type, make, model, year *etc.*), vehicle operating state (e.g. idling, creep, cruising *etc*.), in addition to environmental conditions (e.g. temperature, humidity, *etc*.). Traffic emission factors, which quantify the emission strength of traffic flow, are critical inputs to perform air quality modeling.

To compile a vehicle emission inventory and model, it requires extensive vehicle testing and model structuring, with frequent calibration and update to reflect new vehicles and environmental policies. A comprehensive vehicle emission model covers most types of in-use vehicles (e.g. light duty automobile, various trucks, motor homes, buses, motorcycles *etc*.) and operating states. The emissions evaluated usually include GHG (e.g. carbon dioxide (CO_2)) and primary pollutants (e.g. carbon monoxide (CO), nitrogen oxide (NO), nitrogen dioxide (NO_2), sulfur dioxide (SO_2), fine particles). Depending on the developing scope of vehicle emission models, emission calculations can be performed at a range of geographical (e.g. county, state, nation *etc*.) and temporal (winter, summer, annual *etc*.) resolution, for historical, current and future years.

A few emission models are established to support air quality/GHG emission plans and regulations. From temporal and spatial scale point-of-view, emission modeling analyses can be categorized into microscopic, mesoscopic, and macroscopic scales. Microscopic emission modeling needs input of second-by-second vehicle operation data (e.g. speed trajectory) and produces second-by-second emission rate for specific vehicles. At a mesoscopic level, for example, roadway links, combined emission factors are calculated given overall traffic activities (e.g. speed, fleet composition and volume) or aggregated from microscopic emission rates. To consider total emission from all-category vehicles on various transportation facilities, mesoscale emission factors can be aggregated to regional emission at macroscopic level [*10*].

Currently, up-to-date models include EMFAC (EMission FACtor model) developed by the California Air Resources Board (CARB) and is used for regulatory purposes in California [*11*]. EMFAC can be applied in both mesoscale and macroscale modeling analyses. MOVES (MOtor

Vehicle Emission Simulator) by the U.S. Environmental Protection Agency (EPA) is recommended for regulation analysis in the other 49 states [*12*]. CMEM (Comprehensive Modal Emission Model) is a microscopic emissions model developed by Center for Environment Research & Technology, UC Riverside [*13*, *14*]. VT-Micro is also a microscopic emission model that evaluate hot-stabilized emission and fuel consumption [*15*]. Meanwhile, European countries have made great efforts to characterize on-road vehicle emissions. For example, COPERT (COmputer Programme to calculate Emissions from Road Transport) is an emission model widely used in European countries to calculate air pollutant and GHG emission factors [*16*]. COPERT is supported by the European Environment Agency and is capable of estimating macroscopic and mesoscopic emissions at national, regional and local scale [*17*]. In complementary, VERSIT+ is a microscopic emission model for light duty vehicles developed by the Netherlands Organization for Applied Scientific Research [*18*].

In contrast, in developing countries, vehicle emission problem are not well understood. The International Vehicle Emissions (IVE) Model is designed to fill in the gap and help developing countries for their emission research and regulations. Up to now, IVE has collected traffic activities and evaluated vehicle emission in multiple cities in South American and Asian countries [*19*].

Because emission models are region sensitive, this dissertation focuses on U.S. emission models. EFMAC and MOVES estimate emission based on average trip speeds and are intended to predict macroscopic emission for large regional areas. In microscopic scenarios, such as ramp metering, signal coordination, intersection turns, a modal emission model is needed to evaluate emissions of small operational changes. CMEM and VT-Micro are examples of modal emission models. Table 2-1 is a brief summary of the concurrent emission models develop in the United States.

Table 2-1 Summary of concurrent emission models in the United States

	Analysis Scale	Developer Institute	Emissions included	Vehicle type included	Geographic scale	Temperal resolution
MOVES2014a	Macroscale and mesoscale (R)	U.S. EPA	Comprehensive	All	50 states and counties	Hourly to annually
EMFAC2011/ EMFAC2014	Macroscale and mesoscale (R)	CARB	Comprehensive	All	California counties and air basins	Summer, winter, and annual
CMEM	Microscale (NR)	UC Riverside	HC, NO_x, CO, CO_2	LDA, LDT, HDT and total 28 types	Not limited by geographic scale	Second-by-second
VT-Micro	Microscale(NR)	Virginia Tech	HC, NO_x, CO, CO_2	LDA	Not limited by geographic scale	Second-by-second

Note: (R) means regulatory use, (NR) means non regulatory use

In the real-world, roadways carrying mixed flow of motor vehicles are viewed as continuous line-source of traffic pollutants. To better simulate the real-world emission from roadways, mesoscale and microscale modeling are frequently applied. For vehicles that maintain driving speed (e.g. cruising, creep, accelerating), emission factors are expressed in the unit of grams per mile per vehicle. To address the mesoscale emission factor from mixed traffic flow of various vehicle categories, the emission factors are aggregated by vehicle category as in Equation 2-1.

$$EF_k = \sum_g EFv_{k,g} \times q_{k,g} \qquad (2\text{-}1)$$

where EF_k = emission factor on link k (*gram/mile*)
$EFv_{k,g}$ = emission factor of vehicle group g, at speed v on link k (*gram/mile/vehicle*)
$q_{k,g}$ = traffic flow (*vehicles/hour*) on link k of vehicle group g
k = index of links in the network
g = vehicle group, e.g. light duty automotive, heavy duty trucks of specific model and age

For vehicles in a stopped state (e.g. idling at intersection, stop/starts in parking lots), emission factors are assessed in grams per unit time per vehicle. The stopped-state analyses can be categorized as microscale and considered as point sources in air pollution modeling.

2.2 Prediction of Mobile-Source Emissions Concentration

2.2.1 Introduction

In order to assess human exposure to mobile-source pollutants and develop mitigation strategies, it is critical to predict temporal-spatial distribution of mobile-source pollutants. Measurement and modeling are frequently used methods for both research and regulatory purposes.

Measurement studies utilize monitoring devices and instruments to measure ambient pollutant concentration. Mostly they focus on instrumentation and pollutant characterization, which allow for accurate quantification and chemical composition assay of pollutant species from sampling locations. Beckerman *et al*. measured several pollutants perpendicular to a major expressway in Toronto, Canada. Results showed that levels of NO_2 decay with increasing distance from the expressway, declining to background levels by 300 m. Similar distance-decay were also observed for NO_x, VOC, PM_{10}, $PM_{2.5}$, and Black Carbon (BC) [*8, 9*]. In addition, pollutant dispersion range were generally observed to be larger in stable atmospheric condition (e.g. morning, nighttime) than that during daytime [*9, 20, 21*], where the temporal variations are results of ever-changing atmospheric turbulence levels during different time of the day. While measurement studies reveal temporal-spatial variations of pollutant distribution in the real world, they are spatially sparse and expensive to operate. Also it takes further instrumental analysis to apportion source contributions from on-road vehicles. Therefore, prediction models are developed to predict concentration at a large scale, where measurements can serve as complementary validations. Hence, measurements are not further discussed in this section.

2.2.2 Modeling Techniques

With the development of traffic activity monitoring programs, mobile emission models and land-use maps, it is possible to predict pollutant concentration at a large-scale with relatively low cost.

Extensive air quality prediction research is conducted with the aid of modeling techniques. Referring to Health Effects Institute literature, there are five major categories of models that widely applied in concentration modeling and exposure assessing research: 1) proximity-based models, 2) geostatistical interpolation, 3) land-use-regression (LUR) models, 4) dispersion models, and 5) hybrid models [*Chapter 3 of Reference 22*]. To clarify, in this section, studies which only consider concentration prediction, are categorized as concentration prediction studies. Exposure studies which involve microenvironment concentration modeling or personal inhalation quantifications is introduced in Section 2.3.

The five categories of models have their own strength and weakness. Proximity models use simple surrogates, such as road-to-receptor distance and traffic counts. It is acceptable for comparing time-averaged concentration within a small area by roadways. However, it cannot characterize variant weather conditions, complicated roadway network and terrains. Geostatistical interpolation method integrates data from ambient air monitor network and interpolates pollutant concentration for unsampled locations. This method works well for dense sampling networks, but it is unable to separate the contribution of mobile source from regional background, additionally spatial resolution and interpolation coverage is limited. A Land Use Regression model predicts pollutant concentration at locations based on the surrounding land use and traffic activities. However, the absence of meteorology inputs make LUR unable to capture accurate temporal variations of pollutant concentration.

In contrast, dispersion models directly formulate critical factors into concentration prediction. The critical factors include road-to-receptor locations, road geometry, micrometeorology parameter, and roadway emission strength. They match well with the physical world, therefore, established dispersion models are used in this study.

For a primary pollutant, it's concentration value at a base receptor is typically the summation of three major parts: a regional contribution from long-range (hundreds of kilometers) transport, an urban "background" from sources tens of kilometers away, and a local contribution from sources ranging from meters to hundreds of meters, for example, mobile sources. However, regional and urban scale background are usually well diluted and mixed for an area, where the local source causes major intra-urban pollutant variations. To map the intra-urban variations and plan for corresponding exposure mitigation strategies, dispersion models that predict local scale pollutant distribution are ideal tools for this study.

Transportation air-quality dispersion models have been developed to estimate concentrations from emission sources since early 1960s. They apply atmospheric boundary layer theories and Gaussian distribution to predict time-averaged concentration from various emission sources [*23*], including point sources, line sources, area sources and volume sources. In mobile-source emission studies, roadway links with motor vehicles travelling can be considered as line sources or area sources. Locations of interests, such as elementary school near roads, are assigned as receptors for concentration prediction.

The core point source dispersion equation is still Gaussian dispersion given as:

$$C(x,y,z) = \frac{a \cdot Q}{\pi \bar{u} \sigma_y \sigma_z} F_y \cdot F_z \quad \textbf{(2-2)}$$

where *C (x, y, z)* is the concentration at coordinates of *(x, y, z)* in g/m^3, *a* is a constant coefficient, *Q* is the emission rate in *g/second*, $\bar{u}$ is the wind speed in *meter/second*, and σ_y, σ_z are the lateral and vertical dispersion coefficients respectively, in *meter*. F_y and F_z are dimensionless lateral and vertical dispersion functions, respectively. $\sigma_y, \sigma_z, F_y, F_z$ are functions of the relative position from the source and a number of micrometeorology parameters, which are estimated from micrometeorology theories [*24*, *25*]. The line source dispersion is computed with numerical integration.

There are several established atmospheric dispersion models in the United States. For example, CALINE3 is a steady-state Gaussian dispersion model designed to determine emission concentrations near transportation facilities in relatively uncomplicated terrain [*26*]. CALINE3 is incorporated into the more refined CAL3QHC and CAL3QHCR models to consider modal vehicle activities at roadway intersections. CALINE4 is an upgrade version of CALINE3 issued by California Department of Transportation (Caltrans) [*27*]. CALPUFF and AERMOD are two EPA-approved models for non-steady state and steady state dispersion modeling, respectively. The two models require sophisticated micrometeorology inputs and are able to compute receptor concentrations in complex terrains. Recently, EPA released R-LINE, a research grade dispersion model for near-roadway assessments. It is based on a steady-state Gaussian formulation and is designed especially to simulate line source emissions [*28*]. A list of model documentations and executables can be accessed on EPA Regulatory Atmospheric Modeling website [*29*], and several example models are listed in Table 2-2.

Table 2-2 Summary of atmospheric dispersion models in the United States

	Authorizing Developer	Steady or non-steady	Sources	Meteorology inputs	Terrain
CALINE4	Caltrans	Steady (R)	Line source	Simple (wind, temperature, stability class etc.)	Simple
CAL3QHC/ CAL3QHCR	U.S. EPA	Steady (R)	Line source	Same as CALINE4	Simple
AERMOD	U.S. EPA	Steady (R)	Point, Line, and area source	Complicated (u*, MO-length, w* etc.)	Complex
R-LINE	U.S. EPA	Steady (NR)	Line source	Same as AERMOD	Complex
CALPUFF	U.S. EPA	Non-steady (R)	Point, Line, area, and volume source	Very complicated (wind flow vector, short-wave solar radiation etc.)	Complex

Note: (R) means regulatory use, (NR) means non regulatory or research use

2.3 Assessment of Exposure to Mobile-Source Air Pollution

A broad definition of exposure refers to the amount of a suite of pollutants (or one pollutant) intake by a group of population through inhalation, ingestion or dermal intake. Another important term in exposure study is the microenvironment, which means a space or location where humans are in contact with homogeneously distributed pollutants [*30*]. In this dissertation, we specify exposure as inhalation intake from mobile-source emissions, mostly in outdoor microenvironments.

There are three levels of exposure assessment: 1) microenvironment concentration; 2) exposure, which is usually the product of concentration and time spent in the particular microenvironment; and 3) dose, which is the amount of inhaled substance retained in the human body. Many exposure studies focus on estimation or measurements of pollutant concentration in microenvironments. Lately more studies step further to assess the actual inhalation of pollutants. To walk through the many details of exposure study, two exemplary models and related research are introduced in the following sections.

2.3.1 Estimation of Exposure Concentration in Microenvironments

One example model of concentration estimation in microenvironments is the Hazardous Air Pollutant Exposure Model (HAPEM). It has been designed by U.S. EPA to estimate exposure concentration for selected population groups to various air toxics. The latest HAPEM6 is able to estimate exposure concentration of hazardous air pollutants (HAPs) for six age-group population at a census tract level. It incorporates stochastic processes to model a group's averaged exposure concentration based on human activity pattern (model datasets included by HAPEM), and ambient HAPs concentration (as inputs to HAPEM). It is a very versatile model which accounts for HAPs exposure from multiple sources (mobile source, indoor source *etc*.) and 14 microenvironments (residential, restaurant, office, in vehicle, outdoor *etc*.). HAPEM6 derives microenvironment (ME) concentration from outdoor concentration:

$$ME\ concentration = PROX \times PEN \times Outdoor\ concentration + ADD \quad (2\text{-}3)$$

The proximity factor, *PROX* (dimensionless), is an estimate of the ratio of the outdoor concentration in the immediate vicinity of the ME to the outdoor concentration represented by the air quality data. For example, for an outdoor ME, *PROX* value is 1.0. However, *PROX* value can exceed 1.0 when the ME is near major roadways. This factor serves similarly as a proximity surrogate.

The penetration factor, *PEN* (dimensionless), is an estimate of the ratio of the ME concentration contribution (from a given emission source category) to the concurrent outdoor concentration contribution in the immediate vicinity of the ME. For instance, for a residential house, *PEN* value for PM10 could be 0.9 because the house blocks a fraction of the particles.

ADD ($\mu g/m^3$) is an additive factor that accounts for emission sources within or near to a ME, i.e., indoor emission sources. This enables HAPEM to estimate contribution from indoor emission source. The two terms, *ME concentration* ($\mu g/m^3$) and *Outdoor concentration* ($\mu g/m^3$), are self-explanatory. *Outdoor concentration* values should be obtained from air quality models or large sample of measurement data.

Equation 2-3 is an exemplary formula for ME concentration estimation. Ott *et al.* compiled detailed calculation for various pollutants in different microenvironments [Chapter 8 of *31*].

Özkaynak *et al*. examined personal exposures for over 30 gaseous and particulate HAPs from outdoor sources using HAPEM. They conclude that increased personal exposures to HAPs (e.g. VOCs) occurs near localized sources, especially mobile sources, which underscores importance of reducing exposure during commuting and daily activities near localized sources [*32*].

HAPEM considers many facets of personal exposure and it is appropriate for assessing average long-term inhalation exposures for general population. However, there are two major limitations. The first limitation is that the analysis is at census tract level. In California, an average census tract covers 50 square kilometers [*33*]. This is course resolution, therefore the local scale (meters to hundred meters) exposure cannot be presented. The second limitation is that the output is averaged exposure concentration, which is not an additive metric. For example, the exposure concentration values of a group of young children in school for 8 hours and at home for 10 hours cannot be added up to form a sum of exposure concentration. To allow addition and comparison, we need a metric which can be summarized, for instance, across various ME and a group of population.

2.3.2 Inhalation Assessment of Mobile-Source Pollutants

To consider further, exposure duration is introduced. Ott *et al*. defines integrated exposure as follows (Chapter 19 of Reference *22*):

$$E_i = \sum_{j=1}^{m} C_{ij} T_{ij} \quad (2\text{-}4)$$

T_{ij} (*min*) is the time spent in microenvironment j by individual i, C_{ij} is the air pollutant concentration individual i experiences in microenvironment j ($\mu g/m^3$), E_i is the integrated exposure for person i ($\mu g/m^3/min$), and m is the number of different microenvironments.

Quiros *et al*. applied portable instrument to measure ultrafine particle (UFP) concentration for commuters and used Equation 2-4 to calculate UFP exposure of drivers, cyclists and pedestrians. Measurements show that UFP concentration is highly elevated in 200-meter range of a major freeway. Exposure assessments indicate that respiratory UFP exposure (particles inhaled per trip) was 15 times higher when cycling and 30 times higher when walking, compared with driving with windows closed [*34*].

Rank *et al*. measured benzene concentration for drivers in vehicles and cyclists by streets. They found that benzene concentration in vehicle cabin were 2 - 4 times greater than in the cyclists' breathing zone. They conclude that even after taking the increased respiration rate of cyclists into consideration, car drivers seem to be exposed to more airborne pollution than cyclists [*35*].

However, concentration, breathing rate and exposure duration should be all considered at the same time. For example, given that a pollutant concentration is 4 times greater in an automobile cabin than a cyclist' proximity, we assume an adult male cyclists breathe 3 times greater than driving. Therefore, if a driver is traveling at 65 km/hour and a cyclist is biking at 16 km/hour, the cyclist's exposure duration is 3 times greater than that of the driver when traveling the same distance. Under this circumstance, cyclists inhale two times more pollutant than the driver. On the other hand, if the driver is moving slowly in congested traffic at 20 km/hour, the driver will experience same level of exposure with that of the cyclists.

Therefore, to access the actual amount of inhalation, *inhaled mass (IM)* is applied to quantify the mass of pollutants inhaled by a group of exposure subjects, as expressed in:

$$\boldsymbol{IM = C \cdot Pop \cdot t \cdot BR} \qquad (2\text{-}5)$$

Where *C* is the mobile-source pollutant concentration ($\mu g/m^3$) in a given microenvironment. *Pop* is the number of population in the microenvironment. *t* (*hour*) is the duration spent in microenvironment, and *BR* denotes breathing rate ($m^3/hour/capita$) of subjects exposed to the pollutant. Equation 2-5 is applied through this dissertation with various forms.

An example models that applies *IM* is Integrated Environmental Health Impact Assessment System (IEHIAS). IEHIAS is a conceptual and analytical framework established by European Union researchers (*36*). It is a broad collection of aspects relating exposure and health impacts assessments with similar formulations (*37*).

2.4 Environmental-ITS Applications

The concept, Connected Vehicles (CV), envisions a connected network of vehicles (e.g. cars, buses, trucks *etc*.), traffic signals, mobile devices, and traffic management centers through wireless communications. CV technologies enable vehicle-to-vehicle (V2V), vehicle-to-infrastructure (V2I), and infrastructure-to-vehicle (I2V) communication and operations. Latest ITS trends are elaborated by Barth *et al*., and most of them also bring environmental benefits [*38*]. Environmental-ITS applications apply CV technology to achieve harmonized traffic flow, which not only improve safety and mobility, but also fuel economy. In nearly all cases, the main goals of these environmental-ITS applications is to reduce overall vehicle emissions on a large regional basis. By reducing GHG emissions (primarily carbon dioxide), there is a proportional reduction in energy consumption. Further, pollutant emissions (e.g. carbon monoxide, hydrocarbons, nitrogen oxides, and particulate matter) are also reduced through these GHG emission mitigation strategies.

Environmental-ITS programs are underway in North America, Europe and Asia. Example applications include eco-signal operations, lane-changing management, eco-integrated corridor management, low emission zones, and eco-traveler information systems [*39*]. In addition, new eco-routing algorithms are being developed to provide drivers alternative routes to reduce fuel and emissions. This section introduces applications of Low Emission Zones, Eco-Driving, Eco-Signal and Eco-Routing, because potentially they can be integrated into this dissertation research to achieve substantial exposure mitigation.

2.4.1 Low Emission Zone

Low Emission Zones (LEZs) are areas (usually populated city center) where the heavy-polluting vehicles are prohibited to enter, or can enter at a monetary cost. The future dynamic LEZ management will be realized by communication between the vehicles and the geo-fenced designated zones, where vehicle emission categorization, pricing and permission issuing process will be automatically executed upon the arrival of vehicles at the LEZ [*40*]. Currently, LEZ are enforced by human inspections, and widely implemented in Europe since 2008, where LEZ practice demonstrate significant air quality improvement.

London, capital city of England, is one of the top cities that suffer air pollution. London effectuated LEZ in a staged process starting from year 2008. In the same year the proportion of high-emitting vehicles in LEZ decreased from 47.4% to 31.9%. Following ambient air quality measurements in year 2009 showed that concentrations of particulate matter within the low emission zone had dropped by 2.46 - 3.07% compared to 1% for areas just outside LEZ [*41*].

Munich, the large city in Germany, implemented LEZ in year 2008. In year 2009, air quality studies estimated that the overall mass emission from transportation factor was decreased about 60% within the LEZ boundary. The average concentration of elemental carbon from mobile source decreased from 1.1 to 0.5 $\mu g/m^3$ [*42*].

Lisbon, capital city of Portugal, applied ‘aggressive fleet renewal program’ as a phase in LEZ implementation, starting in July 2011. Subsequent studies showed that within LEZ, PM_{10} mass emission decreased 34% (8 tons per year), and NO_x mass emission was 7% lower (reduced 57 tons per year) [*43*].

Five cities in Netherlands implemented LEZ in year 2008. Two years later, measurements in the five cities and control measurements in suburban locations showed that the air quality of urban street environment was significant improved, where $PM_{2.5}$, NO_x and NO_2 concentrations were reduced substantially [*44*, *45*].

LEZs are effective for straightforward reasons: heavy-emitting vehicles are excluded in populated city center for selected time windows, where the general public in LEZ directly benefit from the pollutant concentration reduction hence exposure mitigation through emission source control. A major limitation is that LEZs restrict heavy-duty vehicle transportation and mobility in implemented area and impede related businesses. Also, before the advent of dynamic automatic LEZ system, it heavily relies on human inspection to enforce LEZs.

2.4.2 Eco-Driving

In early 1990s, automobile ownership surged and inter-vehicle communication systems emerged to improve traffic safety. In late 1990s, researcher started exploring the environmental benefits of vehicle inter-communication systems. For example, Widodo *et al*. proposed a new V2V communication system in 1998 [*46*]. In 2000, they introduced environment-adaptive driving (EAD), and evaluated the fuel consumption as well as emission reduction applying EAD with a traffic simulator. They found that fuel consumption and CO emissions are effectively reduced when simulating vehicles were equipped with EAD [*47*].

Barth *et al*. investigated freeway-based dynamic eco-driving systems, where advice was given in real-time to drivers when traffic conditions change in the vehicle's vicinity. Both simulation and real-world freeway driving showed that, by providing dynamic advice to drivers, approximately 10-20% fuel can be saved with only a small increase in travel time. [*48*]

Further, Barth *et al*. introduced dynamic eco-driving for signalized corridor traveling. In their simulation, vehicles were assigned for different velocity planning when traveling through signalized intersections, then their fuel consumption is evaluated with microscopic emission model CMEM. When comparing two same-length trips for a vehicle: (1) hard accelerates then steady cruises to trip's end point, (2) slow acceleration to reach end point of a trip, it was found that the velocity plan (1) is 10% to 15% more fuel efficient comparing with the second one [*49*].

2.4.3 Eco-Signal Operations

Eco-Signal Operations apply CV technologies to reduce vehicle stops, idling time, unnecessary accelerations and decelerations at signalized intersections, hence reducing fuel consumption, GHG and air pollutant emissions. The overall operations feature specific applications such as: (1) Eco-Approach and Departure at Signalized Intersections, (2) Eco-Traffic Signal Timing, (3) Eco-Traffic Signal Priority [*50*]. They are pioneering research that are mostly in simulation and modeling stage.

Further, Xia *et al*. developed an enhanced eco-approach and departure algorithm which considered not only the phase and timing of the signal but also the estimated intersection delay in front of the subject vehicle. Simulation results showed that, 20% penetration rate contributed up to 11% of network-wide fuel saving, and 100% penetration rate would reduce network-wide fuel consumption by 30% [*51*].

Kamalanathsharma *et al*. also investigated Eco-Speed control near signalized intersections. They simulated different speed adjustments for four type of vehicles at signalized intersections, and compared the fuel consumption with microscopic emission model VT-Micro. It showed that eco-speed control can reduce fuel-consumption up to 50% in the vicinity of signalized intersections in their setting [*52*].

Kari *et al*. [*53*] introduced a multi-agent systems based freight signal priority (FSP) algorithm to reducing network-wide energy and emissions. In a series simulation with varying freight agents penetration rate, traffic volume and communication radius, it is found that FSP can improve system-wide fuel economy by 5%-10%, and reduce freight vehicle travel time by up to 26%.

Even though eco-signalization have not been widely operated in real world, they are expected to effectively reduce pollutant concentration at intersections. For example, Wang *et al*. monitored UFP concentration at a busy intersection in Corpus Christi, Texas. Repeated measurements showed that UFP number concentration was 3.5 times greater when traffic was idling at a red light than moving at a green light [*54*]. Therefore, Eco-Signal and Eco-Traffic Signal Priority are potentially effective ways to mitigate roadside pollutant exposure for general public. The environmental benefits depend on moderate penetration rate of CV technology in vehicles and infrastructures in the future.

2.4.4 Eco-Routing

Considering potential energy saving from standpoint of vehicle trip selection, eco-routing applications are developed to give travelers alternative routes which minimize fuel and emissions. Eco-routing focuses specifically on individual vehicles with the goal of minimizing energy and emissions on a large regional basis. The energy saving is usually accompanied with slight travel time penalty. Fortunately, most of the environmental-ITS applications are additive. For example, if Eco-driving can be integrated with Eco-routing, the travel time penalty can be compensated and environmental benefits will double.

Barth *et al*. performed systematic research on Eco-routing feasibility, benefits and applications. An Eco-routing navigation system was developed where network-based fuel consumption and emissions were estimated. The estimation used CMEM that has been calibrated with real-world vehicle activity patterns. Routing experiments showed that moderate speed routes were often more environmental friendly than fast or slow routes, hence road congestion level played an important factor in routes selection [*55*]. Based on this Eco-routing navigation system, Boriboonsomsin *et al*. incorporated historical and real-time traffic information, as well as detail road grade data into a user-friendly platform. These critical functions allow for a better emission/energy prediction and clear route visualization for users [*56*].

Ahn *et al*. simulated Eco-routing in a roadway network starting with a market penetration rate. Is was found that in most cases eco-routing system contribute to reduction of network-wide energy consumption and emission levels. The reduction ranged between 3.3% and 9.3% when compared to conventional shortest duration routing strategies [*57*].

To summarize, environmental-ITS applications are mostly focusing on overall energy/emission reduction from the vehicle's tailpipe. In the ultimate goal to mitigate human exposure to mobile-source pollutants, more work is needed to identify exposure subjects and link energy/emission to population exposure assessments. Only with this connection it is possible to plan for exposure mitigation applications.

3 Vehicle Roadway Navigation to Mitigate Pollutant Exposure

3.1 Introduction

In a routing scenario described in problem statement (Section 1.1), a heavy-emitting truck plans to travel from Grocery Store 1 to Grocery Store 2. Traditional routing firstly aims at shortest distance. With the improving technologies that collect real-time traffic speed and estimate arrival time, least duration routing is widely used today to minimize the total travel time for drivers. However, without information of pollutant dispersion and population distribution, a least duration trip is likely to traverse populated areas and impose excessive exposure to public population. For example, the blue route in Figure 3-1 may cause excessive exposure to young children who attend schools by major streets.

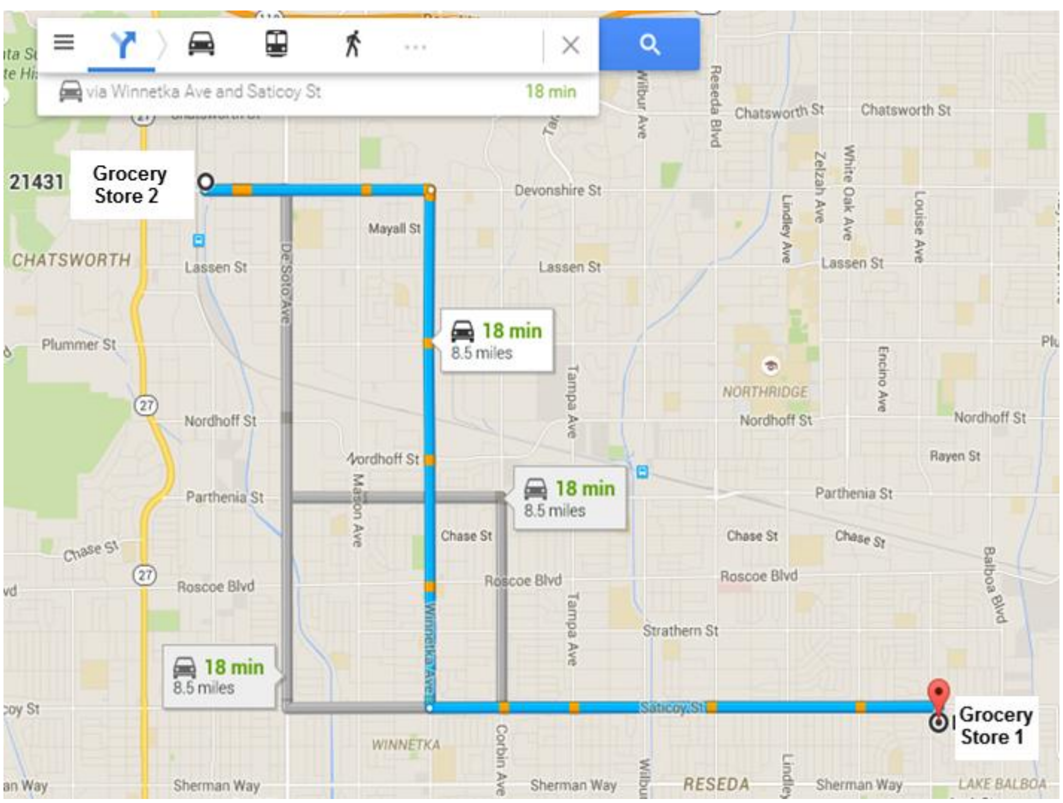

Figure 3-1 An example of heavy-emitting truck routing scenario

This chapter introduces a novel vehicle routing methodology that goes beyond simply minimizing total emissions, instead minimizing pollutant exposure to localized populations along the roadways. As part of the overall methodology, a unique modeling suite has been developed to estimate pollutant exposure based on specific vehicle activity, considering both spatial and temporal factors. Essentially, the pollutant exposure to residents near roadways is estimated and used as an index for vehicle routing to minimize overall exposure, while also considering economical routing distance and duration. This concept is particularly valuable for routing or regulating high-emitting vehicle fleets in sensitive communities such as schools, residential zones, or hospitals.

3.2 Methodology

There are three major calculation components to apply vehicle roadway navigation to minimize pollutant exposure. First, temporal-spatial distribution of pollutant concentration is modeled for area of interest. Secondly, the pollutant concentration map is spatially matched with road network, and local population exposure is assessed for each link in the network. Thirdly, the link-based exposure is integrated with driving duration as a new routing cost of the network. Then the new routing cost is used in the routing tool to find alternative routes that cause lower exposure than traditional least duration routes. The first two components are also applied in studies in Chapter Four and Five.

Modeling concentration of mobile-source air pollutant is a multi-step process. Figure 3-2 shows the flow diagram and model selection of traffic emission exposure modeling methodology: (1) with traffic activity datasets, an emissions model is firstly used to quantify source emissions factor from on-road traffic (2) next, a dispersion model is applied to compute the target area emission pollutant concentration; and (3) a pollutant exposure model is then utilized to account for how much emission pollutant is actually inhaled by a target population group, and in the case studies *inhaled mass* (*IM*) is used as the exposure quantification. The final exposure estimates can be generated on a link-by-link basis in a roadway network, and used as input to a routing engine as the routing costs. Figure 3-3 maps the link-based critical inputs and their dimension in each modeling step.

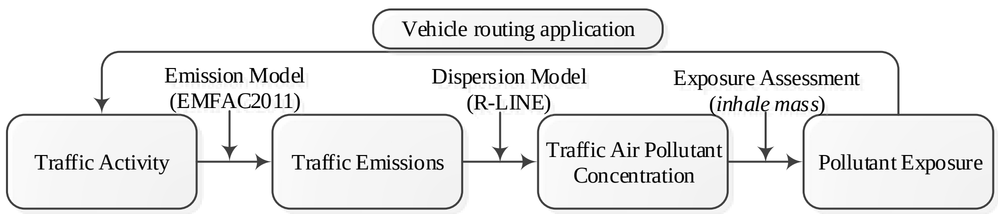

Figure 3-2 Overall traffic pollutant exposure modeling methodology flow diagram

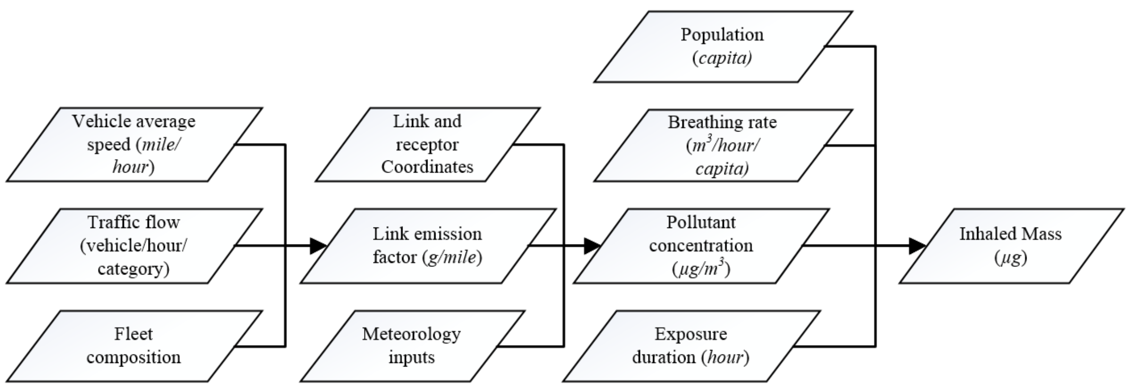

Figure 3-3 Critical link-based inputs for the overall traffic pollutant exposure modeling methodology

This emission-dispersion-exposure modeling method has been applied by several researchers using a variety of model combinations. For example, Amirjamshidi *et al*. modeled the general public exposure at peak hour in Toronto Waterfront Area. Results mapped that total exposure is highest in the densely populated area such as a central business district [*58*]. In this research, we step further to design a routing method to reduce exposure for susceptible groups in an effective and dynamic fashion. The established models are introduced in Chapter Two, specific model selection and data source in the case studies are described in the following sections. To interface with the various models and datasets, and maximize the modeling accuracy, considerable efforts of spatial analysis and data processing are needed.

3.2.1 Traffic Activity Acquisition

First, a digital roadway map is the heart of any navigation applications. It symbolizes the roadway network, including small lanes, arterials, ramps and freeways in line segments. Geographically, the map represents the location, length, shape and stores static attributes (road type, lane number, speed limit *etc*.) of the roadway network in the real world. Then traffic activities are estimated based on roadway links in the network map. For traffic activity parameters, many traffic measurements and models focus on overall traffic speed, traffic flow, and fleet composition. These parameters are available either from real-world measurements (e.g. Caltrans Freeway Performance Measurement System (PeMS) [*59*]), or microscopic vehicle trajectory can be simulated by various traffic simulation software (e.g., Paramics [*60*]) on a roadway link-by-link basis.

In this case study, we use street map of North America provided by ESRI due to the high level of details [*61*]. Posted speed limit values are assigned as average traffic speed in this study. Microscopic vehicle operations, such as speed fluctuations, idling, and accelerations tend to have great impacts towards localized emission. For example, when vehicles stop at an intersection, higher pollutant concentration was observed at the intersection [*54*]. The concentration change will in turn affect *inhaled mass* of localized population. In this exposure modeling, however, microscopic traffic events are not considered. It is a great research topic to explore. This chapter focuses on the overall implementation shown in Figure 3-2 and Figure 3-3.

3.2.2 Traffic Emission Modeling

An emission model is required to determine the emission factors given specific vehicle activities. As introduced in Section 2.1, there are several emission models developed for regulatory or research purposes in United States. To evaluate the mesoscale emission factors (usually in units of *gram/mile/link*), previous link-based travel activities are feed into an emission model. For this particular implementation, EMFAC2011 (introduced in Section 2.1) is applied for mesoscale emission factor calculation, because EFMAC has well-established vehicle activity database for California counties and air basins. Instead using the EFMAC user interface, the emission factors for specific vehicle categories are downloaded from EMFAC2011 online database [*62*] and saved as Matfile [*63*]. Then, link-by-link emission factors are calculated with a scripting language (e.g. Matlab [*64*] is used throughout this dissertation) as a new attribute of the roadway network.

3.2.3 Geometry Refinement of Roadway Network

In this research, not only does the roadway network serve as a navigation graph, but also as the line-source of pollutants. In dispersion modeling, a good representation of the roadway geometry, such as curves, turns and segments, is critical for rendering the relative locations between the line sources (e.g. roadway links), receptors (e.g. schools, residential homes) and other spatial inputs (e.g. weather stations).

Most of the original network shapefiles (a file format that stores geometry, location, and static attributes [*65*]) contain curved links, because curved links in transportation modeling and navigation are acceptable as long as one link has corrected length and consistent road attributes (e.g. level of service, number of lanes). However, a curved link cannot be well represented in dispersion models because it is taken as a straight link given two vertices (as the dashed line in Figure 3-4a). Hence, curved links are not desirable in this study and the geometry should be refined.

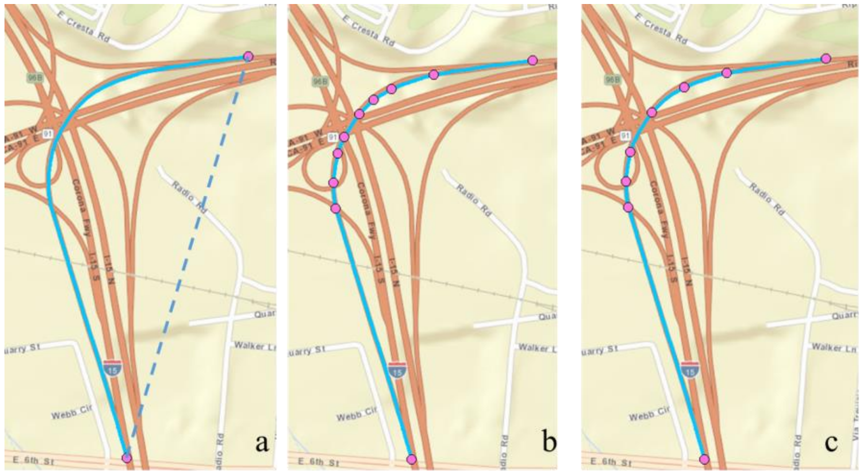

Original link
Original link is split into 9 segments using 'Split' tool
After 'Generalize', the link is split into 7 segments

Notes: b: The original curved link is split into 9 segments using 'Split line at vertices' [*69*] tool in ArcMap, the number of segments are determined internally with ArcMap's geoprocessing algorithm that splits straigh-line segments within a curve. c: After using 'Generalize' tool [*68*] on the original link, the geometry of the curve is simplified and it only produces 7 links using 'Split line at vertices' tool, hence reducing number of links to process. Users need to specify a generlaization tolerance when using this tool; the larger the tolerance is, the more simplified the resutls are.

Figure 3-4 'Generalize' and 'Split Line at Vertices' tools used to simplify and preserve link geometry

The flaws can be corrected by a string of spatial analysis in Geographic Information System (GIS) software. In this dissertation, ESRI ArcMap is applied for all GIS operations [*66*]. The first blue oval, 'network_flow_emi', is the original network shapefile that contains curved links, with flow and calculated emission values tabulated for all links. 'Project' [*67*] transforms the original geographical coordinate of network shapefile into a projected coordinate system (PCS, e.g. UTM), because PCS preserves true distance to the best extent. 'Generalize' [*68*] simplifies curved links, reducing number of links to be generated in the next step (as Figure 3-4b and 3-4c show), hence reducing total number of links to be processed in the overall calculation of subsequent modeling compoments (e.g. dispersion modeling and routing). 'Split line at vertices' [*69*] breaks simplified curves into straight segments (as Figure 3-4c shows).

After the geoprocessing suite, the final network shapefile contains significant more links than the original network (due to the split operations), but they are all straight segments that characterize the network geometry at great details. Moreover, traffic flow and emission factors are passed to every link. This geometry-refined network will be the data source of location inputs in dispersion modeling, routing implementation and data visualization in the following sections. The geometry refine process will also be applied to the following two chapters.

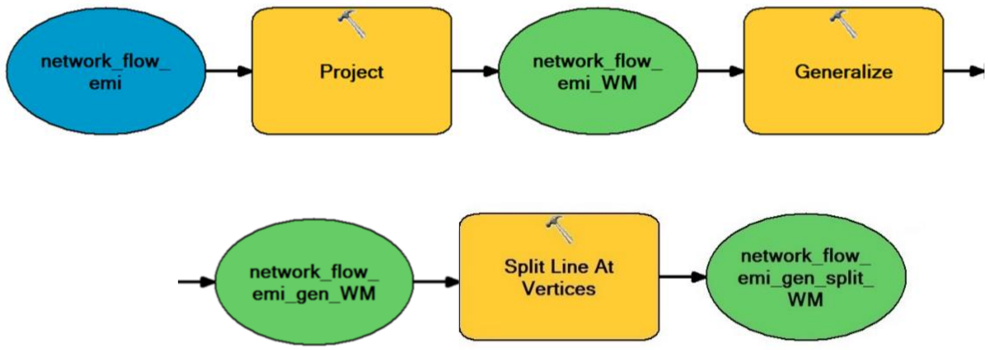

Figure 3-5 Workflow of roadway network characterization

3.2.4 Dispersion Modeling

Next, an atmospheric dispersion model is utilized to predict mobile-source pollutants concentration for specific locations. Among all the established dispersion models introduced in Section 2.2.2 Modeling Techniques, R-LINE is used in this study, because it applies advanced micrometeorology inputs and performs accurate estimation [*25*]. Moreover, R-LINE has a succinct input configuration, and computes fast. The underlying relationship between concentration at receptors and the line sources in R-LINE can be expressed as Equation 2-2.

While all other variables retain the same for Equation 2-2, emission rate of on-road vehicles Q (*g/meter/second*) is given by $N \times e_f$, where N (*vehicle/second*) is traffic flow and e_f (*g/meter/vehicle*) is averaged emission factor acquired from previous traffic emission modeling. Source location, nodes coordinates of each line segment are extracted from the roadway shapefile (e.g. processed in Section 3.2.3) with ArcMap [*66*]. Typical meteorology data for R-LINE includes hourly temperature, wind speed, wind direction, surface friction velocity, Monin-Obukhov length *etc*.

(datasets for several Southern California sites are available from the Southern California Air Quality Management District (SCAQMD) website [*70*]). R-LINE provides options of both analytical solution and numerical integration for concentration calculation, and in this study we choose analytical solution for better performance.

An example R-LINE input file is provided in Appendix A and partially in Figure 3-6. The blue lines mark the mandatory inputs and they should be placed at exact corresponding lines that are also marked in blue color (note: line number are added by the author for clarification, and they are not needed in computing). More details about configuration please refer to R-LINE user guide [*71*].

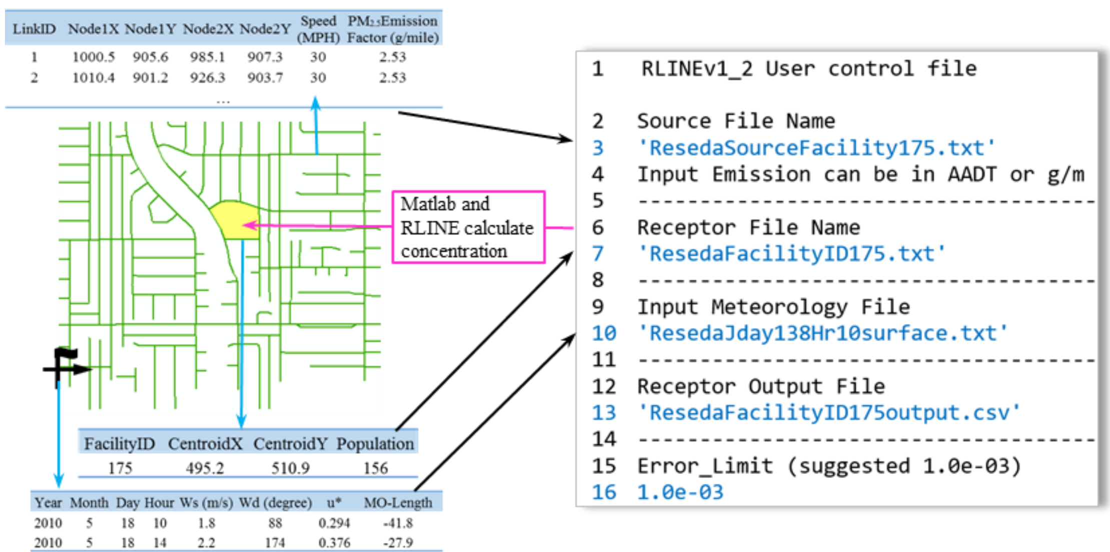

Note: Blue arrows point to pre-calculated attributes of geographic features (e.g. facilities, street links, and weather stations). Black arrows indicate Matlab scripting to select attributes and generate input control files. Pink arrows represent that Matlab calls R-Line and compute receptor concentration. This schematic graph applies to mobile-source pollutant concentration estimation for all point receptor in this dissertation.

Figure 3-6 Schematic graph of transition from spatial feature attributes to dispersion modeling implementation

Combining Figure 3-3 and 3-6, it is clear that there are three major inputs for R-LINE: link-receptor location, roadway emission factors, and meteorology parameters. For a large area (more than 100 Acres), the three major inputs are grouped and indexed based on link-receptor relative location. Matlab is used to write the inputs into text files, process using R-LINE, and read the outputs. The

R-Line program suite coded in Fortune is applied because it can be conveniently called by Matlab and batch processed.

3.2.5 Exposure Assessment

As the last step in the modeling process presented in Figure 3-2, an exposure model is used to estimate how much a pollutant is intake by an individual or a group of population. As discussed in Section 2.3, *inhaled mass* (*IM*) is applied for exposure assessment in this dissertation as in Equation (2-5), and all the variables retain the same meaning. *C* is the mobile-source pollutant concentration ($\mu g/m^3$) in a given microenvironment, which is calculated with R-LINE. *Pop* is the number of population assigned for the facility. *t* (*hour*) is the duration of each trip, and *BR* denotes breathing rate ($m^3/hour/capita$) of subjects exposed to the pollutant.

To assign an exposure value to roadways, *IM* is used to quantify the total mass of vehicular emissions inhaled by nearby population when vehicles traverse a roadway link, for the entire road network. It is of strong research interests to reduce susceptible population's *IM* to vehicular pollutants, because exposure quantities of the primary emissions, such as fine particles, nitrogen oxides (NO_x), and volatile organic compounds (VOCs), are positively associated with health risks to young children, older adults, patients and even healthy adults [*22*]. The goal of this study, is to apply a routing approach for heavy-emitting vehicles, so that the target population's *IM* to certain emissions can be minimized, for the purpose of protecting their health.

The underlying assumptions and hypothesis are as follows. (1) For now, vehicle acceleration/deceleration/stop and building downwash are not considered; (2) The traffic emissions rapidly and uniformly disperse into ambient environment; (3) Only the inhalation exposure mechanism is considered; (4) The dispersed concentrations in indoor and adjacent outdoor areas are the same; and (5) The less *inhaled mass* is for an individual or a group, the better it is.

3.2.6 Vehicle Routing Problem Statement

Normally a route is found with an expectation of a least cost. For example, in our daily life, driving distance or time as a cost is widely used to find a shortest-distance or least-duration route. In this study, given a pair of origin-destination (OD) points, it is desirable to minimize *inhaled mass* and constrain increase of routing time within a practical range for a trip that connects an OD pair. This is a multi-objective vehicle routing problem (VPR) studied by Grodzevich *et al.* [*72*]. Several solving methods for multi-objective VPR were summarized by Demir *et al.* [*73*].

Mathematically, the roadway network is described by a graph $G = (N, L)$, where $N = \{1, ..., n\}$ is the set of nodes. $L= \{(i, j): i, j \in N, \text{ and } i \neq j\}$ is the set of links, also known as arcs in other VRP studies. Two nodes, i and j, determines a link l_{ij}, which belongs to link set L. Each link l_{ij} has several attribute or costs, such as length (d_{ij}), travel time (t_{ij}), in this study, *inhaled mass* (IM_{ij}) as well. The objective is to minimize the collective *IM* for a route *R* (also a subset of *N*): $\sum_{i,j\in R} IM_{ij}$, given an OD pair (O, D). At the same time, the total routing time should be constrained:

$$\sum_{i,j\in R} t_{ij} < (1 + a) \cdot (\sum_{i,j\in R_0} t_{ij}) \text{ (3-1)},$$

where a is a constrain factor, R_o denotes the least duration route that connects (O, D).

A widely used method to address the multi-objective VPR is the weighting method (WM), where multiple objective costs are summed into a single combined cost with a set of weight factors. Thus, the multi-objective VPR is transformed back to a classic VPR. A second method is an extension of WM - the weighting method with normalization (WMN), where the values of objective function are normalized between 0 and 1 [*72*]. The exact solution can be calculated by an epsilon constraint method (ECM), where one of the objective functions is selected to be optimized, while all others are converted into constraints, usually by imposing an upper bound [*74*, *75*]. A fourth method, hybrid method (HM), integrates adaptive weighting and the constraint method. It was found that hybrid method is highly effective in solving good-quality routes in a network of 100 nodes [*73*].

In this chapter, the example network to be tested has more than 13,000 nodes, and hundreds of trips will be experimented. A modified weighting method is applied as in Equation 3-2. The future improvements will include using more efficient routing algorithms.

In this particular research, the new cost is used to find a path with possibly lowest traffic emission pollutant exposure to the target population within a practical driving duration. The final routing is implemented with Matlab, in which the underlying least-cost algorithm is Dijkstra's algorithm [*76*].

$$weighed\_cost_k = \sum_{f=1}^{F} w_f \times cost_{f,k} \qquad (3\text{-}2)$$

In Equation 3-2, $weighed\_cost_k$ is the combined cost for each link k; w_f is the weigh factor for $cost_{f,k}$ (a single cost f for link k). $cost_{f,k}$ can be distance, time, monetary cost, or exposure in this study. There are total F single costs and weigh factors, and it is usually determined that $\sum_{f=1}^{F} w_f$=1. t_k is the driving time for each link k derived from link length and speed limit. In this trade-off routing scenario, for each OD pair, there are several extreme cases: w_f for duration is 1, which means duration is the only cost, and w_f for exposure is 1, which means exposure is the only cost. Because facilities with dense population are normally located near easily-accessible road, the least-duration route tends to cause a large exposure cost, and least-exposure route is likely to be tortuous to avoid all the populated locations. The detour will add excessive routing time to the driver, which makes the path impractical. Since the two costs have different units and numerical ranges, normalization is applied as:

$$IM_k = IM_{orig}/(IM_{max} - IM_{min}) \ (3\text{-}3)$$

$$t_k = t_{orig}/(t_{max} - t_{min}) \ (3\text{-}4),$$

where iM_{orig}/t_{orig} is original *inhaled mass*/*duration* cost of a link with its original dimension. IM_{max}/t_{max} is the maximum *IM*/duration cost of a link among the entire network. Likewise, $IM_{min}/t_{min.}$ denotes the minimum value of a link among the entire network. Note that the normalization here is different from the weighting method with normalization (WMN) mentioned above [*72*].

The overall routing application finds the route with least total cost for a given OD-pair:

$$minimize \sum_{k\in R_1} cost_k \quad (3\text{-}5)$$

where R_1 is the set of links in least-cost path computed by the routing program. Total cost is very sensitive with the variation of weight factor *w*. Specific sensitivity analysis is presented in previous studies [*77*]. Section 3.3 provides more details about experiment values of weight factor. Also, least duration route R_0 is calculated as: $minimize \sum_{k\in R_0} t_k$ (3-6).

Then the total routing time and *IM* values are compared between R_1 and R_0. If R_1's overall *IM* values are lower than that of R_0, and R_1's total routing time is within a reasonable range with that of R_0, R_1 is considered as a low exposure route. Future improvement will be focused on using efficient routing algorithm to solve for low exposure routes.

During data process described above, the format of each data source could be very different, but the datasets are all extracted and computed on a link-by-link basis and passed as binary files which can be directly manipulated by programming tools. It is important to note that routing occurs at specific time of a day with different weather condition and human activities; hence the dispersion, population and resultant routing cost for each link are highly dynamic for a network in the real world. In this experiment, we need to specify time scenarios to determine static parameters. Once link costs and OD-pairs are determined for a scenario, least-exposure routes can then be calculated and visualized. For faster and more comprehensive OD-pair tests, routing programs compiled in advanced computer languages would be very computational efficient.

3.3 Experiments and Results

3.3.1 Experiment Setup

While the methodology can be widely applied to urbanized area, a case study is needed. This section presents experiment area for the low exposure road navigation in calendar year 2010. Also, the experiment vehicles, target pollutants, and susceptible population groups chosen in this modeling study and related data processing are introduced.

We consider the local roadways in Reseda-Northridge area, located in Los Angeles (LA) County as our experiment area as in Figure 3-7. This area was chosen because it has a high percentage of seniors and children population. Also the road network represents a variety of road types, such as freeways, highways, arterial and small roads. According to 2010 U.S. Census, in year 2010, this 64-square-mile area is home to more than 531,000 residents and 192,000 housing units. Adults who are 65 years and older make 11.8% of the total population in this area, which is 2% higher than the average of LA County. Children who are 5 years old and below make 6.3% of the local population [*78*]. Additionally, there are dense residential houses, stores, daycare facilities, primary schools, senior centers, and hospitals located near roadways in this area.

As Figure 3-7 shows, the area is bounded by Interstate-405, U.S. Route-101, State Route 118 and State Route 27. I-405 and US-101 freeways are heavily traveled by both commuters and freight-movement fleets. When heavy duty trucks enter this community to restock goods in local stores, they are likely to pass the daycare centers, senior homes and other facilities which are located right next to roadways, and the emissions will pose potential health risks to sensitive people in those facilities. Therefore, it presents an interesting study area where least-exposure routing can be applied to reduce the susceptible population's *inhaled mass* of vehicle emissions.

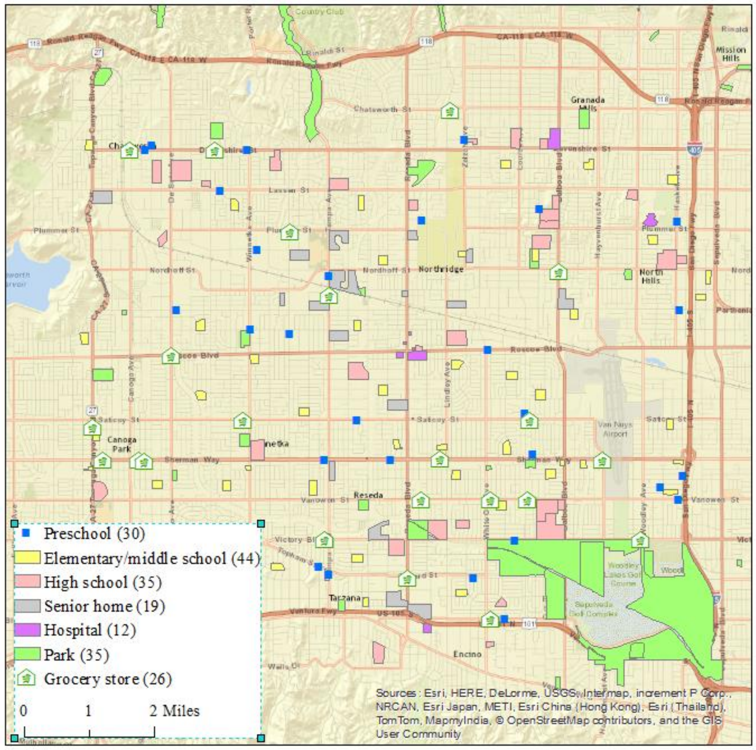

Note: Facilities which occupy more than 100 acres are characterized as polygons, otherwise points
Figure 3-7 Map of Reseda-Northridge area and facilities

3.3.1.1 Traffic Activity and Emission Estimation

The experiment street network contains 17,977 roadway links and 13,664 nodes. To construct *inhaled mass* cost for population in such a large network, we consider diesel-fuel trailer trucks as the source of diesel exhaust. When a fleet of five trailer trucks traverse a section of road, the diesel exhaust disperse into nearby facilities and are inhaled by people in proximity. Diesel exhaust is a mixture of gases and particles pollutants. Extensive health studies show that even acute exposure to diesel exhaust triggers transient irritation and inflammatory symptoms. Chronic inhalation exposure of diesel exhaust is likely to cause severe damage to human lung function, and lung cancer hazard [*79*]. EMFAC2011 (introduced in Section 2.1) is applied for mesoscale emission factor calculation, because EFMAC has well-established vehicle activity database for California counties and air basins. Among various pollutants assessed by EMFAC2011 (PM_{10}, $PM_{2.5}$, CO, NO_x, Reactive Organic Gas (ROG), and Total Organic Gas), $PM_{2.5}$ and ROG are chosen as the toxic surrogates in particle and gaseous phase of diesel exhaust, respectively.

The experiment vehicle is chosen as model-year-2005 diesel tractor trucks. Trailer trucks are frequently seen on streets and widely used in goods distribution are top heavy emitters among on-road vehicles. EMFAC2011 specifies tractor trailer as T7 Tractor category. In this experiment year 2010, mostly traveled T7 tractors in LA County are of model year (MY) 2005, according to EMFAC2011's database [*62*].

MY-2005 T7 tractors have high emission factors compared with regular cars and newer trucks equipped with advanced emission control devices. For example, compared with an average MY-2005 passenger car, an average MY-2005 T7 tractor emits 50 times more ROG, and 2,400 times more primary fine particle ($PM_{2.5}$), when both cruising at a speed of 40 mph. Figure 3-8 compares the emission factors of MY-2005 T7 tractors and MY-2010 T7 tractors.

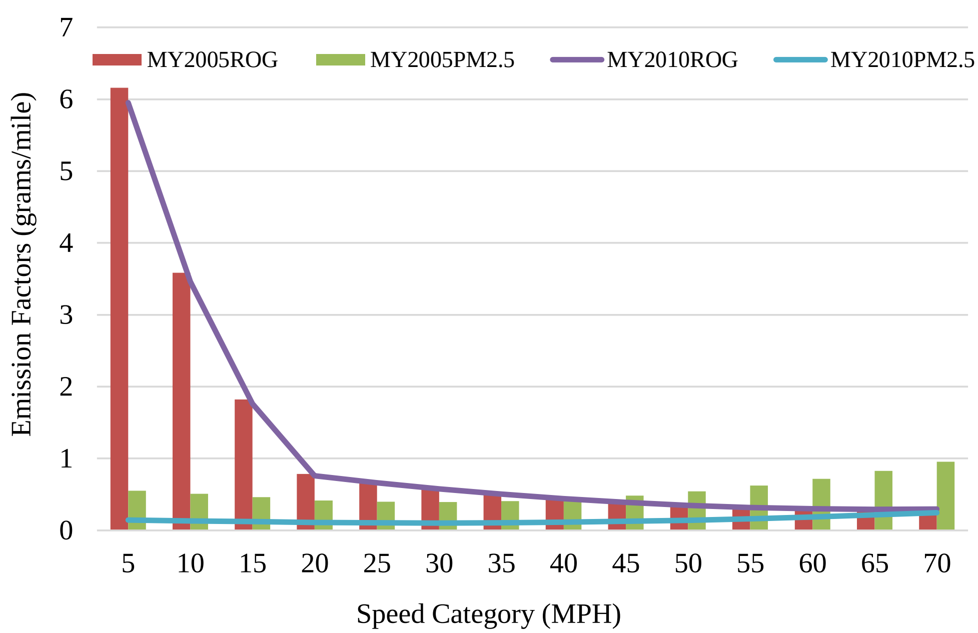

Figure 3-8 ROG and $PM_{2.5}$ emissions comparision between model year 2005 and 2010 T7 tractors.

3.3.1.2 Dispersion Modeling Implementation

As indicated in Figure 3-3, there are three major inputs for dispersion modeling: receptors where target population are located at, roadway links as line-sources, and meteorology parameters.

For receptors, we consider six types of facilities as well as residential homes, and the associated populations of interests. They are preschools, elementary schools, high schools, hospitals, senior centers, and parks (Figure 3-7). Table 3-1 tabulates the major inputs, data sources, and data processing to implement R-LINE. Figure 3-6 provides a schematic graph to understand the transition from spatial features' attributes to dispersion inputs.

Table 3-1 R-LINE major inputs and data sources

Input part	Description
1	File title
Source	User specified text to differentiate each run, e.g. '2010ResedaPM2.5_T7MY2005_Hr10'
2	Input source file: Link Index and 3-demention coordinates for both nodes, offset distance, initial σ_z, number of lanes, emission factor, road barrier location and height, suppressed source specification
Source	All facilities' centroids are indexed uniquely, and centroids of residential area buffers are indexed uniquely. Cartesian coordinates of receptors are extracted using ArcMap tool 'Add XY' [*80*]. Elevations are mapped from USGS DEM database [*81*]. A link is considered as the center line of a road so offset distance is zero. Road barrier and suppressed road are not considered. σ_z please see R-LINE user guide [*71*]. Emission factor is calculated in Section 3.3.1.1.
3	Receptors Index and 3-demention Cartesian coordinates
Source	Receptors Index is nominal. Cartesian coordinates of receptors are extracted using ArcMap tool 'Add XY' and saved in matfiles. Receptors are placed at a typical breathing height of 1.5 m. Receptor elevations are mapped from United States USGS DEM database.
4	Meteorology inputs: date, hour, sensible heat, surface frication velocity, vertical convective velocity, Vertical Potential Temperature Gradient, Monin-Obukhov length, wind speed, wind direction, reference height, temperature, convective and mechanical boundary layer height *etc.*
Source	All the inputs are provided by South Coast Air Quality Management District meteorology data [*70*]. The meteorology station is Reseda Station which is located in the south of the experiment network.
5	Run specifications, e.g. time average options, analytical or numerical solution *etc.*
Source	This experiment choose 1 hour average with analytical solution. Lane width is set as 3 meter. Other options please see user guide [*71*].

3.3.1.3 Exposure Assessment and Network Characterization

Recall Equation 2-5, *inhaled mass* is proportional with microenvironment pollutant concentration, exposure duration, breathing rate, and population. In this experiment, hourly averaged pollutant concentration is estimated, and the exposure duration is set as one hour. Pollution distribution becomes an important parameter that affect the collective *IM* that trailer trucks could impose.

Table 3-2 tabulates the facility types and population estimation methods. Figure 3-7 maps the spatial distribution of the facilities. The general reasons for selecting these facilities and population are based on humans' susceptibility to various pollutants [*1-6*]. Other than the facilities, residential homes are also considered because they should be protected from heavy duty vehicles' entry. A breathing rate of 15 *L/min* is assigned to all the population [*82*].

Table 3-2 Facilities with involved population and data source

Facility type	Preschool	Elementary/ middle school	High school	Senior center	Hospital	Park
Target population	Children 5 years old and below	Children 6-14 years old	Teenager 15-17 years old	65 years old and above	All age	All age
Population data source	Census 2010 and US preschool enrollment rate	Esri[a], Census 2010, and California elementary school enrollment	Esri, Census 2010, and US high school completion rate	Census 2010 and review websites	Esri, Census 2010, and hospital websites	Esri and Census 2010
Number of facility	30	44	35	19	12	35
Average population per facility during experiment hour	202	254	176	596	454	36

Note: the source data is introduced in *Reference 83*

Population estimation requires considerable amount of data preprocessing. For example, local population of different age groups at block level are extracted from Census 2010 data depository and linked to GIS shapefiles [*84, 85*]. Next, we use geoprocessing tools in ArcMap to join the nearby census blocks to facilities and summarize population of appropriate age for each facility respectively [86, 87]. Then, each facility's population value is calibrated according to California schools' enrollment rates and other available information to simulate the real-world situation to the best extent. Facilities selected in this experiment are well-established entities and are confirmed from review websites and their own websites. In the future we would work on obtaining comprehensive and real-time information of facilities and involved population.

The emission concentration and total *inhaled mass* at each facility from each link is calculated with Equation 2-2 and 2-5. Each link has a unique Link-ID but may influence several facilities, then the *IM* values are summarized by Link-ID.

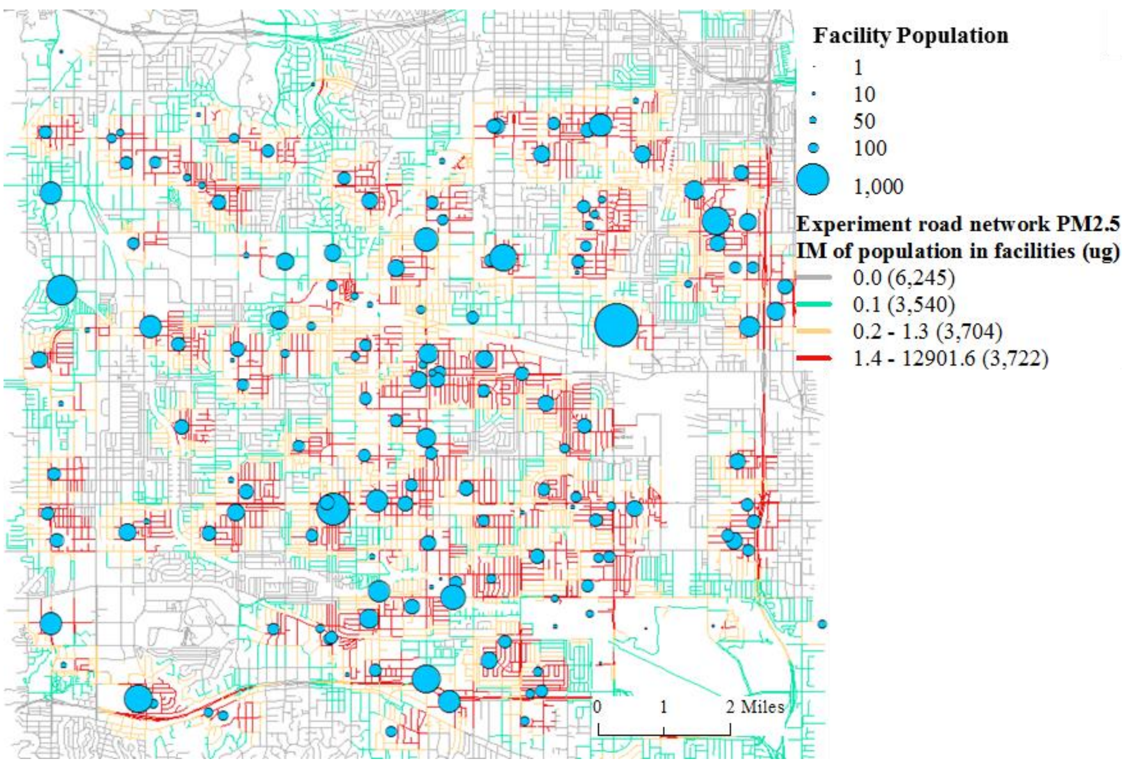

Note: *IM* is from a fleet of five MY-2005 T7 tractor

Figure 3-9 Facility population's $PM_{2.5}$ *inhaled mass* (*μg/link*) values for experiment network

Figure 3-9 presents facilities' $PM_{2.5}$ *inhaled mass* for all links in the network. In this case, for example, an *IM* value of 3,000 *μg/link* means that there is 3,000 *μg* of $PM_{2.5}$ inhaled by nearby target population during the hour, when a fleet of five year-2005 tractor truck is driven along this part of roadway. Figure 3-9 shows that according to R-LINE's computation, as distance to facilities increases, the impacts of emissions decrease. The spread distance of emission ranges from half to one mile, which agrees with roadside measurement studies [*8*, *9*].

Population distribution in residential areas are derived from U.S. Census 2010. *IM* values of population in residential homes are calculated independently from that of facilities. First, local population count at block level are extracted from Census 2010 data depository and linked to GIS census block shapefiles [*84*, *85*]. Population density for each block is calculated as the registered total population divided by the area of a census block (the area of a census block is given in the table or it can be calculated with ArcMap tools [*88*]). Then, we generate a left-side 200-meter buffer and a right-side 200-meter buffer for each link in ArcMap [*89*]. Emission concentration at each buffer are calculated using R-LINE (as shown in Figure 3-3, 3-6, and Table 3-1), assuming that the centroid of each buffer is a receptor and the roadway is a line source. Then we calculate the population within the buffer polygons based on the overlying census block's population density and buffer's area, assuming that 20% residents are at home and they are uniformly distributed within each buffer zone. Then the left and right side residential *IM* are calculated (Equation 2-5) and summarized into a total residential *IM* value for each link. 10 shows that *IM* values in residential area are proportional with the nearby population density.

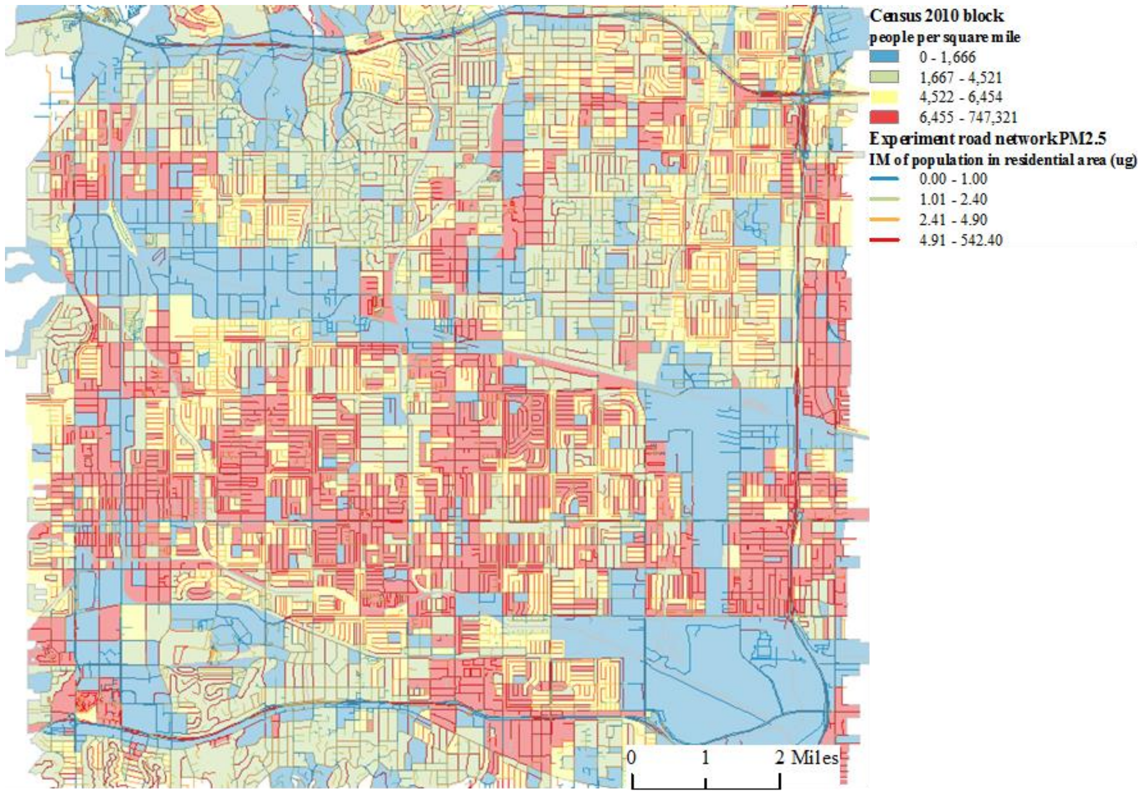

Note: *IM* is from a fleet of five MY-2005 T7 tractor

Figure 3-10 Residential population's $PM_{2.5}$ *inhaled mass* (*µg/link*) values for experiment network

Then the two layers of *IM* are aggregated by unique LinkID, and a final *IM* map of network is shown in Figure 3-11. Generally, the aggregated *IM* values for the entire network are sensitive towards critical variables, including traffic activity, dispersion condition, and adjacent population. For instance, a roadway link will have zero *IM* if there is no residents count (from Census 2010) within 200 meters nor any facilities within 500 meters. In contrast, a link will accumulate high *IM* if there are dense residential houses and several facilities nearby. *IM* calculation for entire network needs to be repeated if any critical variables marked in Figure 3-3 have changed. This facility and residential *IM* calculation is carried on for ROG as well.

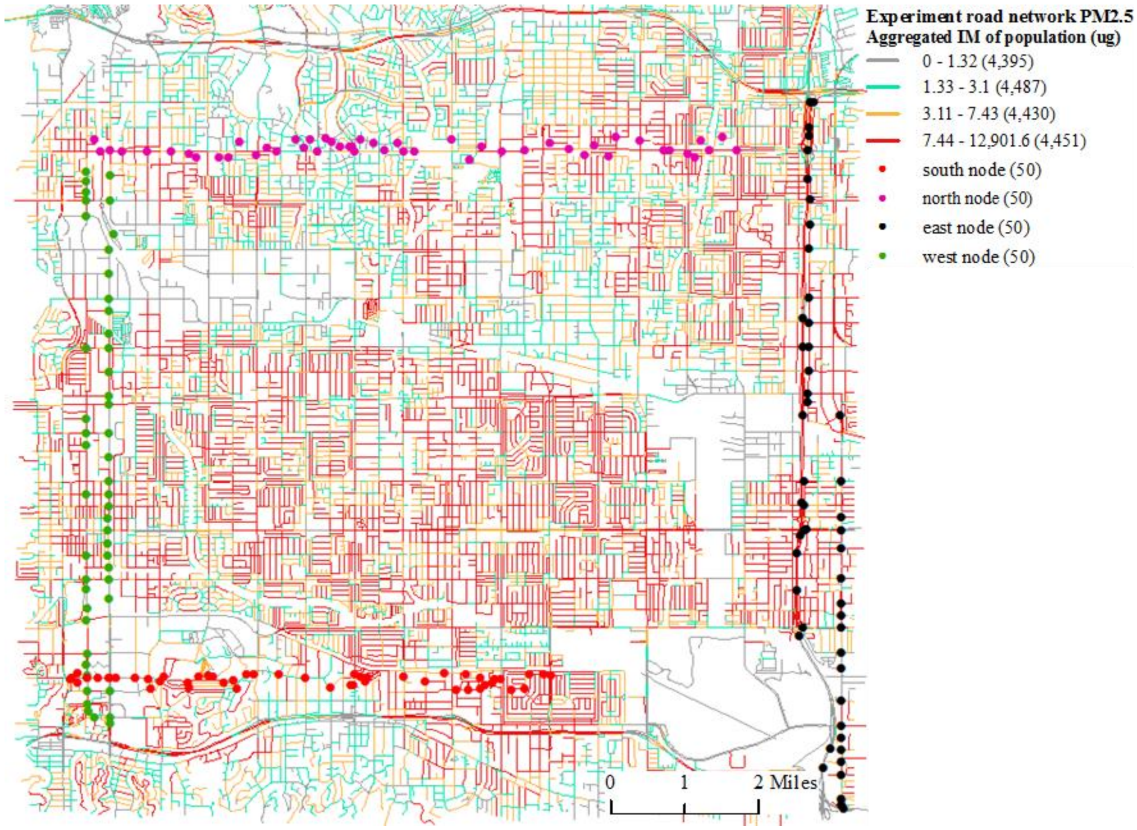

Note: *IM* is from a fleet of five MY-2005 T7 tractor, test junctions are selected approximately 0.2 miles apart in commercial zones

Figure 3-11 Aggregated $PM_{2.5}$ *IM* ($\mu g/link$) values for and test nodes in experiment network

With *IM* values constructed for the network, Equation 3-2 can be applied to prepare the weighed routing cost. Traverse duration for each link is derived from link length and posted speed limit. To restrict routing time and achieve exposure reduction, sensitivity analysis suggest it is good enough to incorporate a moderate portion of *inhaled mass* into the total cost. Combined cost of each link is weighed with three costs in this experiment:

$$cost_k = w_1 \cdot t_k + w_2 \cdot IM\_ROG_k + w_3 \cdot IM\_PM_{2.5_k} \qquad (3\text{-}7)$$

Driving duration (t_k), ROG *inhaled mass* (IM_ROG_k) and $PM_{2.5}$ *inhaled mass* ($IM\_PM_{2.5k}$) are normalized. The weight factor w_1 for t_k is assigned as 0.5, while w_2 and w_3 are given arbitrarily equal as 0.25, 0.25, respectively. This combined cost is calculated for each link k and updated for the entire network. Then an adjacency matrix is constructed with Matlab scripts based on the combined link cost and ready for route calculation. Given an OD pair, we expect that Dijkestra's routing program will compute a route with reduced ROG and $PM_{2.5}$ impacts and practical routing time, which we call low exposure routes.

3.3.2 Experimental Scenarios

As an illustration of the detailed overall process described in the previous sections, we set up a few experiment scenarios. We first consider a baseline scenario A, where a MY-2005 tractor trailer are driven towards several chain grocery stores in the community at 10:00am on a typical work/school day in May 2010. The truck takes a least duration route (LDR). To investigate the *IM* reduction for low exposure route (LER), other three scenarios are performed as listed in Table 3-3.

Table 3-3 Specifications of experiment scenarios

Scenario	Description	Routing Type	Tractor Model Year
A	Baseline route	LDR	2005
B	Test LER's results	LER	2005
C	Test clean vehicle impacts only	LDR	2010
D	Test LER and clean vehicles' impacts	LER	2010

To test more trips, we choose 400 OD-pairs that represent potential driving trips. Figure 3-12 shows 50 test nodes for four directions. First 50 OD-pairs are from east to west parallel (Figure 3-12a). Second 50 OD-pairs are from east to west diagonally (Figure 3-12b). Another 100 south-to-north OD pairs are selected with the same way. For south-to-west and east-to-north OD pairs, they are connected as illustrated in Figure 3-12c and 3-12d. The complementing table also shows the configuration. This setup can generally show patterns of route directions and related *IM*-duration tradeoffs. The 400 OD pairs are solved with both low exposure routing (LER) and least duration (LDR). Then the total routing time and *IM* values are compared between LER and LDR.

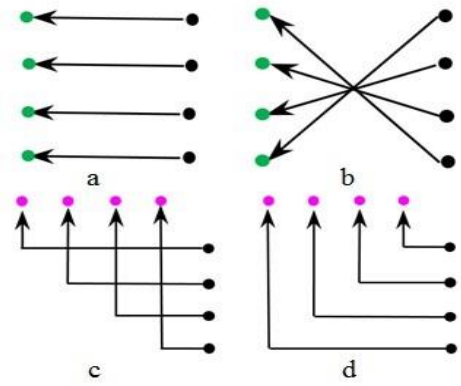

RouteID	Route direction	Route description
1-50	E - W	Parallel, as in Figure 3-12a
51-100	E - W	Diagonal, as in Figure 3-12b
101-150	N - E	Parallel, as in Figure 3-12a
151-200	N - E	Diagonal, as in Figure 3-12b
201-250	E- N	Inner corner, as in Figure 3-12c
251-300	E- N	Out corner, as in Figure 3-12d
301-350	S - W	Inner corner, as in Figure 3-12c
351-400	S - W	Out corner, as in Figure 3-12d

Figure 3-12 A schematic graph and table to explain the configuration of OD pair test

3.3.3 Experimental Results

In experiment scenarios where a fleet of five MY-2005 tractor trailer are driven by two grocery stores (described in last section), example routes are mapped in Figure 3-13 with satellite image overlay. The pink line is the regular least-duration route (Scenario A in Table 3-3), and green line marks low exposure route (Scenario B in Table 3-3). The benefits are summarized in Table 3-4. It can be seen that by choosing a low exposure route for this typical OD-pair on a school/work day, it results in a significant *IM* reduction because the green trip traverse less facilities and residential areas (generally the dense points in satellite image represent residential homes).

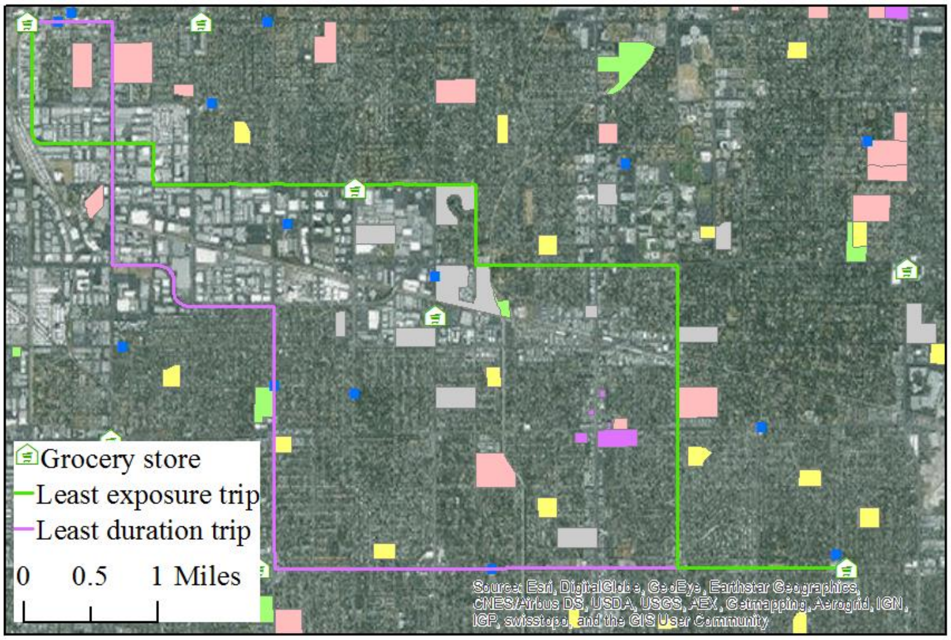

Note: For facility type please refer to Figure 3-7

Figure 3-13 An example routing map of LER and LDR

Table 3-4 Routing results of experiment scenarios

Scenario	Driving duration (min)	CO_2 emission (g)	PM2.5 *IM* (µg)	ROG *IM* (µg)
A (pink, MY-2005 LDR)	20.3	18752.8	588.2	1238.5
B (green, MY-2005 LER)	21.0	19068.1	74.7	297.3
Change (%)	3.3	1.7	-87.3	-76.0
C (MY-2010 LDR)	20.3	18634.0	5.8	87.3
Change (%)	0	-0.6	-92.2	-70.6
D (MY-2010 LER)	21.0	19068.1	5.8	87.3
Change (%)	3.3	1.7	-99.0	-93.0

Note: Route C is the same with that of Route A, and Route D is the same with Route B, hence not shown on map. Change is relative to the baseline scenario A. The mass emission and IM are averaged per truck.

Meantime, comparing Route B to A, driving duration increases 40 seconds (3.3%). It suggests that with a relatively small adjustment, the LER can lead to significant less pollutant exposure to susceptible population. Mass emission of CO_2 only increases 1.7%, indicating that the LER's fuel consumption is not exactly proportional with driving time. In fact, an LER can potentially consumes less fuel than that of LDR given the same OD pair, which can be seen in the following 400 OD test results.

Simply comparing with a MY-2005 trailer truck, a MY-2010 trailer truck emits 92% less $PM_{2.5}$, and 70% less ROG in mass (as shown in Figure 3-8). Therefore, it is expected to see the exposure reduction, because the clean vehicle technology significantly reduces source emission factor, hence proportionally mitigate localized exposure. It is worthy to point out that in Scenario C, even the MY-2010 truck is equipped with advanced emission control, the ROG *IM* reduction (70.6%) is still less than that of Scenario B (76.0%). It is because the MY-2005 truck in Scenario B is informed of the exposure condition when performing low exposure routing. It indicates that even before old vehicles could be retrofitted or replaced, LER offers possibilities to further mitigate their exposure impacts to public population. When looking at Scenario D, it is clear that when clean vehicle technology is coupled with LER, the exposure reduction can be more effective. In the long run, it is desirable to achieve both pollutant mass and exposure reduction. To better understand the effects of LER, we need to look at larger scale routing test.

IM reduction and duration trade-off results for the overall 400 LER trips are compared with their LDR counterparts. Figure 3-14 and 3-15 indicate that both $PM_{2.5}$ and ROG's *IM* can be significantly reduced by low exposure navigation. Also, for 30% of the routes, the LER and LDR are identical, resulting *IM* reduction as zero. Exposure to the two pollutants shows similar level of mitigation (up to 80%), and 40% of the trips have more than 30% reduction of both pollutants. *Inhaled mass* cannot be 100% eliminated because residential exposure is associated with most of the roadway links.

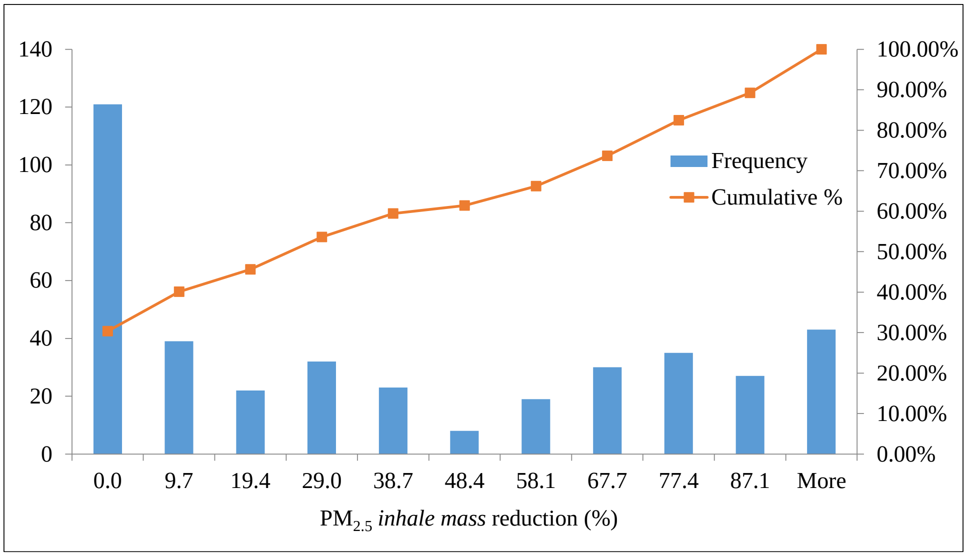

Figure 3-14 $PM_{2.5}$ *IM* decrease for 400 OD-pair test

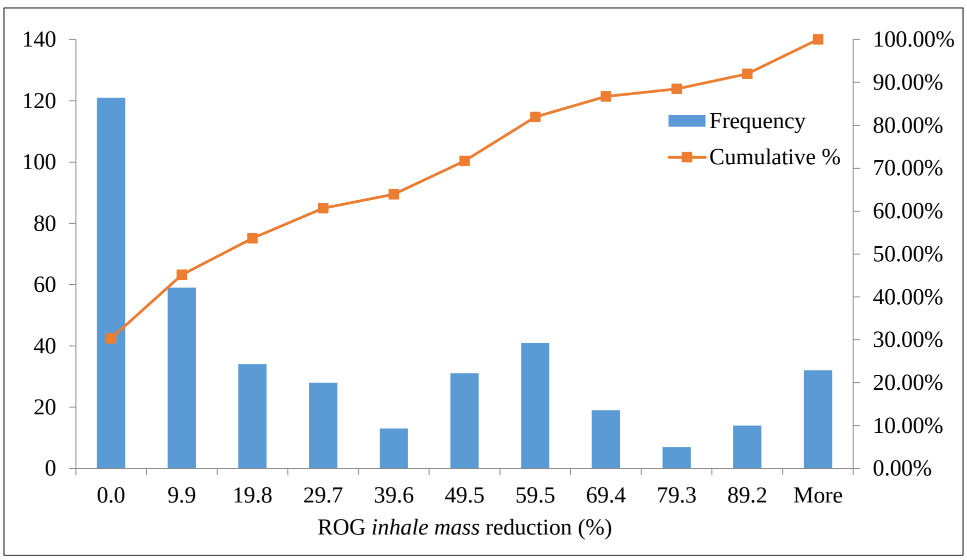

Figure 3-15 ROG *IM* decrease for 400 OD-pair test

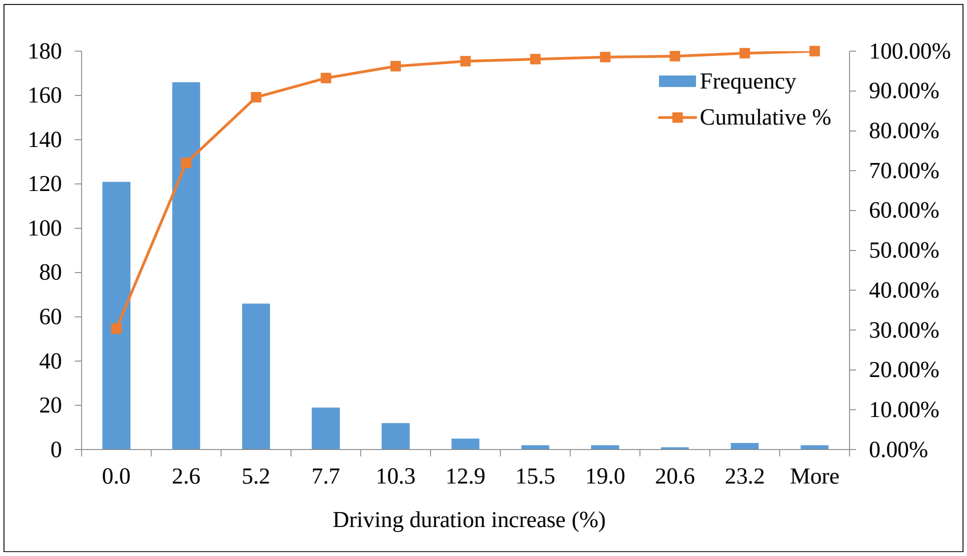

Figure 3-16 Driving duration increase for 400 OD-pair test

Figure 3-16 shows that 96% of the LER trips' driving duration increase are controlled within 10%. Meanwhile, moderate driving speed and increased driving time of LER may also contribute to a reduced fuel consumption. Figure 3-17 presents change of CO_2 emissions for the 400 low exposure trips compared with their least duration trips. Since CO_2 emission is proportional with fuel consumption, it indicates that more than 14% of LER trips actually consume less fuel than their LDR counterparts. 90% of LER trips have an increase of CO_2 consumption within 10%. For LER of prolonged driving time and excessive CO_2 emission increase, we can adjust the weigh factors and iterate LER calculation until it reaches a desired driving time and *IM* reduction.

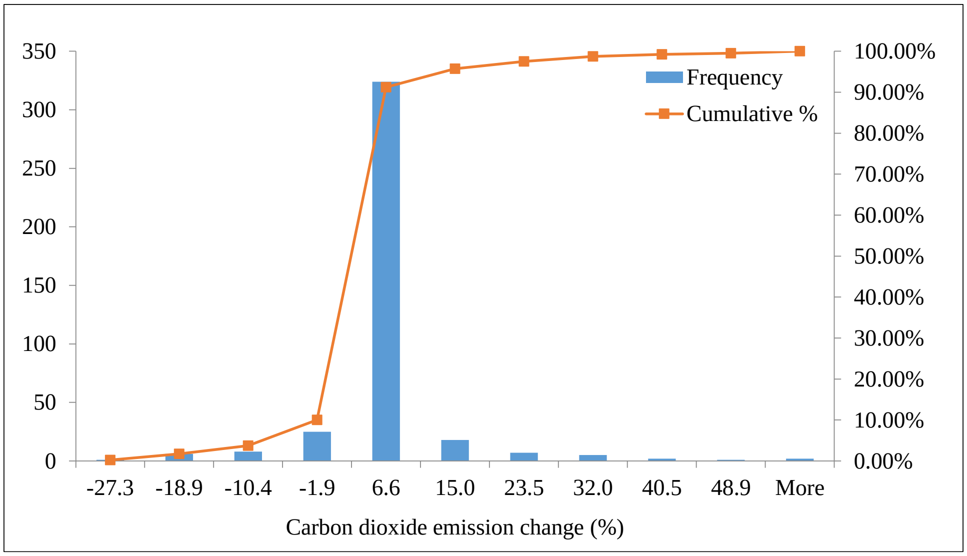

Figure 3-17 CO_2 mass emission change for 400 OD-pair test

When looking at the direction of the 400 OD trips illustrated in Figure 3-12, locations of origin/destination nodes, and proximity to facilities/residential areas/freeways all play important roles in determining changes of driving time and *IM*. For example, When an OD pair is close to freeway, the LER tends to avoid high-exposure freeway links and choose a portion of local roads with less facilities and residential homes, also usually a reduced speed limit than that of freeways. Hence OD pairs close to freeway are more likely to be associated with significant *IM* reduction, slight CO_2 emission reduction, and moderate driving time increase. In contrast, for OD pairs that are further from freeways, the LER's routing time could go to both directions - either very small or large increase compared with LDR. And the *IM* reduction depends on the relative locations between facilities and alternative trips. This also indicates that LER is highly sensitive towards population distribution. Generally, in a diverse roadway network such as in the case study, there are always alternative routes for heavy-emitting vehicles to travel so that their pollutants impact to the local population could be mitigated.

3.4 Conclusions and Discussions

In this chapter, we introduced a novel vehicle routing methodology that builds upon typical eco-routing which attempts to minimize overall population *inhaled mass* for driving trips. In the new routing method, we consider spatial and temporal exposure of pollutants to humans in the routing events. This methodology is accomplished using a unique modeling suite that relates traffic activity, to emissions production, to dispersion modeling, and finally to a human exposure factor - *inhaled mass*. Using local population activity and dispersion parameters, it is possible to then choose routes that least endanger the pollutant sensitive public. To date, this is the first research that targets at vehicle navigation to reduce human exposure to the mobile-source emissions.

A series of experiments were carried out in a street network in Southern California. Susceptible population are defined accordingly with resident homes and diverse facilities (Table 3-2). The calculation of pollutants' dispersion range agrees with that of previous studies. Further, it is found that the least-exposure routing is highly dynamic and sensitive towards input variables, such as vehicle age, dispersion condition, and population activities, *etc*.

It was seen that within a local scale, total exposure (susceptible population's *inhaled mass*) can be greatly reduced (more than 50%) with small adjustments to routing compared to a least duration route. Driving duration can increase, but they can be controlled within a small amount (typically less than 10%). In addition total CO_2 emission of a LER trip can be reduced because LER may choose a street with moderate driving speed limit. Low exposure routing coupled with clean vehicle technology results in larger exposure reduction.

In general, future work will include real-time traffic data collection, refinement to emission modeling modules, and dynamic routing implementation. Specific improvements are as follows:

(1) In the case studies, population activities are estimated statically. Also, traffic speed and weather parameters are retrieved from historical database. With the advent of Big Data, it is possible to realize real-time collection of these input datasets.

(2) The accuracy of address locator which converts U.S. address to coordinates needs to be improved. So the relative locations can be characterized more accurately.

(3) Roadway speed limit is used as default driving speed in this study for experiment vehicles. In the future, microscopic traffic simulation and probe vehicles can be applied to represent the acceleration, deceleration, cruising and idling process of vehicles on road. Coupled with detail road grade data and inputs from previous point, it allows for accurate emission estimation and exposure assessment from mobile source.

(4) Apply more efficient algorithms for routing. Integrate Eco-Driving into low exposure navigation and achieve both emission mass and emission exposure mitigation. Also experiment with more scenarios and street networks. These improvements will make the low-exposure navigation methods more practical and beneficial.

3.5 Acknowledgements

This work is sponsored by the UC MRPI Program in Sustainable Transportation. The authors would like to thank Alexander Vu, for his excellent technical support. The authors also appreciate GIS Academy of UCR Extension for providing the map sets for research.

4 Pedestrian Navigation to Mitigate Pollutant Exposure

4.1 Introduction

Active transportation modes, such as walking, is a fundamental form of sustainable transportation. Walking is advocated as a way to reduce automobile dependency [*90*], foster community livability [*91*], and boost local economy [*92*]. From a health perspective, walking is one of the simplest exercises that help keep fitness and prevent diseases [*93*, *94*].

However, with ever increasing urbanization and vehicular traffic, pedestrians often find themselves walking by streets with heavy traffic and exposed to various traffic emissions, such as hydrocarbon, carbon monoxide, and fine particles. Exposure to the mixture of airborne pollutants, unfortunately, has been proven to contribute to a wide range of health problems [*5*-*7*]. Roadside measurements reveal that concentration of traffic emission is elevated near roadways [*8*, *9*, *20*]. Among the various road users such as pedestrians, cyclists, drivers, and transit riders, pedestrians and cyclists face risks of higher exposure to particle and gaseous emissions, due to their proximity to the emission sources and increased breathing rate during walking and bicycling [*34*, *95*]. Recent research even suggests that the benefits of walking could be offset by exposure to these traffic emissions [*96*].

4.1.1 Research Motivation

Extensive studies have investigated the relationship between traffic air pollution, walking, and health effects. Only a few have sought exposure mitigation methods that pedestrians can practically use to protect themselves from excessive traffic emission exposure. Kaur *et al*. suggested that individuals should be encouraged to use less-busy street routes to reduce their exposure to vehicular emission [*97*]. However, the publicly available information about air quality (e.g., the Air Quality Index on http://www.airnow.gov/) does not have adequate resolution to support pedestrian route choice.

In recent years, route planning and navigation tools that find travel routes between an origin and a destination are widely available. These tools are available in several platforms (e.g., web-based tool, smartphone app, *etc*.) and for many travel modes including auto, transit, and walking. As an example, Figure 4-1 illustrates the web-based Google Map navigation tool for determining walking routes (https://www.google.com/maps). The suggested route options are usually the shortest in terms of walking distance or walking time. In Figure 4-1, the tool suggests three different walking route options for a trip from home to school in Riverside, California, that have the same walking distance and walking time. However, these routes may not have the same level of exposure to traffic-relation air pollution for the pedestrian. Based on the authors' knowledge of the area, Magnolia Ave is a major arterial with heavy traffic. Thus, the pedestrian would likely inhaled a higher level of air pollution if taking the blue dotted route. Also, parallel to Magnolia Ave to the south is California State Route 91 (SR-91) that carries high volumes of traffic and is often congested. When the wind blows in the northwest direction, the blue dotted route would likely experience higher air pollutant concentration levels due to its closer proximity to this major emission source. Therefore, for this particular trip the pedestrian may be better off taking one of the two grey solid routes.

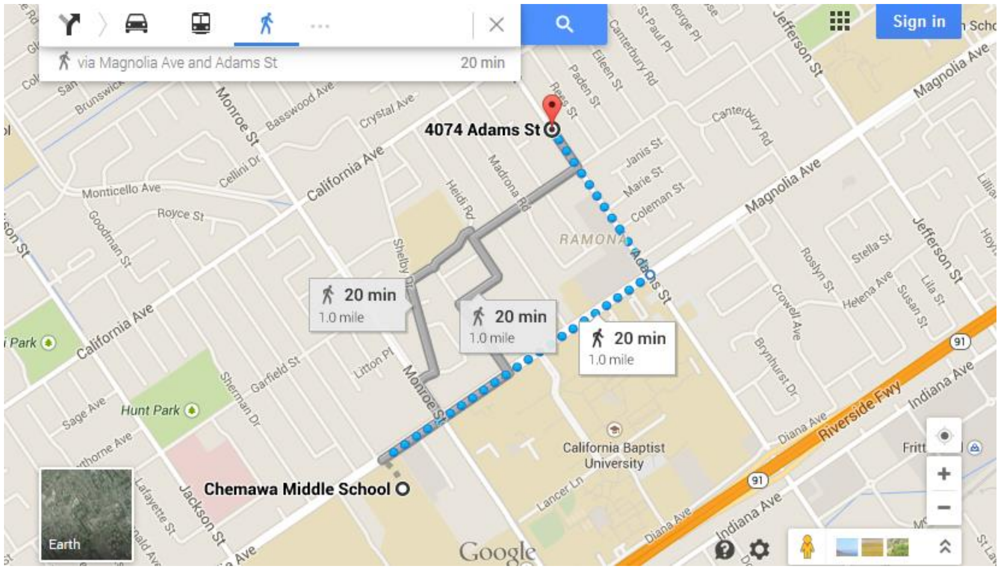

Note: Credit to https://www.google.com/maps

Figure 4-1 Three walking route options for a home-to-school trip in Riverside, California

4.1.2 Objectives and Scope

The main objective of this study is to determine whether and how much route choice decision, such as the one discussed earlier, can help reduce pedestrian's exposure to traffic-related air pollution. In relation to that, another objective of this study is to evaluate the travel time impact of taking a lower exposure route as opposed to the traditional shortest duration routes.

To meet these objectives, we opt for a modeling approach (instead of a measurement approach) so that the method could be widely applied for a large area. As case study area, we choose the Ramona neighborhood and the adjacent Arlington neighborhood in Riverside, California, because at the time of the study, they were engaged in a walkability improvement project by a multi-organization partnership in the city [*98*]. The project involves many facets of improvement, including education outreaches in communities and improvements of pedestrian-friendly infrastructure. In advocating walkability and healthy air awareness to the local residents, our study explores tools that reduce the local pedestrians' exposure to traffic emissions. In this study, we focus on $PM_{2.5}$ because even short-term exposure to this pollutant can trigger a variety of adverse health conditions [*1-4*]. Also, the neighborhoods are in a $PM_{2.5}$ nonattainment area.

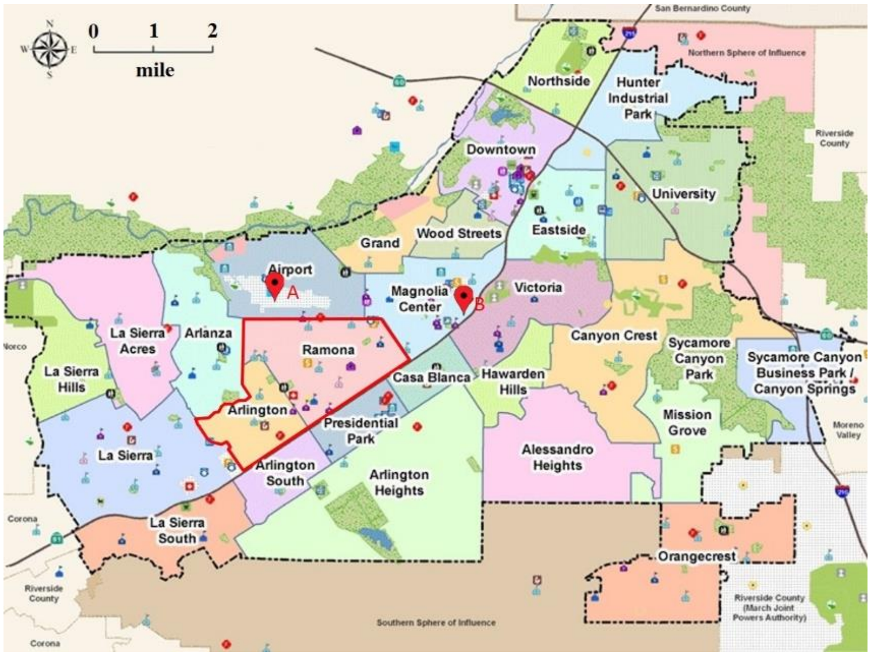

Note: Pin A marks Riverside Municipal Airport Site that provides meteorology data mentioned in Section 4.2. Pin B marks the Riverside-Magnolia Air Quality Monitoring Site mentioned in Section 4.3. Picture courtesy of UCR Today

Figure 4-2 Arlington and Ramona neighborhoods in the city of Riverside

The three major calculation components are previously introduced in Section 3.2. To briefly reiterate, they are: (1) pollutant concentration modeling, (2) exposure assessment, (3) incorporate exposure assessment results into network characterization and implement routing. The method and selected models for first component is presented in Figure 4-3.

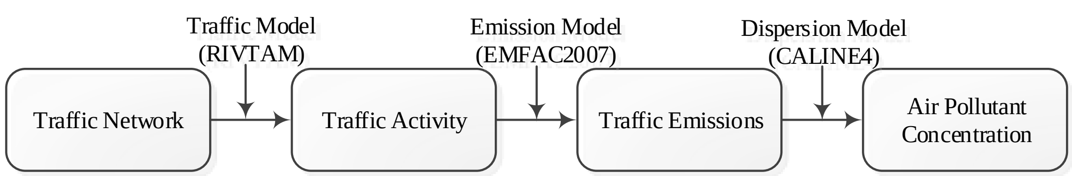

Figure 4-3 Flow chart of model selection for concentration modeling

This pedestrian study shares similar modeling framework with the low-exposure vehicle road navigation (Section 3.2). Meanwhile, there are several distinct differences. For example, in

Chapter Three, the exposure subjects are selected as school children, older adults, patients in hospital *etc*., and they are assumed to be static in selected locations during the modeling time window. In this study, however, the exposure subjects are pedestrians who are assumed to be walking on sidewalks. Another major difference is that, in Chapter Three, the routing subjects are vehicles; however in this chapter, the routing subjects become pedestrians. Some major differences between Chapter Three and Four are compared in Table 4-1. In the following sections, similar process will be briefly described and differences will be emphasized.

Table 4-1 Comparison between vehicle navigation (Chapter 3) and pedestrian navigation (Chapter 4)

Differences	Vehicle (Chapter 3)	Pedestrian (Chapter 4)	Comparison
Emission Source	Heavy-emitting vehicles on roadway network	All vehicles on roadway network	The concentration modeling shares the same method, but slight different in emission factor calculation
Exposure subjects	Clusters of school children, older adults, patients, residents etc., who are assumed to be static in selected locations during the modeling time window	Individual pedestrians who are assumed to be walking on sidewalks	They both apply *Inhale Mass* as exposure assessment. In Chapter 3 population counts vary significantly for facilities, but in Chapter 4 population is always one.
Navigation subjects	Heavy-emitting vehicles	Pedestrians	This results in different navigation network.
Navigation network	Roadway network	Sidewalk network	Roadway networks are well developed for commercial use. Sidewalk networks are not well characterized yet. A sidewalk system is defined and developed in Chapter 4.2.4

4.2.1 Traffic Activity and Emissions Modeling

First component of the study is to model mobile-source pollutant concentration at the street level in the neighborhoods, so that pedestrian exposure could be estimated. The modeling process and specific models are shown in Figure 4-3 and elaborated in Section 3.2.

There are 743 roadway links covering the study area. Traffic activity data (in terms of roadway map, flow and speed) on each link are obtained directly from the Riverside County Transportation Analysis Model (RIVTAM), which is the regional transportation model for Riverside County [*99*]. The data are available for four time periods: morning (6-9 AM), midday

(9 AM – 3 PM), afternoon (3-7 PM), and nighttime (7 p.m. – 6 a.m.). We only consider the morning and afternoon hours in this study, since traffic and walking activities are relatively higher during these periods of the day. We plan to expand our study to include other pollutants and time periods in future work. Traffic flow data include separate values for six vehicle types: (1) DA: passenger car driving alone, (2) SR2: passenger car shared ride with 2 persons, (3) SR3: passenger car shared ride with 3 or more persons, (4) LHDT: light-heavy duty trucks, (5) MHDT: medium-heavy duty trucks, (6) HHDT: heavy-heavy duty trucks. Figure 4-4 shows the total traffic flow, which is the summation of the flow values of all the six vehicle types. On the other hand, traffic speed data only has one value that represents the overall speed of all vehicle types.

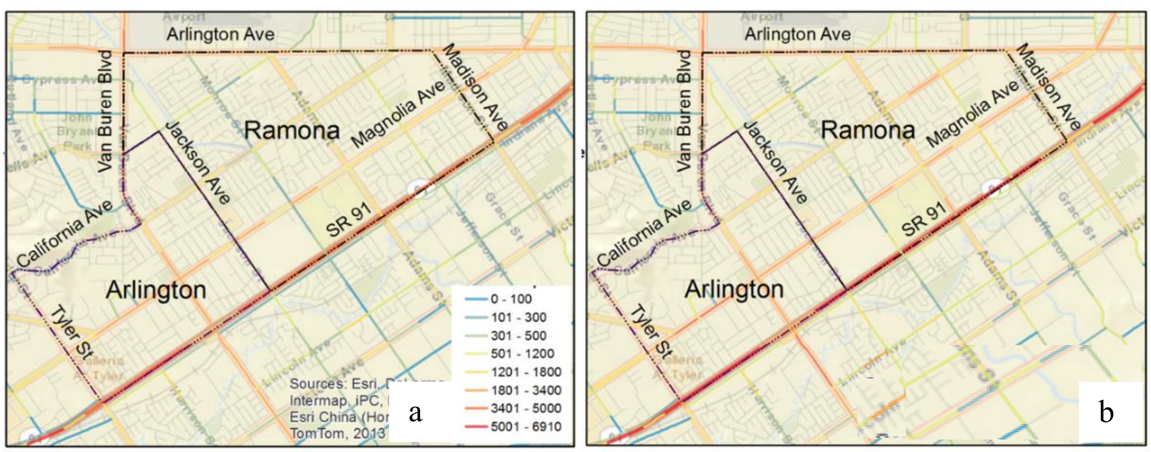

Figure 4-4 Total flow (vehicles per hour) for morning (a) and afternoon (b) periods.

With link-based traffic activity as inputs, EMFAC2011 is applied to estimate emission factors because its emission inventory database includes comprehensive vehicle activities in Riverside County [*62*]. $PM_{2.5}$ emission factors for average speed from 5 mph to 70 mph were obtained for multiple vehicle categories in EMFAC, which are then aggregated according to the vehicle type mapping given in Table 4-2. After that, the total $PM_{2.5}$ emission on each roadway link is aggregated into (*gram/meter/vehicle*) as in Equation (2-1).

Table 4-2 Vehicle Type Mapping

This Study	RIVTAM	EMFAC2011
LDV	DA, SR2, SR3	LDA, LDT1, LDT2, MDV
LHDT	LHDT	LHDT1, LHDT2
MHDT	MHDT	MHDT
HHDT	HHDT	HHDT

4.2.2 Mobile-Source Air Pollutant Concentration Modeling

CALINE4 (introduced in Section 2.2.2), developed by the California Department of Transportation, is used to model $PM_{2.5}$ concentration in the example neighborhoods. Meteorology inputs are obtained from the nearby weather station (Point A in Figure 4-2) [*100*]. On average, the weather data show that air temperature peaks and humidity reaches lowest point around 2pm (Figure 4-5). Figure 4-6 shows wind roses derived from the weather data for the entire year of 2012 (newer data were not available at the time of study). Wind speed increases significantly in the afternoon compared with that in the morning. This is a good representation of inland Southern California weather, where strong solar radiation during noon time drastically increases surface temperature, which induces more atmospheric turbulence. Another two important meteorology inputs, atmospheric stability and boundary layer mixing height, are set as empirical values as in Table 4-3 [*Chapter 5 of Reference 101*]. The spatial data (e.g. roadway maps, meteorology station, receptors) needed to be transferred to tabular data (e.g. roadway location, meteorology inputs) for dispersion input file preparation, and a schematic graph of this transition is illustrated in Figure 3-6 in Section 3.2.4.

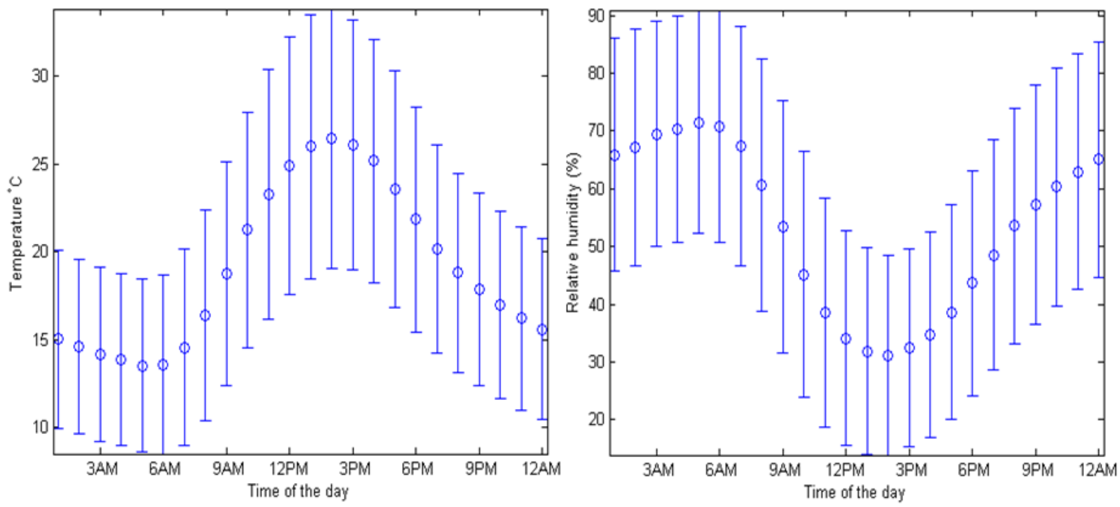

Note: Bars on data points represent standard deviation of the hour through the year

Figure 4-5 Temperature and humidity by hours of the day in experiment neighborhoods in year 2012

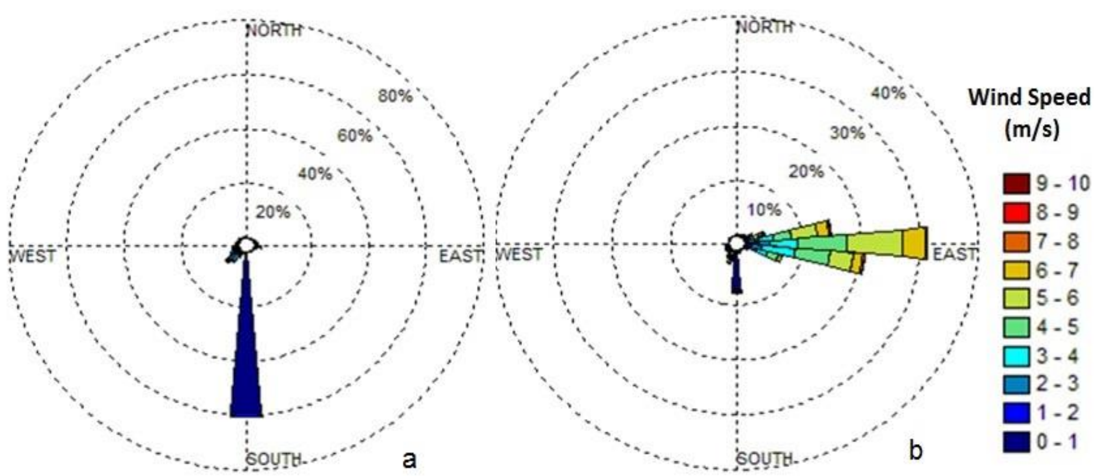

Figure 4-6 Wind rose graphs during the morning (a) and afternoon (b) periods

Table 4-3 Stability Class and Mixing Height for four time periods in dispersion modeling

	Stability Class	Mixing Height (meter)	Wind Speed Limit (m/s)
Morning	2	500	<5.5
Afternoon	3	2000	No limit

In order to obtain detailed $PM_{2.5}$ concentration estimates at the street level, receptors are set up as a 150m×150m gridded network at the height of 1.5 meter (Figure 4-7 4-7) using ArcMap geoprocessing tools [*102*]. This operation yields a total of 1,748 receptors covering the experiment neighborhoods. Since CALINE4 allows at most 20 roadway links and 20 receptors to be modeled at a time, several thousands of model runs are executed in batch mode using a MATLAB script [*103*]. For each receptor, the modeled $PM_{2.5}$ concentration values from all the model runs are summed together to result in the total $PM_{2.5}$ concentration estimate. Figure 4-7 shows the total $PM_{2.5}$ concentration estimates at the receptor grid in the modeling area during the morning period.

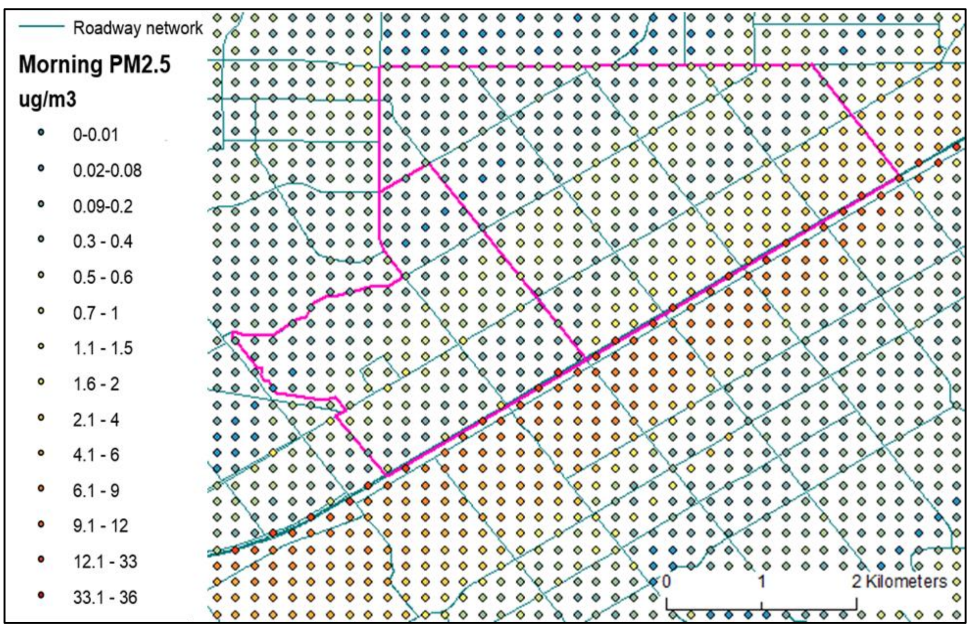

Figure 4-7 Estimated $PM_{2.5}$ concentration at receptors during the morning period.

The estimated $PM_{2.5}$ concentration values at the receptors were used to create concentration surface maps using the 'Spline' interpolation tool in ArcMap software [*104*]. Figure 4-8 reflects the contrast of $PM_{2.5}$ concentration between morning and afternoon scenarios. Although the traffic flows in both periods were similar, $PM_{2.5}$ disperses faster (resulting in lower concentration in the modeling area) in the afternoon due to higher ambient temperature and wind speed. In the morning, the dominant wind blows towards southwest and the high concentration plume from the SR-91 freeway extends 1.5 kilometer wide. In the afternoon, the stronger wind changes direction to southeast, and the plume only spread a few hundred meters from the freeway. In addition, during morning and afternoon peak hours, arterials such as Arlington and Magnolia Avenue contribute to considerable amount of $PM_{2.5}$ in the neighborhoods.

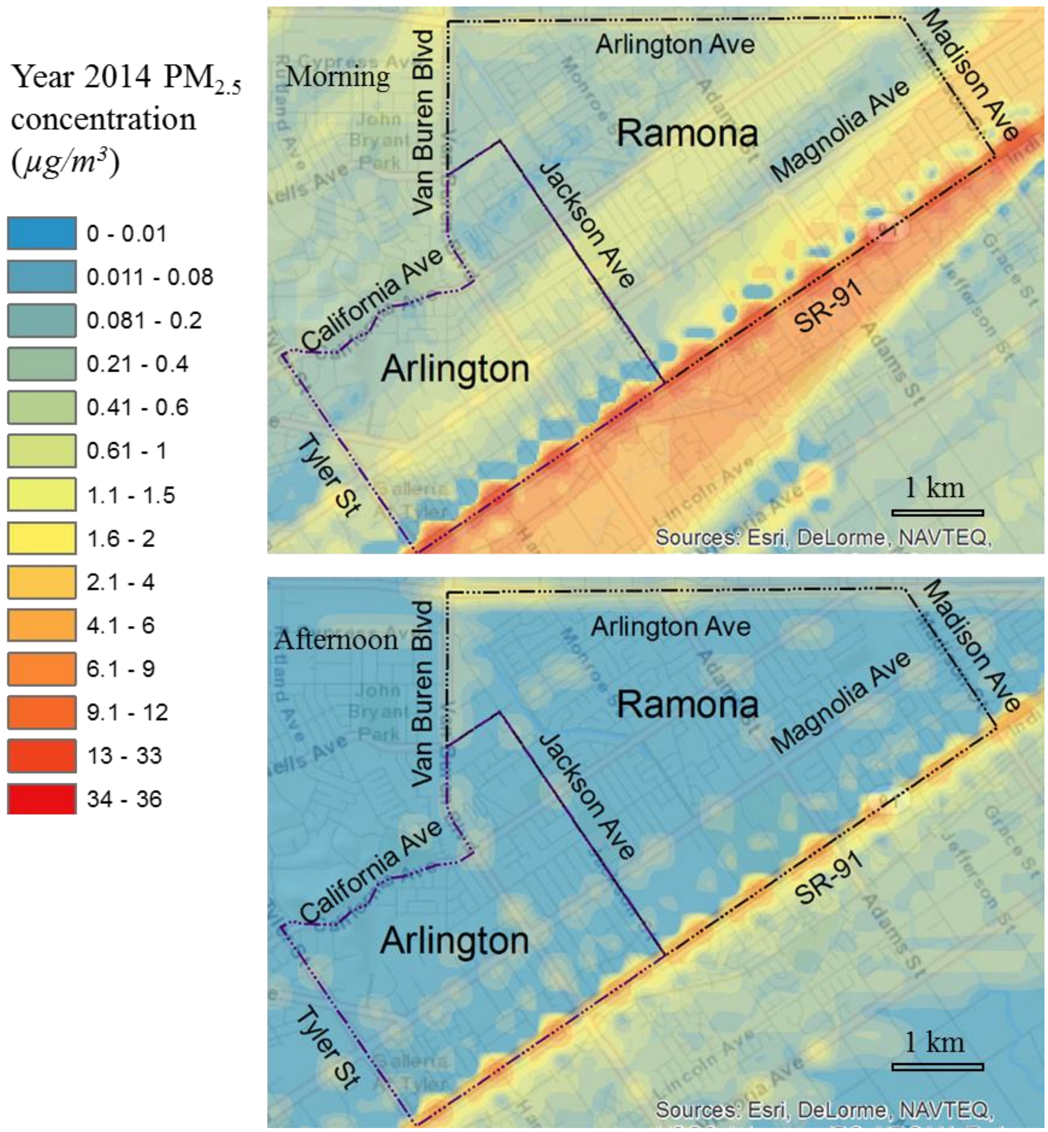

Figure 4-8 Estimated localized mobile-source $PM_{2.5}$ concentration surface maps for morning and afternoon

The contrast between morning and afternoon $PM_{2.5}$ concentration also agrees the air quality monitor station near the study area (marked in Figure 4-2), as plot in Figure 4-9. In previous measurement studies, higher pollutant levels and longer decay distance were observed under stable atmospheric condition (e.g. early morning and nighttime) than in the daytime [*9*, *20*, *21*].

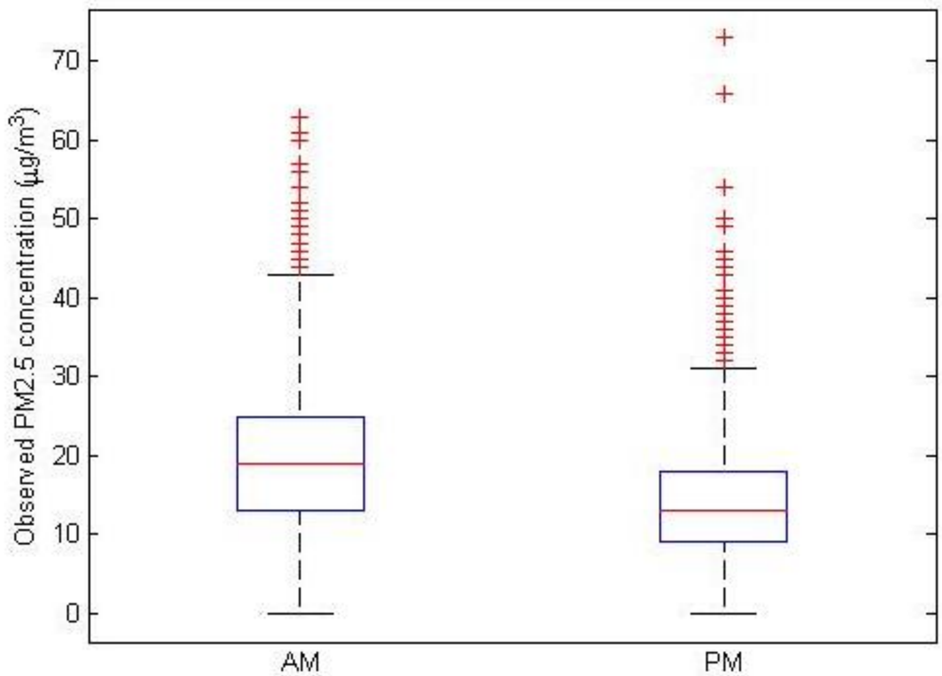

Note: the air quality station is marked as point B in Figure 4-2

Figure 4-9 $PM_{2.5}$ concentration observed in morning (6-9 AM) and afternoon (3-7 PM) by air quality monitor station in year 2014

The plume spread in Figure 4-8 may change when applying different dispersion models, however the concentration variation near major sources adhere to similar concentration decay patterns [*8*, *9*, *21*]. This study estimates annually averaged $PM_{2.5}$ concentration as reasonable illustrative inputs to develop a low-exposure pedestrian routing tool. Upon future implementation, this routing tool will require real-time online traffic/weather data collection and concentration prediction. At the same time complementary air quality measurement will be needed for validation purposes, and the most suitable dispersion model will be applied.

4.2.3 Digitization and Characterization of Sidewalk Network System

At the heart of any navigation application are digital roadway maps. To clarify, a roadway network refers to motor vehicle roadways which are considered as pollutant sources. In the case of pedestrian routing, a digital sidewalk map is critical for pedestrian safety, accurate routing planning, and travel time estimation. Unfortunately, for almost all pedestrian routing applications in the market, vehicle roadway maps are used for pedestrian routing due to an absence of digital sidewalk system. It stems several issues: (1) incorrect navigation direction (e.g. indicated in Figure 4-10a and 4-10b); (2) inaccurate positioning (3) potential safety hazards for pedestrians (e.g. Figure 4-10a indicates crossing roadway where pedestrian crossing is prohibited); (4) inaccurate travel time estimation (e.g. pedestrians need to detour to cross signalized intersections and wait for crossing signals, which are not considered in Figure 4-10a but can be assessed in Figure 4-10b). Therefore, a digital sidewalk system will greatly enhance pedestrian navigation's validity and pedestrian infrastructure planning.

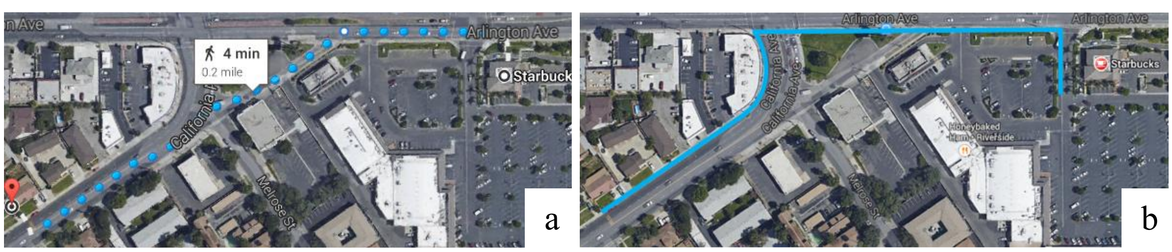

Figure 4-10 Contrast between roadway map (a) and sidewalk map (b) for pedestrian routing

Since walking is a fundamental form of transportation, numerous studies have explored the various aspects of walking, for example, 'Complete Streets'. To advocate and encourage active transportation, the concept of 'Complete Streets', which aims at planning infrastructures for active travelers (pedestrians, bicyclists, skateboarders, wheelchairs *etc*.), is surging in the United States. The plans envision designs and styles of active-traveler-friendly streets and practice [*105*].

Only a few studies attempt to digitize walk ways as a part of GIS training [*106*]. However, not a comprehensive sidewalk system has been mapped for research nor management purposes.

To resolve the issues, a digital sidewalk network system is created by the author for two neighborhoods in Riverside, California. Sidewalk sections are categorized into paved sidewalk, landscape/lawn, crosswalk, parking lot/driveway, and missing sidewalk. Example images of each category and explanations are provided in Figure 4-11.

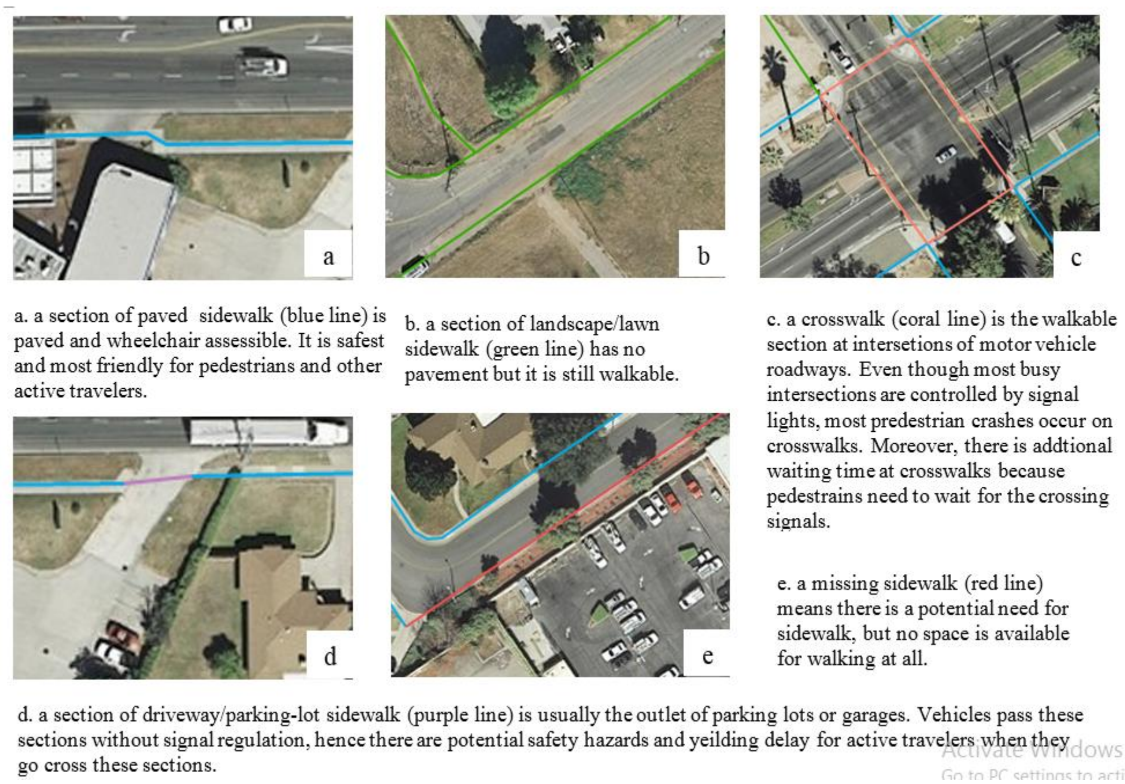

Figure 4-11 Digital sidewalk categories defined by the author

An overview the sidewalk system is mapped in Figure 4-12. In the 35-kilometer-square study area, there are more than 267 km of digitized sidewalk, among which 73% of the total length are paved sidewalks, indicating that the two neighborhoods are moderately pedestrian friendly.

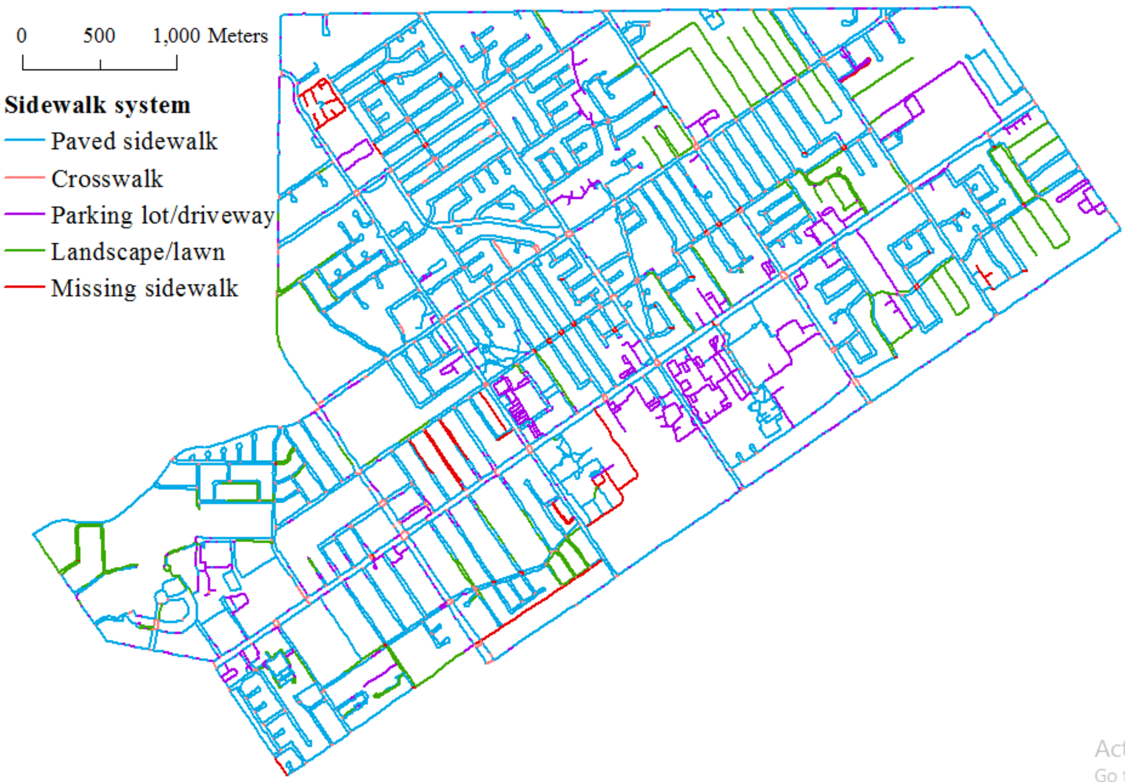

Figure 4-12 Overview of the sidewalk network in experiment neighborhoods

Table 4-4 summarizes the length and number of links for each sidewalk category in the neighborhoods. Also, based on the potential travel delay occurred when pedestrians wait at the intersection for safe cross (described in Figure 4-11), a few seconds of delay time are added to crosswalk, parking lot/driveway and missing sidewalk sections, as the last row in Table 4-4 indicates [*107*, *108*]. The sidewalk network will be applied in the following exposure estimation and pedestrian routing implementation.

Table 4-4 Summary of sidewalk categories and time delay

Sidewalk category	paved	landscape/lawn	crosswalk	parking lot/driveway	missing sidewalk
Number of links	5417	624	609	1073	211
Total length (km)	195.5	23.0	12.3	28.7	6.9
Average link length (m)	36.1	36.8	20.2	26.8	32.7
Travel delay add-on (sec)	0	0	8	2	5

In the case of pedestrian routing, walking distance or walking duration is often used as the only cost in route calculation. Typically, if walking speed is assumed to be a constant, the shortest distance and shortest duration routes for pedestrian are essentially the same. However, a digital sidewalk network enables the incorporation of pedestrian travel delay, now the duration to cross a sidewalk section becomes:

$$t_i = \frac{L_i}{v} + a \qquad (4\text{-}1)$$

where t_i is the walking duration (*second*), L_i is the length of a sidewalk link (*m*), v is the walking speed (1.2 *m/s* [*109*]), and a is the travel delay add-on. For example, if a crosswalk is 20 meters, and travel delay is 8 seconds, then the traverse time will be 20 (*m*) divided by 1.2 (*m/s*) then plus 8 (s), which is 25 seconds. In this study, the walking duration which also accounts for travel delay will be applied in pedestrian routing implementation.

4.2.4 Pedestrian Exposure Estimation

The availability of air pollutant concentration data or estimates allows for human exposure assessment with an exposure model. Studies of human exposure to traffic-related air pollution is discussed in Section 2.3. Customized from Equation 2-5, *inhaled mass* of $PM_{2.5}$ for an individual pedestrian can be expressed as in Equation 4-2, assuming that the breathing rate of the pedestrian remains the same throughout the roadway link.

$$IM_{i,j} = c_i \cdot t_i \cdot BR_j \qquad (4\text{-}2)$$

where $IM_{i,j}$ is *inhaled mass* of $PM_{2.5}$ (μg); c_i is $PM_{2.5}$ concentration ($\mu g/m^3$, average $PM_{2.5}$ values of the starting, mid, and ending points of a sidewalk link) for link i ; t_i is walking duration (minutes, calculated with Equation 4-1); BR_j is the breathing rate of the pedestrian j ($m^3/minute$). The breathing rate of an average pedestrian is assumed to be 0.02 m^3/minute based on health studies [*82*]. *IM* values will be incorporated into network cost for routing implementation.

4.2.5 Pedestrian Routing Implementation

The pedestrian routing is implemented with the graph described in Section 4.2.3. The sidewalk graph has 7934 links and 7143 nodes. As discussed in Section 3.2.6, link traverse time t_i and link-based $PM_{2.5}$ *inhaled mass* IM_i are normalized and integrated as a combined cost $cost_i$ for link i:

$$cost_i = w \cdot IM_i + (1 - w) \cdot t_i \quad (4\text{-}3)$$

When weight factor w is 0, it is a shortest duration route. As w increases to 1, it turns into a least exposure route. Given an OD pair, Dijkstra's algorithm is applied to calculate a route R_1, which has the least summation of Equation (4-4) comparing with all routes that connect (O, D).

$$\sum_{i \in R_1} cost_i \quad (4\text{-}4)$$

We plug Equation (4-2) and (4-3) into (4-4) and it yields:

$$\sum_{i \in R_1} [w \cdot (c_i \cdot t_i \cdot BR_j) + (1 - w) \cdot t_i]$$

Take w and BR_j as constants it gives:

$$w \cdot BR_j \cdot \sum_{i \in R_1} c_i \cdot t_i + (1 - w) \cdot \sum_{i \in R_1} t_i \quad (4\text{-}5)$$

These formulations do not consider background pollutant concentration. c_i is the concentration contributed from line source i. To explore the impacts of background concentration to the routing results. We change c_i in Equation (4-5) into (c_i+ c_b), where c_b is the background pollutant concentration, which is considered as a constant during the routing events. Equation (4-5) becomes:

$$w \cdot BR_j \cdot \sum_{i \in R_1} c_i \cdot t_i + \left(1 - w + w \cdot BR_j \cdot c_b\right) \cdot \sum_{i \in R_1} t_i \quad (4\text{-}6)$$

Equation (4-6) shows that the incorporation of background concentration actually increases the weight of routing duration. For example, if we take BR_j as 0.02 m^3/min and c_b as 30 $\mu g/m^3$, the weight for routing duration increases from (1-w) to (1-w+$0.6w$). It can be anticipated that if c_b

value keeps rising over c_i while w is a constant, due to the continuously increasing weight of routing duration, the time constraint will become more and more stringent, and it will become less likely that an alternative low-exposure route could be found. However, as extensive roadside measurement studies reveal that in the daytime, mobile-source pollutants from heavily travelled corridor would not dissipate to background concentration until several hundred meters away, we think there are still considerable potential exposure benefits of this low-exposure routing tool for pedestrians who walk right next to major roadways. In the following sections, background concentration are not considered. In the future work, reliable estimate values of background concentration may be incorporated in this study.

To evaluate pedestrian route choices, a number of origin and destination points in the study area are used to simulate home-to-amenity trips. Specifically, 242 residential blocks are selected from U.S. Census 2010, and 139 addresses of a variety of amenities randomly obtained from Google Map are used as destination points (Figure 4-13).

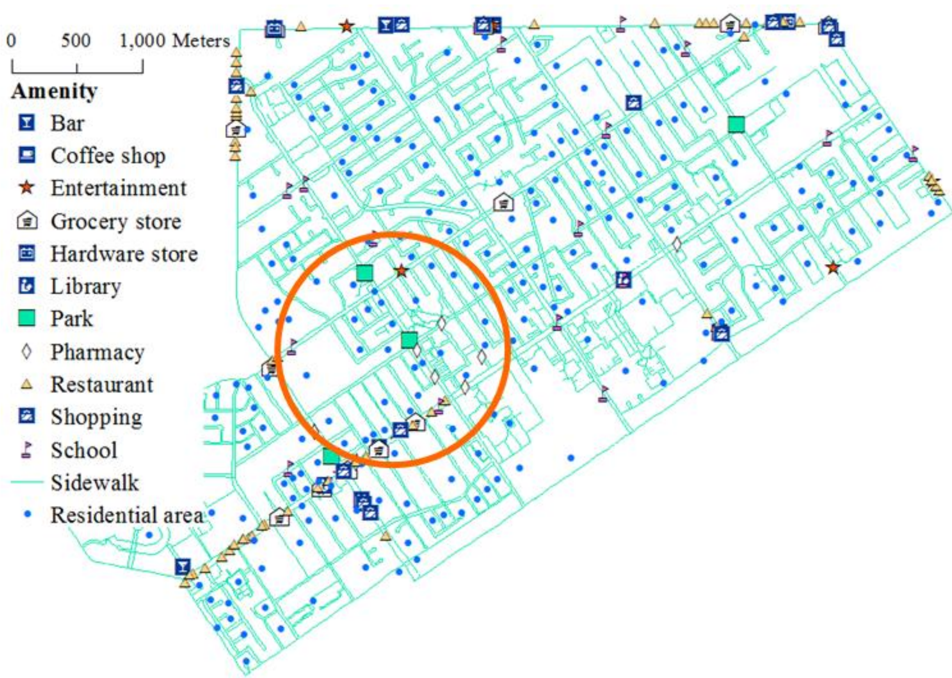

Figure 4-13 Location of homes and amenities used in route choice evaluation

Amenities within 1 mile of each home are searched and paired as potential walking trips, resulting in more than 10,000 home-to-amenity trips. Because desired walking trips are typically within one mile or 30 minutes [*110*], then trips with estimated walking duration greater than 30 minutes are excluded as they are very unlikely to be made by foot. For the remaining 7,223 trips, both the shortest duration route (w = 0) and the low exposure route (w = 0.5) are determined. For both routes, the total *inhaled mass* of $PM_{2.5}$ and the total walking duration for the entire trip are calculated. A trip was designated as an "improved trip" if the low exposure route would result in a reduction in pedestrian exposure to $PM_{2.5}$ as compared to the shortest duration trip. As for the time constraint, an 'improved trip' should take no more than 33 minutes.

In this section, many specific models and datasets are given as examples for clear description. However, this methodology is generally applicable to other areas if required inputs are available. Additionally, it also applies for other en-route active travelers, such as bicyclists. Following the methodology and cases studies, there are several interesting future projects to explore.

Experiment Results

Table 4-5 provides statistics of the improved trips for both morning and afternoon analysis periods. Out from 7223 walking trips, a low exposure route could be found for 5.1% of the walking trips in the morning, and 9.6% of the trips in the afternoon. The trade-off between walking time increase and $PM_{2.5}$ *inhaled mass* reduction are summarized in Table 4-5.

Table 4-5 Statistics of improved trips

Analysis Period	Trips under 30 minutes	Improved Trips		$PM_{2.5}$ Exposure Reduction (%)			Walking Duration Increase (%)		
		Trips	%	Max	Median	Mean	Max	Median	Mean
Morning	7223	367	5.1	84.4	5.2	13.8	16.8	0.04	0.5
Afternoon	7223	697	9.6	98.2	17.7	32.0	45.0	0.1	1.1

On average, in the morning, the low exposure routes would reduce the pedestrian exposure to $PM_{2.5}$ by 13.8% while increasing the walking duration by merely 0.5%. During the afternoon period, the low exposure routes would reduce the pedestrian exposure to $PM_{2.5}$ by an average of 32.0% while increasing the walking duration by 1.1% on average. The median values, however, are significantly lower than that of mean values, indicating there are trips with skewed IM reduction and walking time increase.

Figure 4-14 plots pedestrian exposure reduction versus the walking duration increase for both analysis periods. Data points that are reaching the top of y-axis represent trips with small walking time increase and large exposure reduction, which are desirable low exposure routes for pedestrians. Scatter points whose x-axis values go beyond 10, are those trips with excessive routing time compared with their least duration route counterparts. The further the points reach to the right side of x-axis, the more extra walking time would be needed, hence the less practical the routes are, no matter how high is the $PM_{2.5}$ exposure reduction. The points on the right side of the plot area are also those outliners which make the overall exposure reduction and walking time increase values skewed, as shown in Table 4-5.

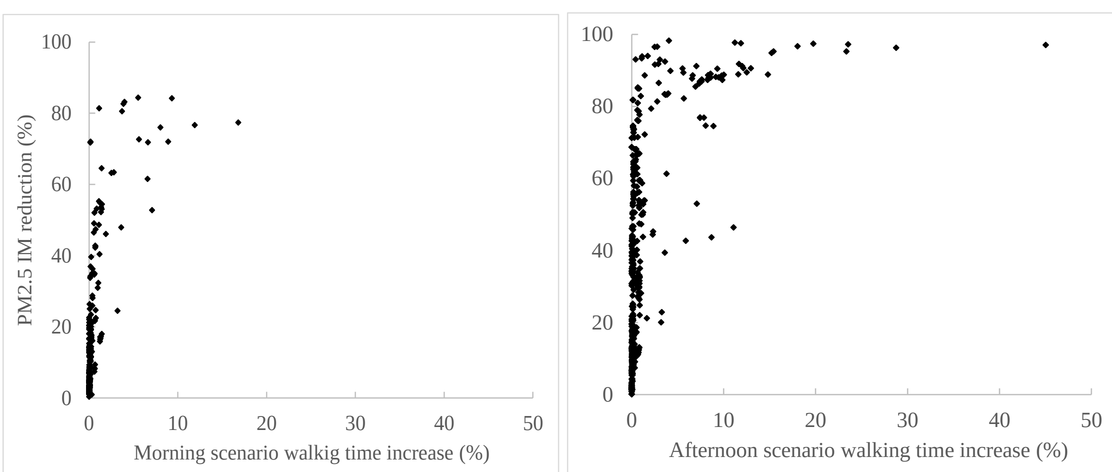

Figure 4-14 Reduction in $PM_{2.5}$ exposure versus increase in walking duration for improved trips.

Figure 4-15 illustrates one example of an improved trip, which is a trip between home and school. The shortest duration route is shown in pink while the low exposure route is shown in green. The shortest duration route remains the same for both morning and afternoon periods while the low exposure route in the morning is different from the one in the afternoon. When overlaid on the $PM_{2.5}$ concentration maps, it can be seen that the low exposure route deviates away from roadway links with relatively higher $PM_{2.5}$ concentration. In the morning, the low exposure route would reduce exposure to $PM_{2.5}$ by 72% with a 1% increase in walking duration as compared to the shortest duration route. In the afternoon, the low exposure route would result in 92% reduction in exposure to $PM_{2.5}$ with a mere 0.3% increase in walking duration.

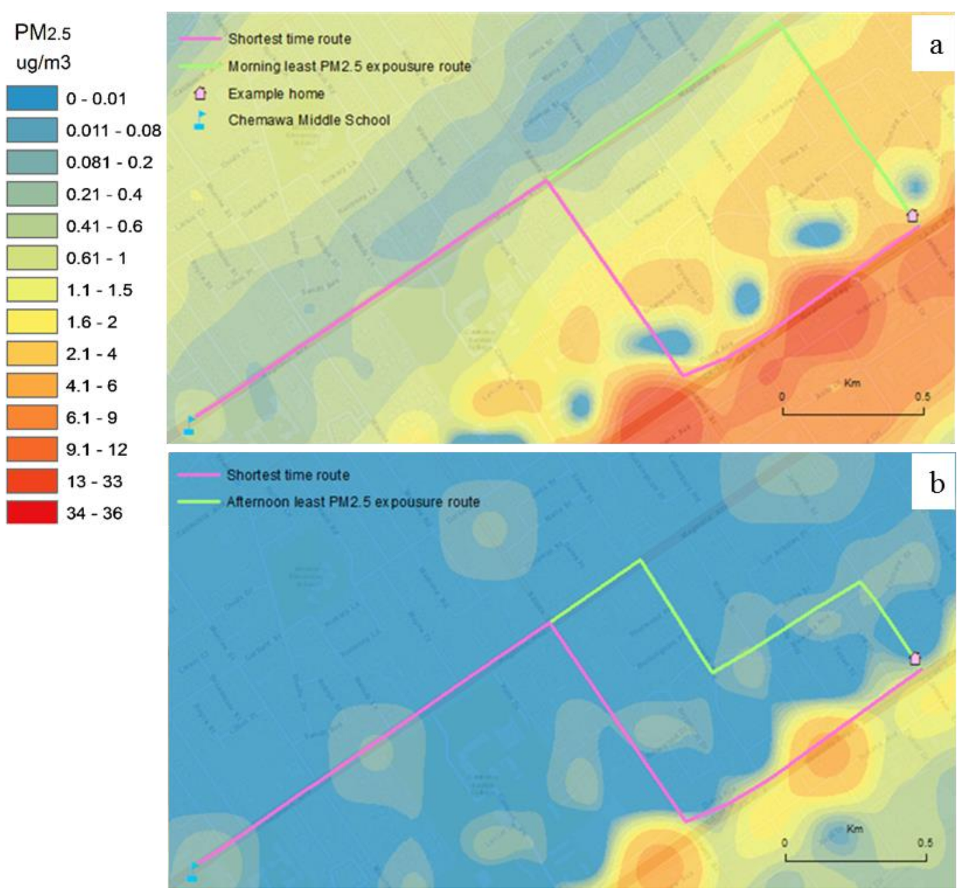

Note: the $PM_{2.5}$ refers to localized mobile-source $PM_{2.5}$
Figure 4-15 Example of improved trips in morning (a) and afternoon (b)

For this particular trip, the very small increase in walking duration coupled with the large reduction in exposure to $PM_{2.5}$ makes the low exposure route appealing and practical. Parents who escort their children to school in the morning can reduce the exposure to localized vehicular $PM_{2.5}$ by 72%, both for themselves and their children, solely by their route choice decision. In the afternoon, on the way to pick up their children, they can also reduce the exposure by 92%. Given the information about $PM_{2.5}$ concentration in the neighborhood, they can also make similar route choice decisions for their other walking trips (e.g., school to home, home to grocery, *etc*.).

4.2 Conclusions and Discussions

Pedestrians face risks of higher exposure to traffic-related air pollution due to their close proximity to the emission sources and increased breathing rate during walking. A number of studies have investigated the relationship between walking and exposure to traffic-related air pollution, but very few have sought mitigation measures that pedestrians can actively use to protect themselves from excessive exposure.

This study examines route choice decision as one such measure and evaluate its potential through modeling. Specifically, a method for incorporating pedestrian exposure to $PM_{2.5}$ into walking route calculation was developed, and the calculated low exposure route was compared against the traditional shortest duration route. For this example case study of neighborhoods in Riverside, California, it was found that among the samples of 7223 walking trip under 30 minutes:

(1) A low exposure route could be found for 5.1% of the walking trips in the morning, and 9.6% of the trips in the afternoon.

(2) On average, the low exposure routes would reduce the pedestrian exposure to $PM_{2.5}$ during the morning period by 24% while increasing the walking duration by only 1%.

(3) During the afternoon period, the low exposure routes would reduce the pedestrian exposure to $PM_{2.5}$ by an average of 32.0% while increasing the walking duration by 1.1% on average.

These results indicate that if the pedestrians can accommodate a moderate increase in walking duration in some of their walking trips, they can substantially reduce their exposure to $PM_{2.5}$ on those trips. This may be particularly important for sensitive population such as children, seniors, and people with respiratory health conditions.

This study has established a framework for modeling low pollution route choice for pedestrian. There are several aspects of the study that can be improved and expanded in the future:

(1) Include emissions from major non-traffic sources (e.g., stationary) in study areas.

(2) Use walking speed and breathing rate values specific to demographic groups (e.g., school-age children), and accounting for possible changes in these values over long walking trips.

(3) Studying potential benefits of low exposure route choices for other pollutants (e.g., NO_2), settings (e.g., central business district), and time periods (e.g., midday).

4.3 Acknowledgement

This study was partially supported by the California Department of Transportation. The authors acknowledge the County of Riverside for providing access to the Riverside County Transportation Analysis Model. The authors also thank Alexander Vu or his assistance and contribution.

5 Application of Pollutant Exposure Assessment in Environmental Inequality Studies

5.1 Introduction

Urban area is usually home to dense population of diverse socioeconomic background (race, income level, education, *etc*.). At the same time, urbanization is often accompanied by high-demand energy consumption, such as in transportation and heating industry. The intense energy consumption are sustained by combustion of large quantities of fossil fuel, which releases harmful pollutants into the environment and causes environmental hazards for humans.

However, it was concerned that people with different socioeconomic status (SES) face different levels of environmental hazards in the same urban area. For example, researchers found that in the United States, low-income or non-white communities tend to be exposed to a higher magnitude of environmental hazards [*111*, *112*, *113*].

As transportation emission forms a major sector in anthropogenic emission inventory, this chapter proposes a mobile-source pollutant exposure assessment framework in large-scale and high-resolution, and applies it to Southern California Association of Governments region. What's more, relationships between residents' SES (e.g. race, income level) and exposure are analyzed.

5.1.1 Research Background

Many efforts have been made in quantifying regional emission sources, estimating pollutant concentration, assessing pollutant exposure, and exploring socioeconomic implications.

Marshall *et al*. computed the inhalation intake (same definition as *inhaled mass*) of five outdoor-originated pollutants for a survey sample of more than 25,000 people living in South Coast Air Basin (SoCAB) in California. The inhalation estimation included commute, outdoor and indoor exposure whose concentration were calculated from sources specified in a 1000 meter grid. For the four primary pollutants studied, estimated median intake rates were higher for non-whites and for individuals in low-income households than for the population as a whole. For ozone, a secondary pollutant, the reverse is true [*112*]. Then, environmental inequality is quantified using linear regression, based on previous inhalation intake. It was found that holding constant attributes such as population density and daily travel distance, mean exposure differences between whites and nonwhites are 16–40% among the five pollutants [*113*].

Su *et al.* proposed a method for creating an index summarizing racial-ethnic and socioeconomic inequalities from the impact of cumulative environmental hazards. Second, they applied the Cumulative Environmental Hazard Inequality Index (CEHII) in a case study for Los Angeles County to illustrate the potential applications and complexities of its implementation. They found that non-white residents were mainly located in the downtown area and along the major traffic corridors. The extremely low-income population displayed a similar pattern but less clustered. A multiplicative model that estimated cumulative hazards demonstrated highest level of inequality among racial-ethnic and socioeconomic groups [*114*].

This study proposes a mobile-source pollutant exposure assessment framework in large-scale and high-resolution, and applies it to Southern California Association of Governments (SCAG) region. SCAG region consists of 6 counties in Southern California - Imperial, Los Angeles, Orange, Riverside, San Bernardino, and Ventura. In year 2000, SCAG region was home to more than 16 million people, which also accounted for half of the total population of California. Figure 5-1 maps the population and major race distribution in SCAG in year 2000. In addition, SCAG had the most dense roadway network, largest private vehicle fleet, and heaviest on-road traffic in the United States. The unique transportation status and diverse-background population in the

SCAG region have presented this intriguing research topic -- the relationships between the residents' exposure and their SES, such as income level, ethnicity, education level, *etc*.

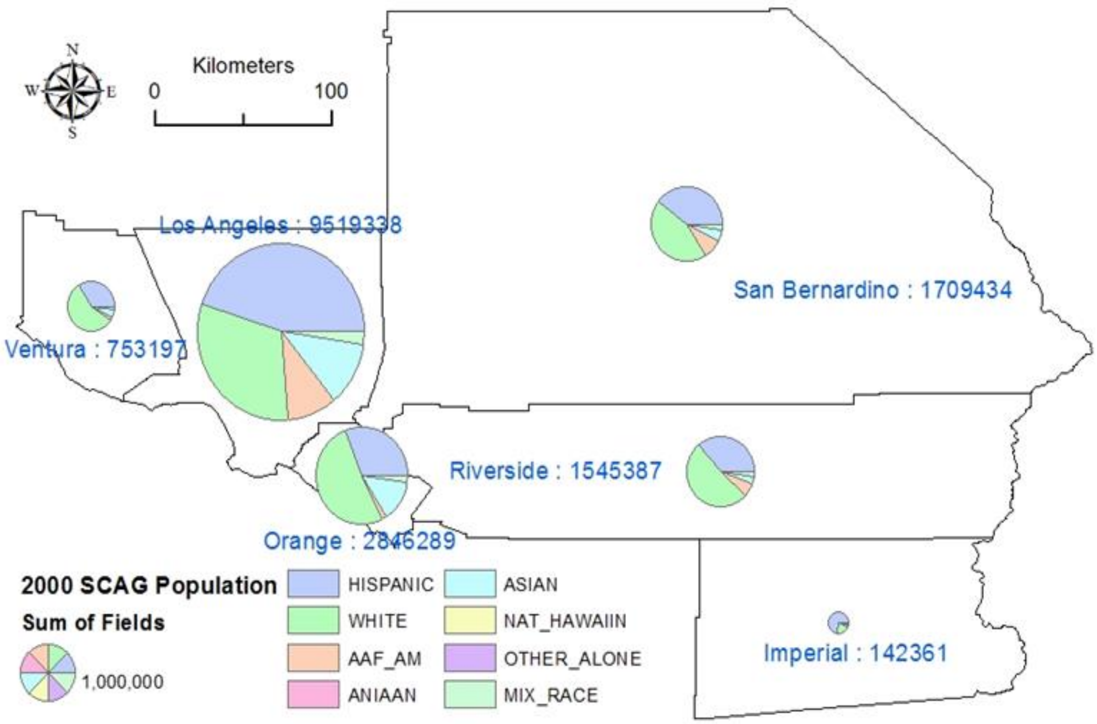

Note: The data source is Census 2000. 'HISPANIC' refers to Hispanic or Latino, which is a racially diverse group. 'AF_AM' refers to African American. 'ANIANA' refers to American Indian or Alaska Native. 'NAT_HWN' refers to Native Hawaiian or Other Pacific Islander. 'OTHER_ALONE' refers to other one race population. 'MIX_RACE' refers to mixed race population.

Figure 5-1 Map of SCAG and population distribution in year 2000

5.1.2 Objectives and Scope

There are three objectives of this study. First, we propose a mobile-source pollutant exposure assessment framework in large-scale and high-resolution. Second, we apply the framework to SCAG region. Third, we use high-resolution residents' SES data provided by U.S. census survey and calculated exposure values to analyze the relationships between residents' socioeconomic parameters (mainly race and family income) and exposure levels.

The pollutant surrogate is chosen as primary out-of-tail-pipe $PM_{2.5}$, which is a pollutant largely contributed by on-road traffic in SCAG region. Health researchers worldwide have suggested that human exposure to vehicular $PM_{2.5}$ causes or triggers an array of health problems. As explained in Section 1.1 Problem Statement, unless otherwise mentioned, $PM_{2.5}$ refers to the localized primary out-of-tail-pipe $PM_{2.5}$ for the rest of this chapter.

This chapter describes the use of the transportation model output for year 2003 to estimate near-road residential exposure of primary mobile-source $PM_{2.5}$ for the entire region in year 2003. The exposure assessment time windows only include morning and nighttime in residential units, assuming residents registered with Census 2000 are at home during morning and nighttime and the daytime activities are not considered. It also explores the statistical implications between the residents' exposure to $PM_{2.5}$ and their SES, as well as screens high-$PM_{2.5}$-exposure census units.

5.2 Methodology and Analysis

There are three major calculation components to achieve the objectives. First two are: (1) pollutant concentration modeling, and (2) exposure assessment. This is the framework of exposure assessment which is applied in previous two studies (please refer to Section 3.2 and Section 4.2). The other parallel component is (3) census data processing, because census data contain two critical datasets - receptor locations (census block centroid) for dispersion modeling and SES data for statistical analysis. The flowchart of the methodology and models in this study are presented in Figure 5-2.

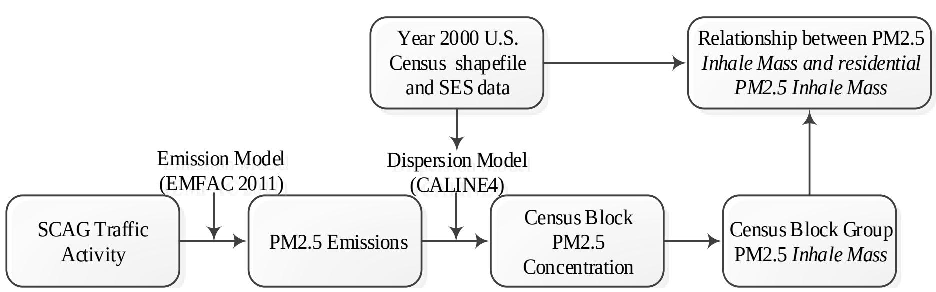

Figure 5-2 Framework of traffic emission concentration modeling applied in this study

The main focuses of this study are $PM_{2.5}$ concentration modeling, exposure assessment, and SES analysis. To clearly illustrate the calculation and data transform processes, specific data sources and implementation for SCAG region are described in the methodology chapter. However, this methodology also applies to other metropolitan areas, and similar high-resolution outputs can also be achieved given required input datasets with appropriate resolution, such as roadway digital map and weather parameters.

Section 5.2.1 briefly summarizes the traffic activity and emission modeling. Section 5.2.2 gives an overview of the U.S. Census GIS files and associated socioeconomic data used in subsequent sections. Section 5.2.3 describes the large-scale implementation of state-of-the-practice CALINE4 dispersion model. Section 5.2.4 assesses residents' exposure to $PM_{2.5}$ in SCAG region. Section 5.3 shows the exposure results and explores the underlying socioeconomic implications.

5.2.1 Traffic Activity and Emissions Modeling

Traffic activities of the roadway network, in terms of traffic flow and speed, are obtained from SCAG Regional Transportation Model (SCAG-RTM). SCAG-RTM simulates traffic volumes and transit usage during a transportation planning cycle for Southern California region.

The digital roadway network provided by SCAG-RTM contains 49,146 links covering SCAG area, which represent a complex freeway system (mixed-flow lane, HOV lane, ramp, *etc*.) and arterials. Small roads and lanes are not included in this system. Centroid collectors, which are presented in original network file, are for trip distribution modeling purposes but not real roadways. Hence, to preserve the geometry of real roads for dispersion modeling, collectors are removed from the original network in this study. The digital map includes traffic flow of various vehicle types (as in Table 4-2) for four time periods of a day - morning, midday, afternoon, and nighttime. It was calibrated based on year 2000's travel survey data and validated with year-2003 travel statistics [*115*]. Therefore, this study aims at the average exposure assessment in calendar year 2003.

5.2.1.1 Traffic Flow Modeling

Total traffic flow of year 2003, provided by SCAG Regional Transportation Model, consist a variety of on-road vehicle types to simulate real-world traffic: passenger car driving alone (DA), passenger car shared ride with 2 persons (SR2), passenger car shared ride with 3 or more persons (SR3), light-heavy duty trucks (LHDT), medium-heavy duty trucks (MHDT), heavy-heavy duty trucks (HHDT).

In consideration of traffic volume variation throughout the day, vehicle flow is modeled for four time periods - morning peak period (6:00 to 9:00 AM), midday period (9:00 AM to 3:00 PM), afternoon peak period (3:00 PM to 7:00 PM), and night period (7:00 PM to 6:00 AM). Because the exposure assessment only includes morning and nighttime time window, analysis of these two periods are presented. Figure 5-3 maps average network-wide traffic flow in the morning in SCAG region, which varies significantly at a spatial scale. Temporally, traffic volume changes substantially as well. Histograms of traffic flow for two time periods are presented in Figure 5-4. As transportation model predicts, heavy traffic volumes occur during morning peak hours; moderate traffic flows are observed in nighttime.

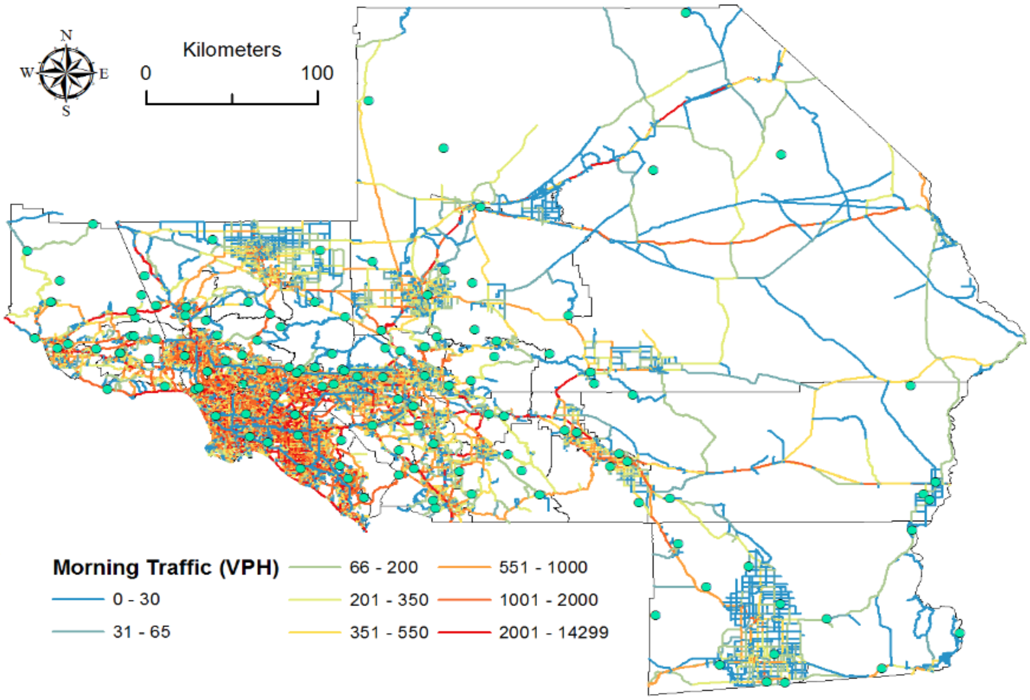

Figure 5-3 Traffic during morning peak and weather stations (in green dot) in SCAG region

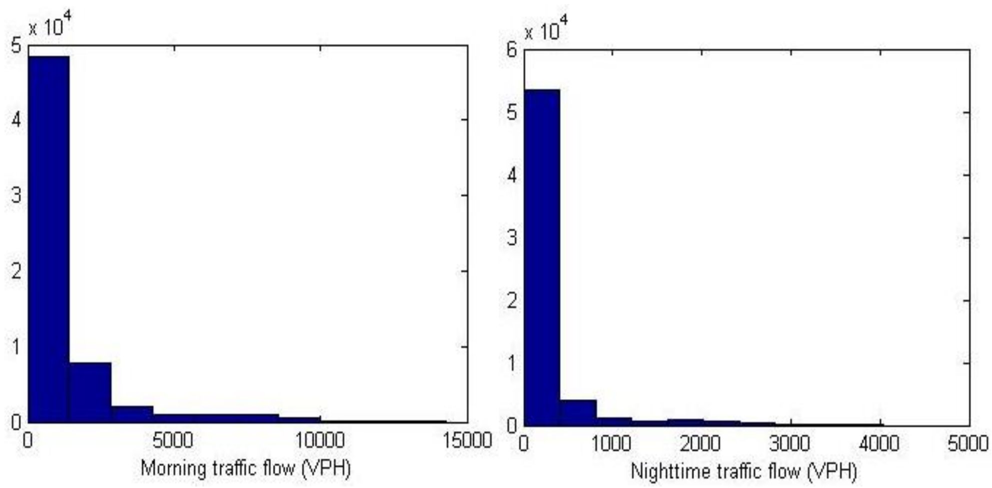

Figure 5-4 Histogram of traffic flow in morning and nighttime period

5.2.1.2 Traffic Speed Estimation

Traffic speed of vehicles traveling on roadways is another important factor of traffic activity and emission modeling. It is estimated with the approach shown in Figure 5-5. Road facility type, post speed limit, area type, traffic flow, lane number are given parameters in network metadata for each roadway link. Also, network's traffic speed values are calculated for four time periods of a day. Formulas and parameters applied are described in Chapter 4 of the Report *116*.

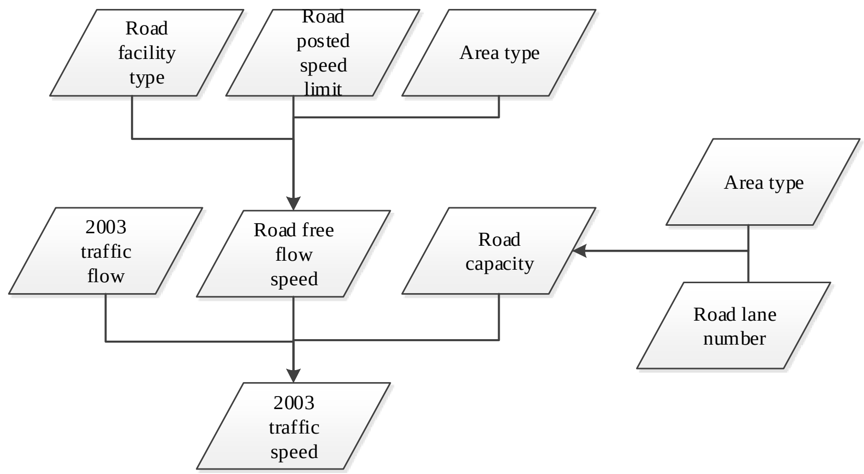

Figure 5-5 Flow chart of year 2014 traffic speed estimation

5.2.1.3 Emission Factors Modeling

Traffic emission factors are retrieved from EMFAC2011 online database [*62*] and results are aggregated for 6 counties. To characterize the 6 vehicle types (introduced in Section 5.2.1.1 Traffic Flow Modeling), they are regrouped into 4 vehicle groups to match EFMAC2011 vehicle category: Light Duty Vehicle (LDV), Light Heavy Duty Truck (LHDT), Medium Heavy Duty Truck (MHDT) and Heavy Heavy Duty Truck (HHDT), as introduced in Table 4-2, Section 4.2.1.

Then, $PM_{2.5}$ emission factors (gram per mile) of EMFAC vehicle categories (listed in Table 4-2) are retrieved from EMFAC online database, for 6 counties in SCAG region. It takes two levels to aggregate $PM_{2.5}$ emission factors for the four vehicle groups applied in this study for SCAG region. First, for each county, emission factors of each new vehicle group are aggregated from corresponding EMFAC vehicle categories. Secondly, for each new vehicle group, emission factors of SCAG region is aggregated from 6 counties. Figure 5-6 plots the aggregated emission factors over speed categories.

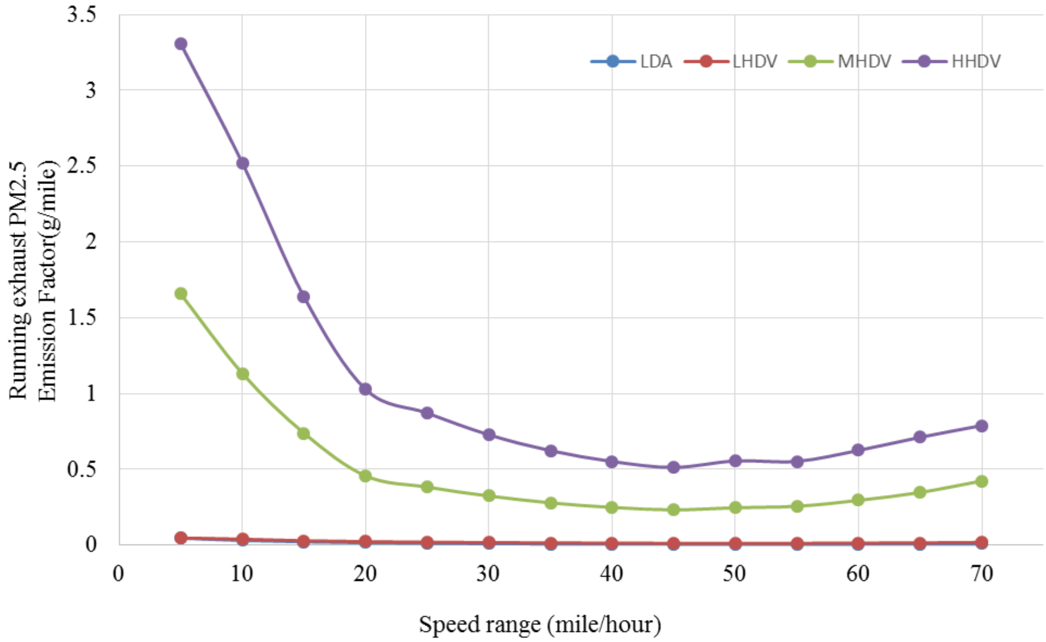

Figure 5-6 Aggregated $PM_{2.5}$ emission factors for 4 vehicle groups in SCAG region

From Figure 5-6, it is evident that particle emissions are more dominant in HHDV than light duty counterparts. $PM_{2.5}$ emission factors for heavy-duty trucks are significantly higher throughout the entire speed range. These emission factors are expressed in the unit of grams per mile per vehicle. Thus, to calculate the emission strength on each link of the roadway network, the emission factors were multiplied with traffic flow on the link according to Equation 2-1.

All aggregation calculation is realized with Matlab script. Emission factor and traffic flow are calculated for all links in the network, saved in matrices in form of matfile [*63*]. They will be input into air dispersion models to characterize traffic emission strength, as described in Section 5.2.3.

5.2.2 Census Data Processing

To investigate the relationship between transportation $PM_{2.5}$ exposure and resident SES at a high resolution, we choose the U.S. Census block as our geographic units for $PM_{2.5}$ estimation. Because the traffic activities are modeled for year 2003, we apply census data of year 2000, for best proximity. Decennial U.S. Census figures are based on survey of persons dwelling in U.S. residential structures. It includes citizens, non-citizen legal residents, non-citizen long-term visitors and illegal immigrants.

Demographically, census data collects wide range aspects of SES of the dwellers in the United States, including population, age, gender, race, education, housing situation, income *etc*. Geologically, it covers entire US (including 50 states, the District of Columbia, and Puerto Rico) in hierarchical sequence or political districts. Take hierarchical sequence as an example, census provides data for big geographic entities (e.g. state and county), and their smaller subareas (e.g. block, block groups).

Census data store large quantities of files regarding demographics and geographic. To access the data in need, there are several steps to take. First, the Topologically Integrated Geographic Encoding and Referencing (TIGER) files [*117*], which are essentially the shapes and geographic locations of all the census blocks (in form of shapefile [*65*]), are needed. So that one can view and analyze them in ArcMap. Second, the demographics tables associated with the TIGER files are needed. Because there are hundreds of SES subjects (e.g. age, gender, race, education, housing situation, income *etc*.), the data are categorized into four major sections - Summary File 1 (SF1) [*118*], Summary File 2 (SF2) [*119*], Summary File 3 (SF3) [*120*], and Summary File 4 (SF4) [*121*]. Table 5-1 lists data content for each Summary File. Upon confirming locations of interest and SES subjects, one can download Census TIGER shapefiles [*122*] and Summary File tables, import tables with database management tools [*123*], and select data according to level of summaries (e.g. tract, block group, block *etc*.). The FTP download websites and technical documentations can be found in Reference *118-122*.

Table 5-1 Overview of content for each Summary File

	Number of Tables	Overview of content
SF1	286	SF1 focuses on age, sex, households, families, and housing units. These tables provide in-depth figures by race and Hispanic origin; some tables are repeated for each of nine race/Latino groups.
SF2	47	SF2 focuses on age, sex, households, families, and occupied housing units for the total population. These tables are repeated for 249 detailed population groups.
SF3	813	SF3 provides social, economic and housing characteristics compiled from a sample of approximately 19 million housing units (about 1 in 6 households) that received the Census 2000 long-form questionnaire.
SF4	323	SF4 contains the sample data, which is the information compiled from the questions asked of a sample of all people and housing units. Each table is iterated for 336 population groups: the total population, 132 race groups, 78 American Indian and Alaska Native tribe categories (reflecting 39 individual tribes), 39 Hispanic or Latino groups, and 86 ancestry groups.

In this study, SCAG region is comprised of 3,402 census tracts, and 10,577 census block groups, which can be further divided into 203,191 census blocks. Population count by age, gender and race are extracted at a census block level; median annual income data is extracted at census block group level, at the best level of details. According to Census 2000, SCAG region is home to 16,516,006 residents. Los Angeles and Orange County have highest population density. The summary plots of population are displayed through Figure 5-7 to 5-9. In the following exposure assessment, it is assumed that in year 2003, all the dwellers still all live in the homes where they reported in year 2000, and the dwellers' age increase 3 years. Newborns during year 2000 and 2003 are not considered.

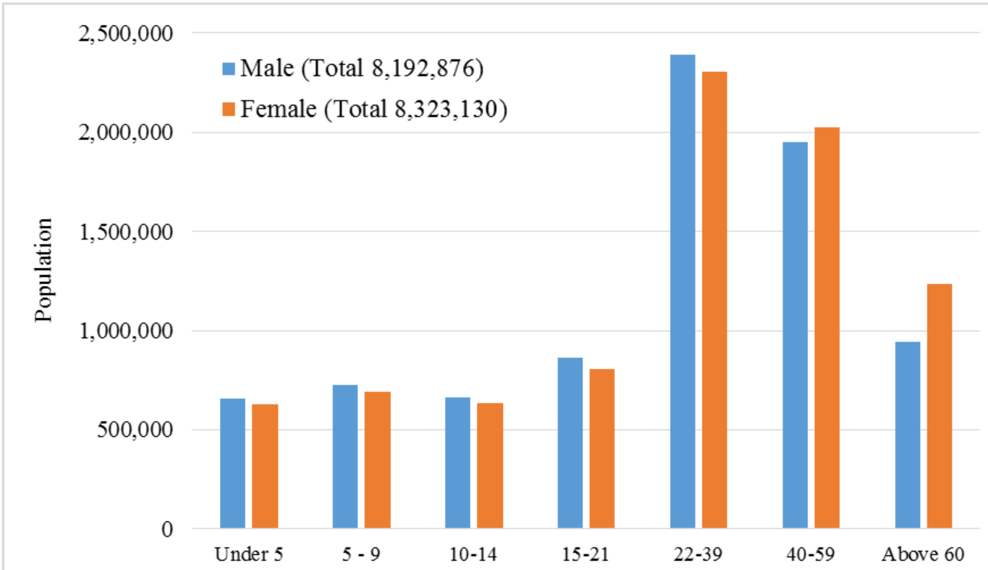

Figure 5-7 Year 2000 Population of age groups by gender in SCAG region

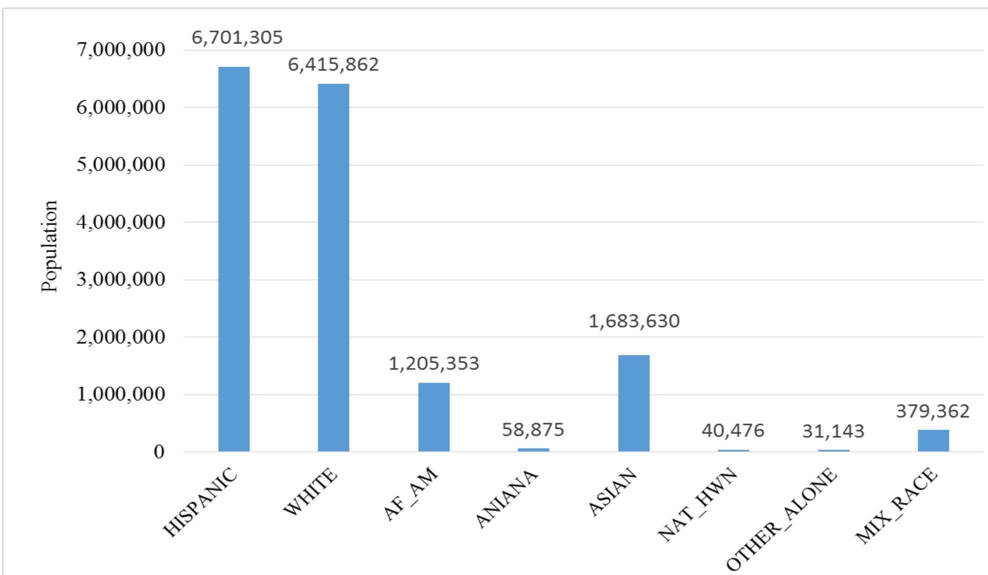

Note: 'HISPANIC' refers to Hispanic or Latino, which is a racially diverse group. 'AF_AM' refers to African American. 'ANIANA' refers to American Indian or Alaska Native. 'NAT_HWN' refers to Native Hawaiian or Other Pacific Islander. 'OTHER_ALONE' refers to other one race population. 'MIX_RACE' refers to mixed race population.

Figure 5-8 Year 2000 population by race groups in SCAG region

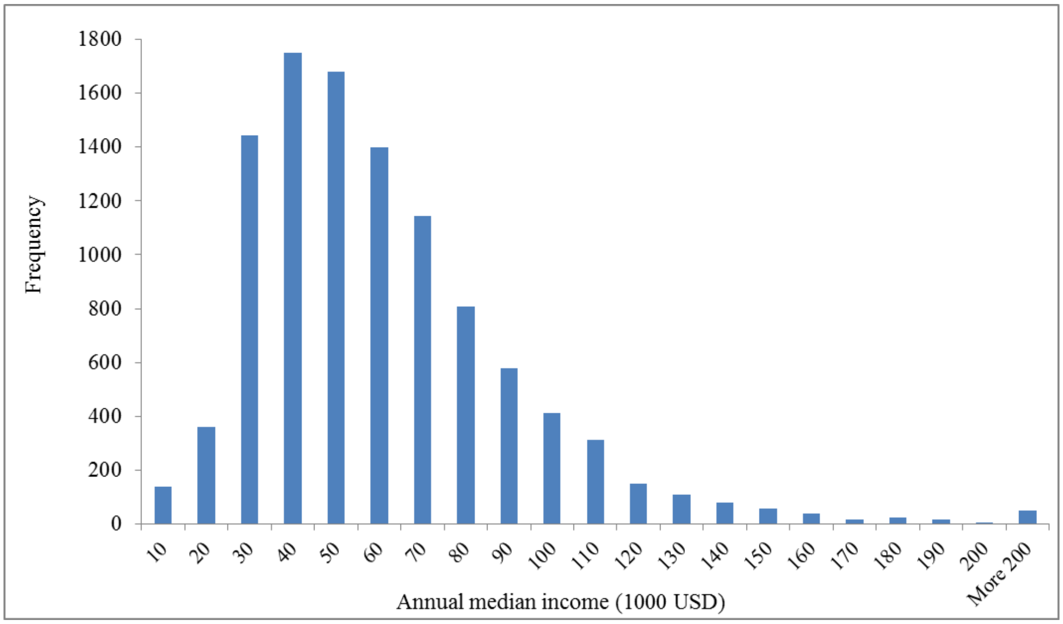

Figure 5-9 Year 2000 annual median income (1000 USD) in SCAG region by census block groups

In this study, census also provides block locations and SES information for $PM_{2.5}$ concentration estimation and exposure assessment. To represent census blocks, centroid of each census block is set as a receptor in dispersion modeling, which is introduced in section 5.2.3.5.

5.2.3 Air Dispersion Modeling

In this step, we aim at estimating transportation $PM_{2.5}$ concentration at census block level. The air pollutant dispersion modeling is conducted using CALINE4.

5.2.3.1 Introduction of CALINE4

CALINE4 (introduced in Section 2.2.2), is a line-source dispersion model developed by Caltrans [*27*]. Caltrans provides two forms of CALINE4 - user interface (UI) and windows executable (‘CALINE4_w32.exe’). Both of them process at most 20 links and 20 receptors at one time. The CALINE4 UI provides a convenient way to enter and visualize parameters of receptors and roadway links, but it requires manual inputs. Therefore, it is only suitable for small-scale modeling projects.

Table 5-2 CALINE4 input file components in this study

Block No.	Description
1	File title
Source	User specified text, such as '2003SCAG_PM2.5'
2	Name of pollutant
Source	Model specified text, for PM, use '4Particulates'
3	Scenario parameters: roughness length in cm (Z_0), molecular weight (M), setting velocity (VS), deposition velocity (VD), number of receptors (Nr), number of links (Nl), hour average (Hr), length unit (1 for meter and 0.3 for feet), run type, altitude above sea level (Alt)
Source	For each run Z0 is determined by one property of census block- urban or rural. Urban is 60 cm, and suburban is 20 cm [*70*]. M, VS and VD are all 0. To uniform the output, Nr and Nl are all set as 20. Since 1-hr average concentration is needed, Hr is 1. Length unit is 1 since metric units is chosen for Alt. Alt for all census block centroids are retrieved from USGS digital elevation map database [*81*], and extracted using ArcMap raster process tools [*124*, *125*]. All data are written into matrices and saved in CSV (Comma-separated values, supported by Microsoft Excel) files.
4	Receptors Index and 3-demention Cartesian coordinates
Source	Receptors Index is nominal index to label receptors (see Appendix C). Cartesian coordinates of receptors are extracted using ArcMap (detail steps are described in Section 5.2.3.3 GIS Implementation), and saved in CSV files. Receptors are placed at a typical breathing height of 1.6 m (5.3 ft).
5	Links index and links parameters: link type, junctions' Cartesian coordinates, mix height *etc*.
Source	Links Index is nominal index to label roadway links (see Appendix C). Link type for all links are set as 1- at-grade - which means no plume mix below ground level (please see Reference *82* for more details). Cartesian coordinates of roadway junctions are extracted from roadway shapefile using ArcMap (detail steps are described in Section 5.2.3.3 GIS Implementation), and saved in CSV file.
6	Run type and time interval specification
Source	Run type is standard and set as 1. Average time interval for dispersion is 1. See Appendix C.
7	Traffic flow for each input link
Source	Estimation of traffic flow for each link is described in Section 5.2.1.1 Traffic Flow Modeling
8	Traffic emission factor for each input link
Source	Estimation of traffic emissions for each link is described in Section 5.2.1.2 and 5.2.1.3.
9	Meteorology inputs: wind direction, wind speed, stability class, mixing height, wind direction standard deviation, background concentration, and temperature.
Source	Raw weather data (wind speed/direction and temperature) are retrieved from CARB website. Other values are derived or empirical data. For data processing please see Section 5.2.3.2.

In order to process more than 200,000 receptors with surrounding roadway links efficiently, an automated execution of CALINE4 executable in batch mode is desirable. In the Windows operating systems, CALINE4 executable can read formatted batch files (in text file format, see Appendix B), execute the corresponding input files (in text file format, see Appendix C), and generate output files in batch mode. Section 5.2.3.6 introduces the automation process using the CALINE4 executable.

The model requires 9 major input blocks as specified in Table 5-2. Various data sources and formats are also referenced in Table 5-2. To summarize, the major inputs are receptor locations, road link locations, traffic flow and emission factor of road links, and meteorology parameters. Report *126* and Guideline *127* provide helpful details of CALINE4 modeling. Data processing of major inputs are described in the following sections.

5.2.3.2 Meteorology Data Processing

Meteorology inputs are critical to air dispersion modeling. For CALINE4, mandatory meteorology inputs are listed in Block 9 of Table 5-2. Among these parameters, raw data of wind speed, wind direction, wind direction standard deviation, and ambient temperature, are obtained from the routine weather monitor system managed by CARB [*100*]. Another two meteorology inputs, atmospheric stability and boundary layer mixing height, are set as empirical values [*101*], shown in Table 5-3. 136 weather stations in the SCAG region are included for a better representation of the weather patterns in Southern California, as marked in Figure 5-3.

Table 5-3 Stability Class and Mixing Height for two time periods in dispersion modeling

	Stability Class	Mixing Height (meter)	Wind Speed Limit (m/s)
Morning	2	500	<5.5
Nighttime	1	300	<4.5

Since $PM_{2.5}$ concentration is required for morning and nighttime periods, every meteorology parameter is averaged into morning and nighttime values regarding the time slot of each period. Hourly observations of each weather station for year 2003 are retrieved and processed using customized Python scripts. For example, for a weather station in Long Beach, 24-hour temperature values for 365 days in year 2003 are downloaded. For the morning period (6 - 9 AM), all the temperature values (for 365 days) between 6:00 to 9:00 are averaged into one morning temperature mean. Then this process is repeated for nighttime periods, as well as other weather stations. Wind speed and wind direction are averaged according to Chapter 6 of meteorological monitoring guidance compiled by U.S. EPA [*128*].

After the meteorology parameters of each weather station are processed, the data table is imported into ArcMap. With the latitude and longitude of stations, ArcMap converts table into a point shapefile that can be used in further spatial analysis. Then, meteorology data of weather stations can be related to receptors and links nearby, as explained in Figure 3-6.

5.2.3.3 GIS Implementation

To prepare the input parameters for dispersion modeling, several suites of GIS operations are required to refine the network geometry, and relate the receptors (census block centroids), roadway links and weather stations spatially. The processes are illustrated in the following figures which clearly display inputs, outputs, and geoprocessing tools applied in GIS implementation. The blue and green oval indicate the input and output file, respectively. A yellow rounded rectangle represents a geoprocessing tool. For more helpful information on geoprocessing, please refer to Book *129*.

5.2.3.4 Roadway Network Characterization

The original road network provided by SCAG-RTM, mapped in Figure 5-3, contains 49,146 roadway links, among which a large number are curved. As discussed in Section 3.2.3, curved links cannot be well represented (Figure 3-4) in dispersion modeling and must be refined. The geometry refinement for this SCAG network applies the same process as in Figure 3-5. After the geoprocessing suite, the final network shapefile contains 500,850 links that characterize the network geometry at great details. Moreover, previously calculated traffic flow and emission factors are passed to every link. The output shapefile 'network_flow_emi_gen_split_WM' is in Web Mercator coordinates and will be one of the inputs in next steps.

Next, as described in Table 5-2 input block 5, 7, 8 and 9, the link activities and meteorology parameters need to be incorporated for dispersion modeling. The spatial to tabular data transition is illustrated in Figure 3-6, except for that the dispersion model in this chapter is CALINE4.

This geoprocessing suite joins meteorology parameters to roadway links, locates link nodes and assigns Cartesian coordinates to them. The other input shapefile 'SCAG2003met_site_WM', contains the 136 weather stations in Web Mercator coordinates with meteorology parameters calculated for morning and nighttime periods, as described in Section 5.2.3.2. The weather stations are spatially joined to the 500,850 roadway links based on their relative location [*86*], hence the meteorology parameters are passed to links. Final output table, 'detail_network_flow_emi_met_X1Y1_X2Y2_table', retains all information from the parent network shapefiles, which covers link-based traffic flow, link-based averaged emission factor, link location, and meteorology parameters for dispersion modeling.

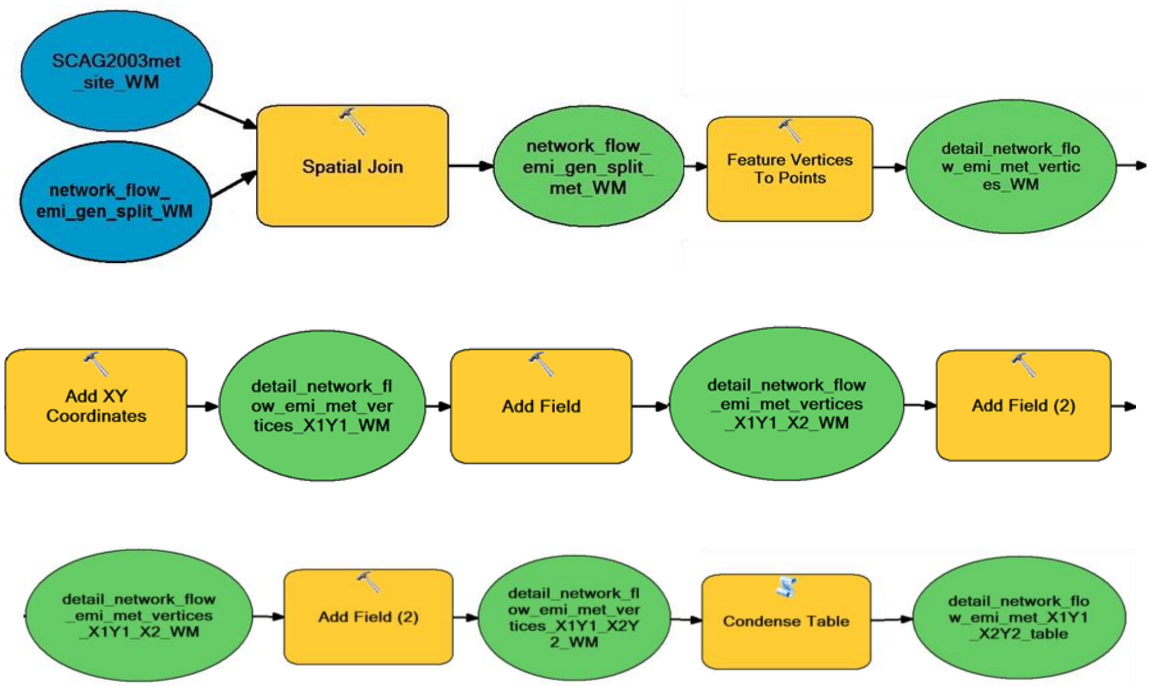

Notes: 'Spatial Join' matches roadways with nearby weather stations [*86*]. 'Feature vertices to points' locates nodes for link segments [*130*]. 'Add XY Coordinates' assigns Cartesian coordinates to nodes [*80*]. Two applications of 'Add Field' add two blank columns for later steps [*131*]. 'Condense Table' tool is scripted using Python, which can be executed in ArcMap. This tool condenses the node lists into node pairs that locate road links.

Figure 5-10 Workflow of roadway network charaterization for dispersion modeling

5.2.3.5 Receptors Setup

In this dispersion modeling component, we aim at estimating transportation $PM_{2.5}$ concentration at census block level. Hence, census blocks' centroids are located as receptors as we assume that they represent the locations of census blocks (Figure 5-13b). As mentioned in Section 5.2.2, there are 203,191 census blocks in SCAG region. Therefore, there are 203,191 receptors that scattering in entire SCAG area. If we iterate block centroids one by one, the computation cost will be enormous. To improve the computation efficiency, the receptors should be grouped into clusters (Figure 5-13c). Based on the cluster location, surrounding links within 2,000 meters are selected as 'influential links' (Figure 5-13d). An underlying assumption is that, roads 2,000 meters away have no impact on a residential block in terms of fine particles pollution. The data source, scripts, tools used are specified in Figure 5-13. After this cluster process, the number of clusters groups becomes 35,109, which is a numeral reduction of 83%, compared with 203,191 individual centroids. Even though the exact time saving of computation is less than 83%, the cluster process significantly reduces computation cost in the following dispersion model execution.

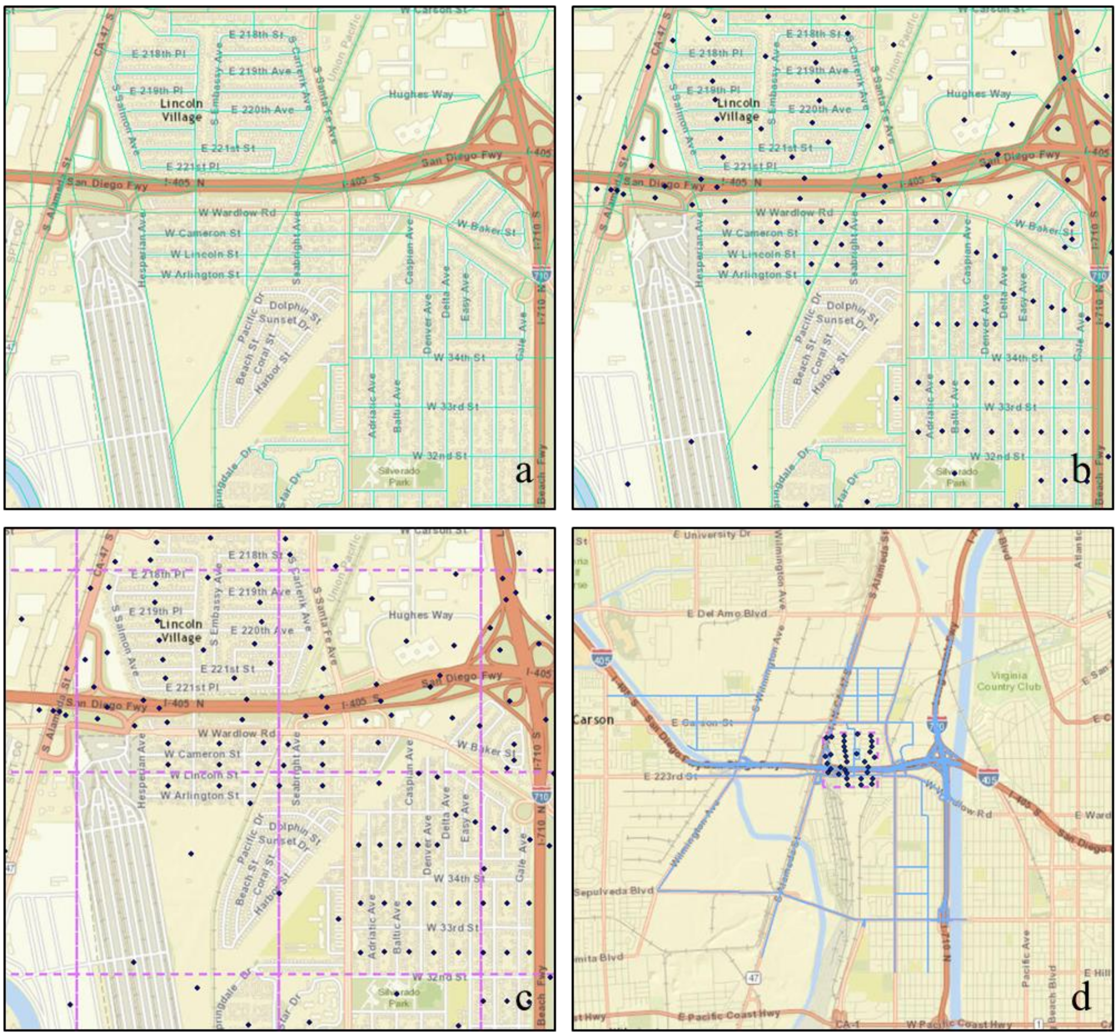

Notes: a - Outline of Census 2000 blocks are drawn in green lines. (source: Census [*122*])
b - Centroids of Census 2000 blocks (marked in blue points) are generated from Census 2000 block polygons, using 'Feature Vertices to Point' tool in ArcMap [*130*], and coordinates are extracted using 'Add XY' tool in ArcMap [*80*].
c - Grid is generated by 'Fishnet' tool in ArcMap [ref], at 1000×1000 meter spacing. The grid coordinates are extracted using 'Add XY' tool in ArcMap. With the coordinates of both grid and centroids, a Matlab script is applied to group the centroids into clusters. Centroid clusters are saved with index as matfile [*63*].
d - Take the patch that covers Lincoln Village as an example, a Matlab script is applied to search and select links that within 2,000 meters of each centroid cluster, named 'influential links'. Influential links are saved with index as matfile.

Figure 5-11 Schematics of receptors setup and clustering

5.2.3.6 Dispersion Model Execution

The previous sections document the preparation of the major inputs for CALINE4 execution. Processed receptor locations, road link attributes (e.g. locations, lane width, traffic flow, emission factor *etc*.), and meteorology parameters, are saved in matfile format [*63*] which are ready for final dispersion calculation.

A suite of Matlab scripts performs the automation process - writing input files from raw data, calling CALINE4 executable to batch process input files and generate output files, as well as reading output files - as the following tasks:

1. Read 'centroid cluster' and 'influential links' file processed in Section 5.2.3.5 Receptors Setup
2. Divide one centroid cluster into groups of 20. Also, divide surrounding links into groups of 20 (because the CALINE4 executable can at most processes 20 links and 20 receptor at one time). Assign a unique link-receptor group index to each combination.
3. Create input text files containing attributes of the link-receptor group, e.g. link location, traffic flow, traffic emission factor, receptor location, meteorology data, and other required inputs (as listed in Table 5-2). At the same time write corresponding command file of batch run. An example of batch file is given in Appendix B.
4. Run the batch command to call CALINE4 to execute the input files for each link-receptor group. Iterate through all link-receptor groups for each centroid cluster. Output files are generated with unique link-receptor group index.
5. Read the output files according to the unique link-receptor group index, and extract the output $PM_{2.5}$ concentration values at each receptor. Iterate through all centroid clusters.

6. Keep count of generated input and output files, create new folder for storage when total number of files in one folder exceeds 900. This step is critical to improve search efficiency.
7. Repeat step 1-6 for all centroid clusters in the network. It takes 5 hours for a personal computer (Intel Core i7 @3.4 GHz) to generate approximately 1 million text files (7GB), for a complete run.
8. Restore and save $PM_{2.5}$ concentration values of centroid cluster into vectors, for the subsequent exposure assessment.
9. Repeat 1-8 for other time periods if needed.

Chapter 4 and Chapter 5 both involves in CALINE4 batch process due to a large number of input links and receptors. The GIS implementation and Matlab scripts applied in this process serve as critical connections between the various input datasets, established models and desired outputs.

5.2.4 Exposure Assessment

Previous sections describe the estimation of $PM_{2.5}$ estimation in SCAG region, in preparation for exposure assessment in this section. Equation 2-5 describes the formulation of *inhaled mass* (*IM*) that is applied to quantify inhalation exposure through this dissertation.

Several assumptions are made to simplify the exposure assessment. First, fine particle exposure in residential homes during morning and nighttime is included; other microenvironments and time periods are not considered. Secondly, $PM_{2.5}$ concentration at home is the same with that of ambient. Hence penetration factor is one for all the scenarios. Thirdly, background $PM_{2.5}$ concentration are not included in exposure assessment. Equation 5-2 sums up the variables to calculate residential *IM* (μg) for population groups in census block *i*:

$$IM_{(i,PM_{2.5})} = \sum_{j=1}^{j} C_{AM,i} \times t_{AM,i} \times BR_{AM,j} \times Pop_{i,j} + \sum_{j=1}^{j} C_{NT,i} \times t_{NT,i} \times BR_{NT,j} \times Pop_{i,j} \quad (5\text{-}1)$$

$C_{AM,i}$ is $PM_{2.5}$ concentration (*μg/m³*) in census block *i* in the morning. $t_{AM,i}$ is duration spent in census block *i* in morning (morning: 3 hours; nighttime: 11 hours). $BR_{AM,j}$ is the breathing rate (*L/min/capita*) of age group *j* in morning. $Pop_{i,j}$ denotes the population of group *j* in census block *i*. Subscript *NT* labels nighttime terms. From a medical standpoint, breathing rate for different age group and gender are different. In this calculation, to avoid the bias brought by different breathing rate, we assign $BR_{AM,j}$ as 20 *L/min* as the average for all gender-age group. The referenced study is one of a series air pollution research sponsored by CARB [*82*]. At night during sleep, breathing volume roughly reduces 8% [*132*]; therefore, we give $BR_{NT,j}$ a value of 18.5 L/min. Final $PM_{2.5}$ exposure assessment for each census block in year 2003 is implemented in Matlab. After that, block level exposure is aggregated to block group level, because the most detailed family income data is at census block group level.

$$IM'_k = \frac{\sum_{i=1}^{i} IM_i}{\sum_{i=1}^{i} Pop_i \times \sum t} \quad (5\text{-}2)$$

IM'_k is the population-time-normalized *inhaled mass* (*μg/hour/capita*) in block group *k*. It means the average *inhaled mass* of $PM_{2.5}$ by one person in block group *k* per hour during morning and nighttime in year 2003. Then, relationships between the normalized $PM_{2.5}$ *inhaled mass*, population by race, and annual income at block group level are analyzed.

5.3 Analyses Results

5.3.1 $PM_{2.5}$ Concentration Estimation at Census Block Level

Figure 5-14 and 5-15 map $PM_{2.5}$ concentration of census block centroids in SCAG region, in morning and nighttime period of year 2003, respectively. The choropleth clearly outlines major roads in Southern California, indicating that the emission source (on-road vehicles) are correctly assigned to receptors (census blocks centroids). The meteorology condition during morning and nighttime are similar. Both time periods feature stable atmospheric stability, low wind speed and low mixing height. However, $PM_{2.5}$ estimation in the morning is generally higher than that of night. In the morning, extremely high concentration values, up to 174 $\mu g/m^3$, occur due to high peak-hour traffic in proximity (more than 12000 vehicles per hour). In contrast, high concentration in nighttime only ranges from 36 to 56 $\mu g/m^3$, due to moderate on-road traffic flow. To reiterate as in Section 5.1.2, $PM_{2.5}$ refers to localized primary out-of-tail-pipe $PM_{2.5}$.

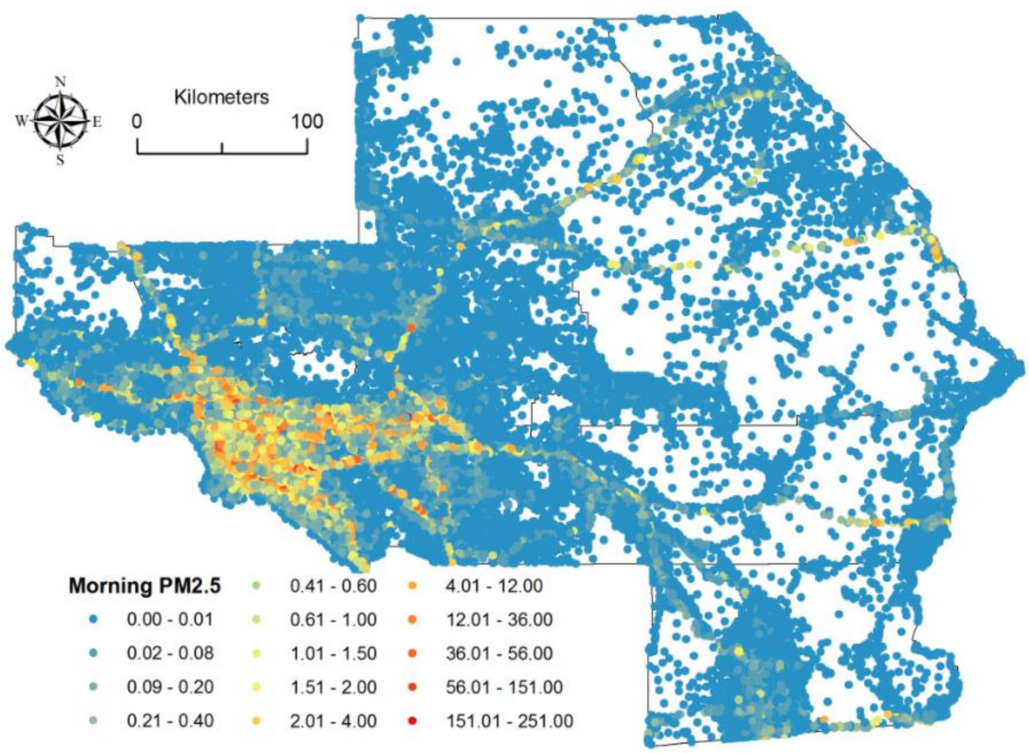

Figure 5-12 Morning localized mobile-source $PM_{2.5}$ concentration at census block level in year 2003

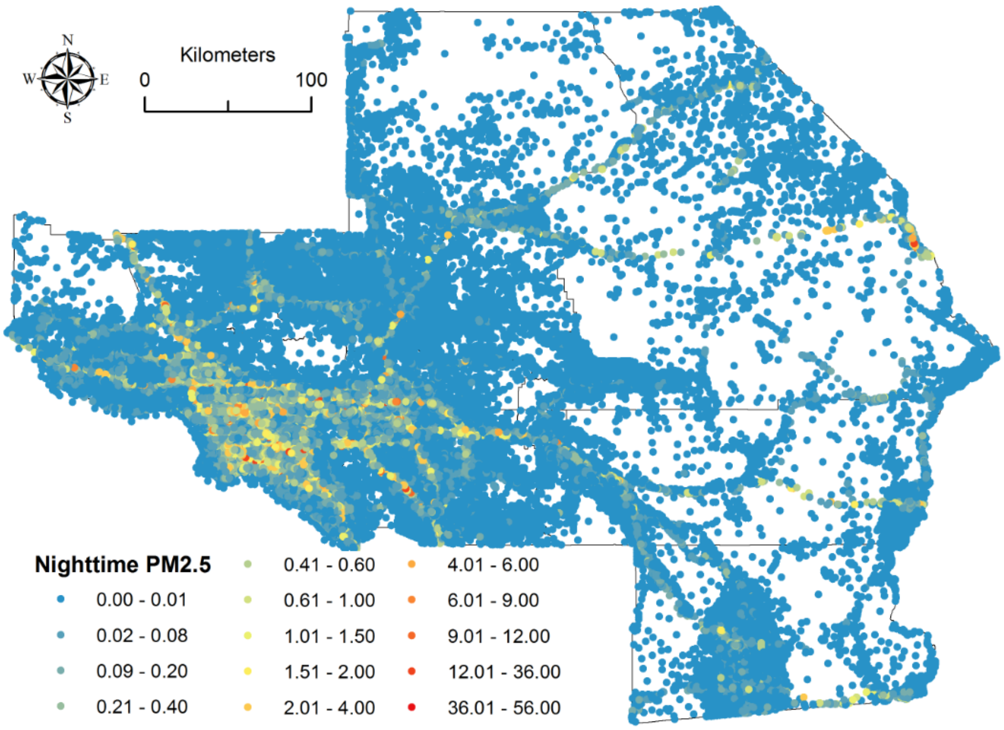

Figure 5-13 Nighttime localized mobile-source $PM_{2.5}$ concentration at census block level in year 2003

These high $PM_{2.5}$ concentration values in year 2003 are rarely observed today, thanks to stringent emission control policies implemented in California during last decades. However, back in year 2003, it is not abnormal to detect ambient $PM_{2.5}$ concentration up to 150 $\mu g/m^3$. According to air quality history data monitored by CARB in year 2003 [*133*], several statistics summaries are displayed in Figure 5-14.

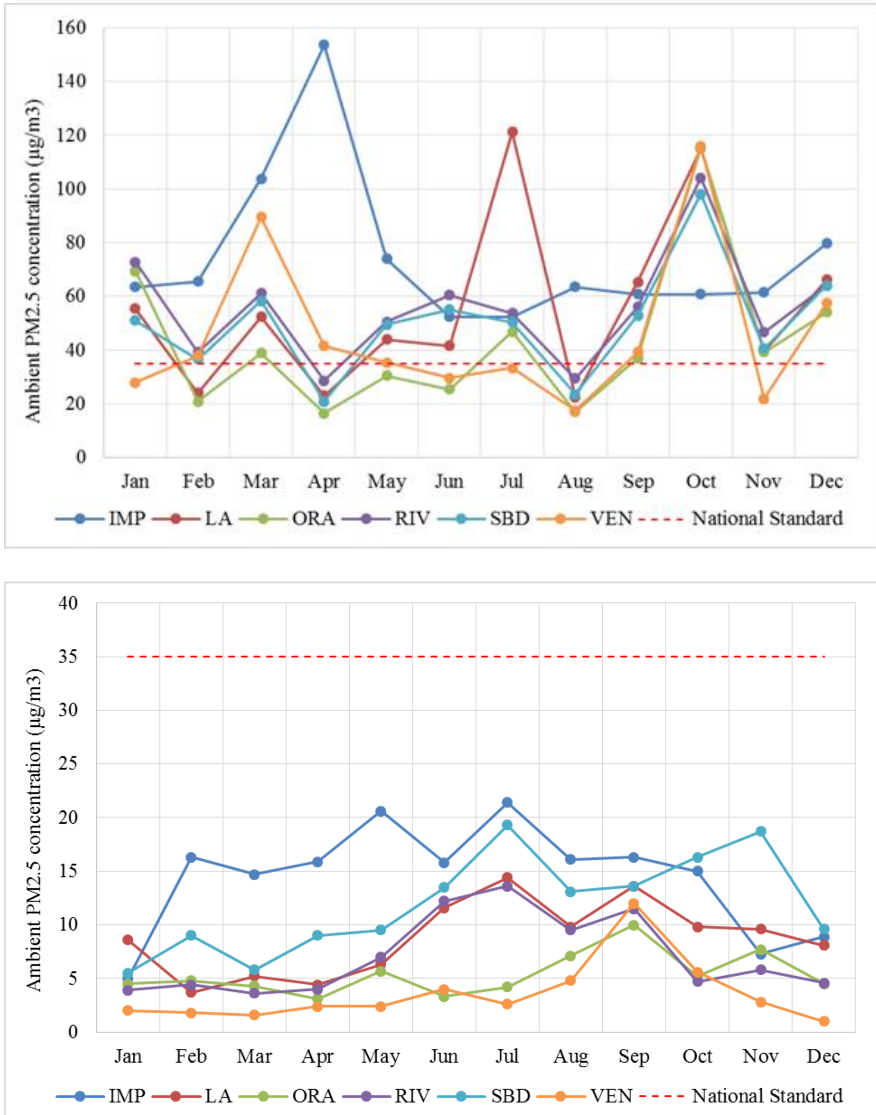

Figure 5-14 Maximum and minimum concentration of ambient $PM_{2.5}$ of annual daily average for each month and county in year 2003

Therefore, the magnitude of estimated $PM_{2.5}$ concentration levels, agrees with monitor records. The comparison, strictly speaking, is not a validation of dispersion modeling results. However, it indicates that the concentration modeling in this study is implemented with reasonable assumptions and operations. The output $PM_{2.5}$ concentration at each census block is not only an estimated value, but also an integrated index of proximity to roadway, traffic volume on adjacent roadways and average weather condition. The higher the $PM_{2.5}$ value is, the higher the exposure impacts are imposed from localized mobile source. Therefore, the output $PM_{2.5}$ concentration provides a solid support for exposure assessment.

Section 5.2 shows the efforts made to implement this framework, and one of the important benefits is that it enables high-resolution and large-scale concentration modeling, which is also the most critical input for exposure assessment. Figure 5-15 and Figure 5-16 present examples of census tract, block groups and blocks to give a visual comparison between the three spatial scales.

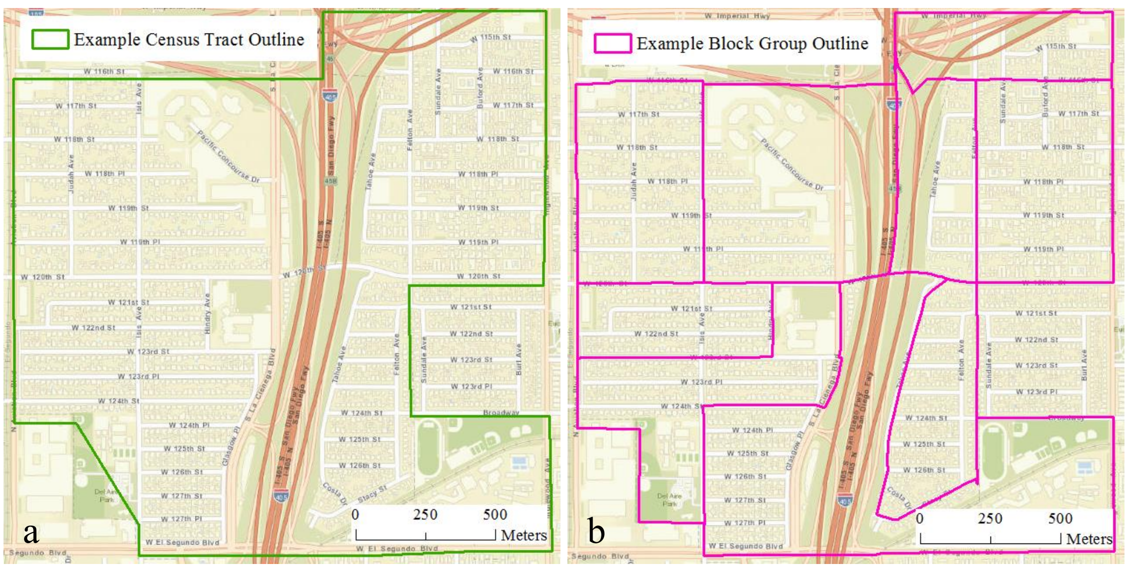

Figure 5-15 An example of spatial comparison between census tract level (a) and block group level (b)

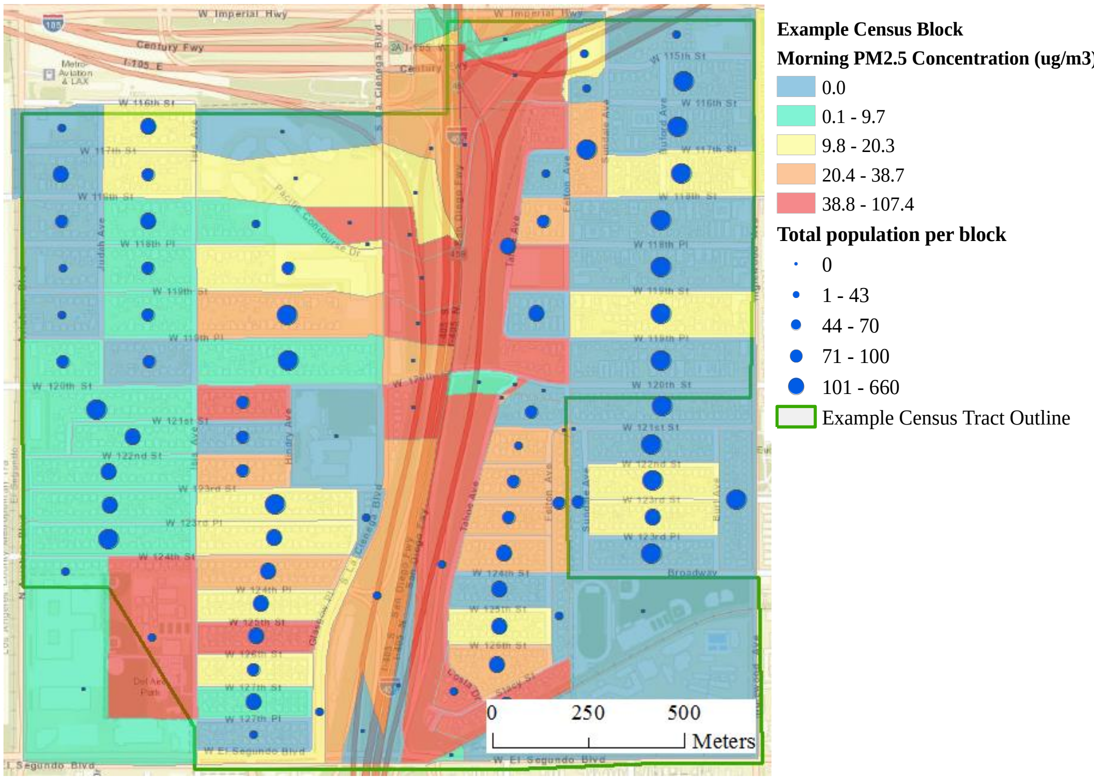

Figure 5-16 An example of concentration and population distribution at census block level in this study

Most of the environmental justice studies are performed at census tract level [*111*, *114*]. Marshall *et al.* applied dispersion results and assessed inhalation intake based on a 1000-meter grid [*112*, *113*]. But for area with dense blocks, such as south LA County whose block density is even larger than that of Figure 5-16, 1000-meter grid resolution is still not adequate.

In contrast, this framework enables concentration modeling at census block level, which is a significant improvement in terms of spatial resolution. In addition, the framework also supports better temporal resolution analyses given required inputs. According to Census 2000, there are 3,402 census tracts in SCAG region, which can be further divided into 10,577 block groups, or 203,191 blocks. Therefore, generally, the block-level resolution in this study is 58 times higher than tract-level studies. Block-group-level resolution in the following sections is 2 times higher than tract-level.

Because detailed family income information provided by U.S. Census 2000 is available at block group level, the exposure assessment is aggregated to block group level (described in Section 5.2.4) so that the relationship between income and exposure can be analyzed.

5.3.2 $PM_{2.5}$ Exposure Assessment at Census Block Group Level

Aggregated $PM_{2.5}$ *inhaled mass* at block group level, calculated in Section 5.2.4, is normalized by total duration (morning plus nighttime gives 14 hours) and total population in each block group. Figure 5-17 presents histogram of normalized $PM_{2.5}$ exposure for 10,457 census block groups (120 block groups with zero population are excluded).

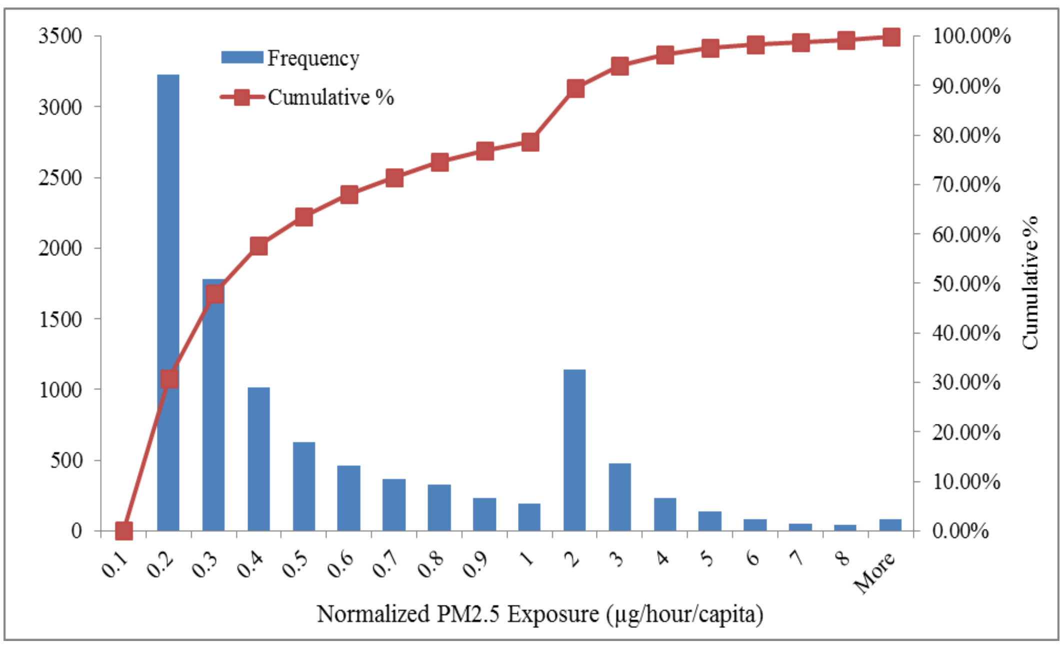

Figure 5-17 Histogram of $PM_{2.5}$ exposure to all population at census block group level

According to U.S. National Air Quality Standards, 24-hour average $PM_{2.5}$ concentration is 35 $\mu g/m^3$ [*134*]. Based on this concentration, we assume an average breathing rate of 20 *L/min* [*82*], and 20% of the ambient $PM_{2.5}$ concentration is contributed by primary out-of-tail emission [*135*, *136*, *137*]. It yields a threshold of 8.4 *µg/hour/capita* that would conform to national standards for the purpose of protecting human health. Figure 5-17 indicates that, for more than 99% of census block groups, their $PM_{2.5}$ exposure are within the $PM_{2.5}$ national standards threshold.

According to Air Quality Index (AQI) evaluation issued by U.S. EPA, air quality is classified into six categories [*138*, *139*], as Table 5-4 illustrates. Accordingly, we divide $PM_{2.5}$ exposure into six categories: low exposure, moderate exposure, unhealthy exposure for sensitive population, unhealthy exposure, very unhealthy exposure and hazardous exposure. The way we calculate $PM_{2.5}$ exposure cut point is multiplying $PM_{2.5}$ cut point concentration ($\mu g/m^3$, listed in Table 5-4) of each category with breathing rate (20*L/min*) and 20% (assume that 20% of ambient $PM_{2.5}$ is contributed by primary out-of-tailpipe $PM_{2.5}$ [*135*-*137*]). After unit conversion, the cut point $PM_{2.5}$ exposure values are 2.9, 8.5, 13.3, 36.1, 60.1, 120.1 *μg/hour/capita* for the six categories, respectively. The highest exposure among all the block groups is 37.3 *μg/hour/*capita, falling in 'very unhealthy' category. And this block group is in Tustin, Orange County.

Table 5-4 AQI categories and corresponding criteria pollutants level

AQI Index Values	Levels of Health Concern	Colors	PM2.5 (24hr-avg, in ug/m3)	PM10 (24hr-avg, in ug/m3)	CO (8hr-avg, in ppm)	NO2 (1hr-avg, in ppb)
When the AQI is in this range:	... air quality conditions are:	... as symbolized by this color:	... concentrations are:			
0-50	Good	Green	12	54	4.4	53
51-100	Moderate	Yellow	35.4	154	9.4	100
101-150	Unhealthy for Sensitive Groups	Orange	55.4	254	12.4	360
151-200	Unhealthy	Red	150.4	354	15.4	649
201-300	Very Unhealthy	Purple	250.4	424	30.4	1244
301-500	Hazardous	Maroon	500.4	604	50.4	2044

Figure 5-18 delineates the exposure level for 10,457 block groups with median income shown on x-axis. To take a close look at the surrounding traffic conditions, weather patterns, and SES statistics, a map of all the block groups whose normalized *IM* values are higher than moderate level (8.5 *μg/hour/capita*) are labeled in this interactive map http://arcg.is/1HAscj2.

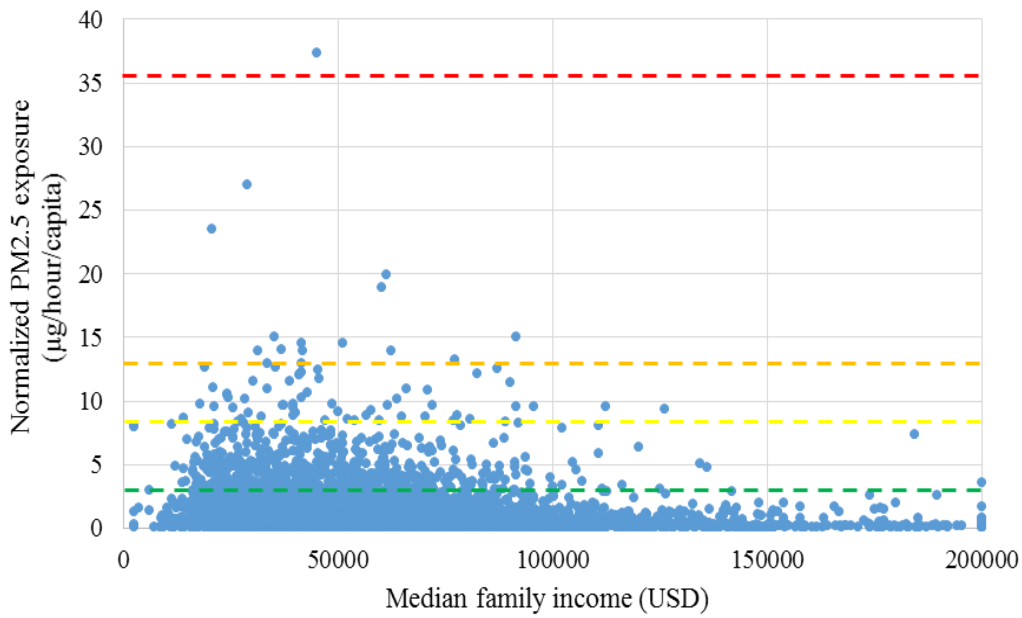

Note: the four dash lines, from bottom up, divide the scatters into five exposure levels: 'low', 'moderate', 'unhealthy for sensitive population', 'unhealthy', 'very unhealthy'

Figure 5-18 Scatter plot of median annual income vs. normalized $PM_{2.5}$ exposure at block group level

5.3.3 Income Level Delineation

Figure 5-19 also plots median income over normalized $PM_{2.5}$ exposure. To delineate income levels, we apply income limit published by U.S. Department of Housing and Urban Development (HUD) [*140*]. Despite different levels for six counties in SCAG region, the average values of the six counties are used. Hence, the 'extremely low', 'very low' and 'low income' limits in this analysis are determined as \$21,100, \$35,170, and \$54,580, respectively [*141*], as marked by vertical lines in Figure 5-19.

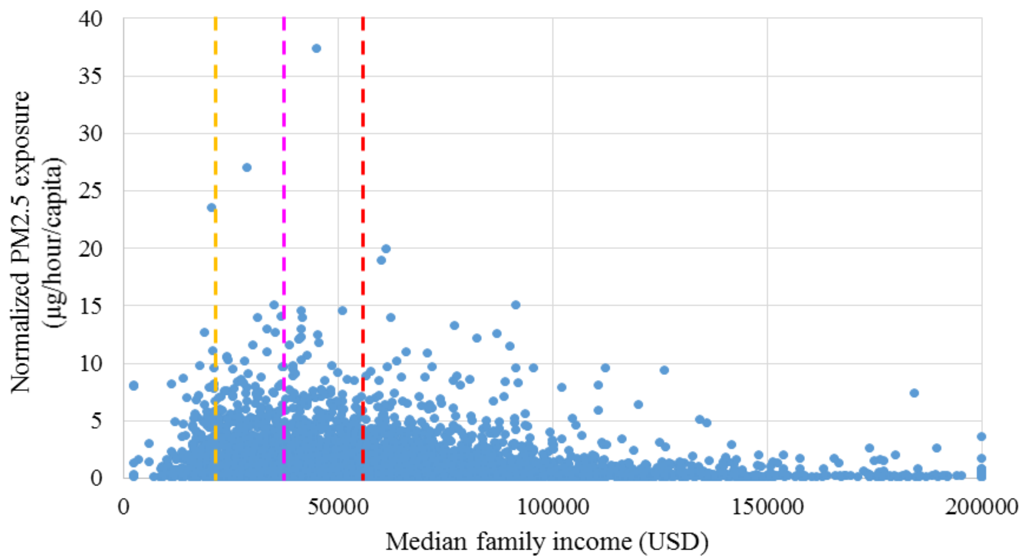

Note: three dashed lines mark three income limits and divided the scatters into four sections: extremely low income, very low income, low income, and normal income from left to right

Figure 5-19 Scatter plot of median annual income vs. normalized $PM_{2.5}$ exposure at block group level

Single-factor ANOVA is performed between the four income groups' normalized exposure values, whose hypotheses is that the four groups of exposure values are not significantly different from each other. According the ANOVA statistics reported in Table 5-5, $F(49,2)$=22.5, which is much higher than *F critical* value 2.6. The extremely small *P-value* indicates that at least two groups' exposure values are significantly different than each other.

Table 5-5 Single-factor ANOVA for normalized exposure from four income-groups

Source of Variation	*SS*	*Df*	*MS*	*F*	*P-value*	*F critical*
Between Groups	148.2264	3	49.40879	22.47617	1.68E-14	2.605759
Within Groups	22978.57	10453	2.198275			
Total	23126.79	10456				

To further analyze their differences, three unpaired T-tests are performed on the four groups. A box plot of normalized $PM_{2.5}$ exposure for the four income levels is presented in Figure 5-20. Results suggest that, in terms of $PM_{2.5}$ exposure values, Group A is significantly higher than Group B, Group B and C are not significantly different, while Group D is significantly lower than

Group C. Table 5-6 tabulates statistics of three T-tests for four income level groups. Based on the income level delineation, we conclude that generally the low income residents (annual income less than 54,580 USD) are subject to higher level localized mobile-source $PM_{2.5}$ exposure.

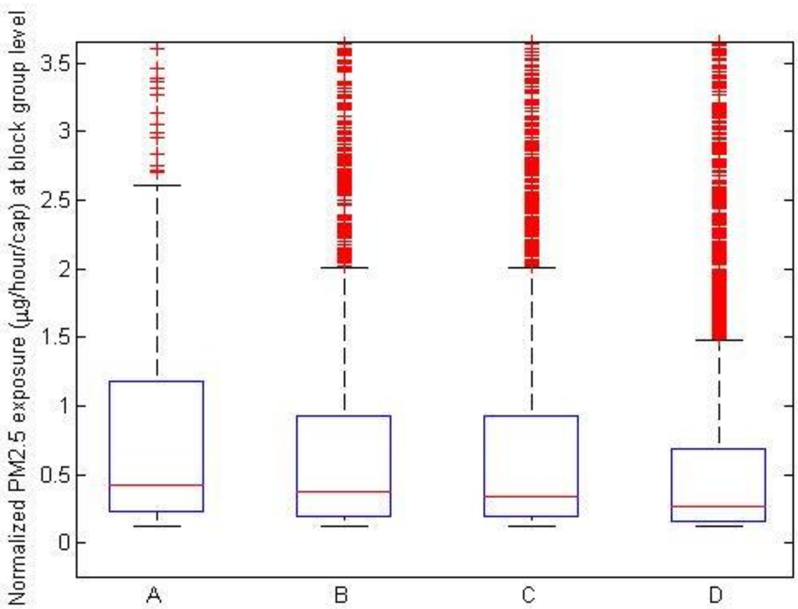

Notes: Group A, B, C, D stands for extremely-low income (483 counts), very-low income (2244 counts), low income (3242 counts), and normal income (4488 counts), respectively

Figure 5-20 Boxplot of localized mobile-source $PM_{2.5}$ exposure at block group level

Table 5-6 Statistics of three unpaired T-tests for four income level groups (α=0.05)

Income Level	*Ext Low*	*Very Low*	*Low*	*Normal*
Mean	1.123	0.924	0.924	0.714
Variance	3.748	2.334	2.685	1.612
Count	483	2244	3242	4488

Hypothesized Mean Difference	0	0	0
df	618	5030	5864
t Stat	2.123	-0.007	6.090
P(T<=t) one-tail	0.017	0.497	0.000
t Critical one-tail	1.647	1.645	1.645
P(T<=t) two-tail	0.034	0.994	0.000
t Critical two-tail	1.964	1.960	1.960

To better understand the general race composition of the four income level groups, the race composition is summarized for each income group, as in Table 5-7 and Figure 5-21.

Table 5-7 Summary of population by race for the four income groups

	Ext Low	Very Low	Low	Normal
Number of Block Groups	483	2,244	3,242	4,488
HISP	477,917	2,499,628	2,467,198	1,247,501
HISP Ratio	65.2%	63.6%	46.6%	19.1%
WHITE	76,209	639,298	1,704,867	3,986,358
WHITE Ratio	10.4%	16.3%	32.2%	61.0%
AFAM	108,125	406,735	416,209	268,028
AFAM Ratio	14.8%	10.4%	7.9%	4.1%
ASIAN	52,817	280,687	534,160	811,583
ASIAN Ratio	7.2%	7.1%	10.1%	12.4%
OTHER	17,589	102,252	169,076	219,614
OTHER Ratio	2.4%	2.6%	3.2%	3.4%
Total	732,657	3,928,600	5,291,510	6,533,084

Note: 'HISP' refers to Hispanic or Latino, which is a racially diverse group. 'AF_AM' refers to African American, 'OTHER' includes American Indian or Alaska Native, Native Hawaiian or other Pacific Islander, and other mixed races. Ratio of each race over total population in each income group is marked in blue)

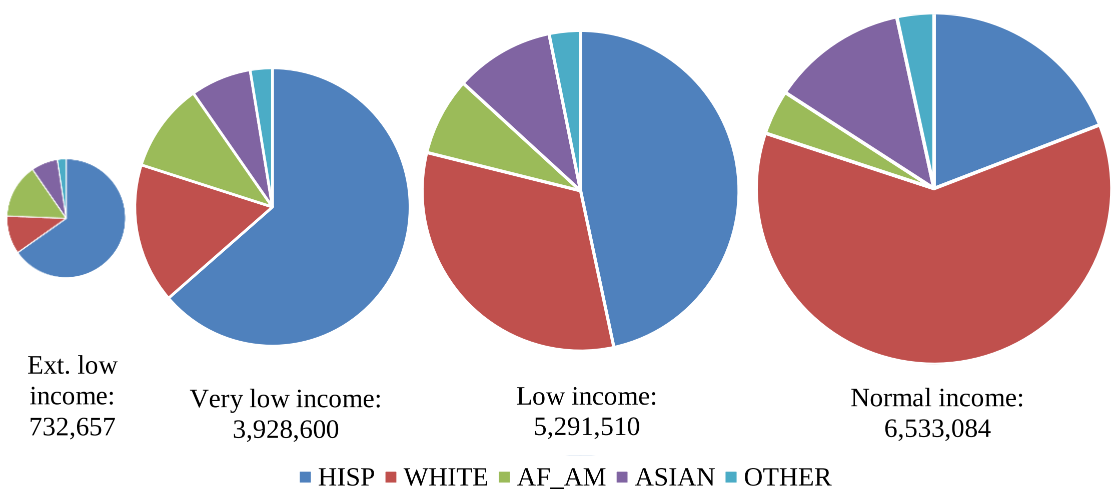

Note: The number and area of each pie chart represents total population in each income group. For income group exposure statistics please see Table 5-6

Figure 5-21 Population by race for the four income groups

Figure 5-21 visualizes that, population ratio of Hispanic decreases significantly between extremely-low income group and normal income group. Population ratio of African Americans decreases steadily as income level increases. Generally, Asian population ratio increases slightly as income level rises. In contrast, White population ratio increases sharply as income level increases. Combined with Table 5-6, localized mobile-source $PM_{2.5}$ exposure per capita steadily decreases as income level increases.

This trend shows that when considering both absolute population and ratio of population, Hispanic population are likely located in low-income communities, and low-income communities tend to reside in locations with higher level of localized mobile-source $PM_{2.5}$. These communities are usually in close proximity to major roadways, and the local meteorology condition contributes to higher $PM_{2.5}$ levels. For White population, the situation is the other way around. White population mainly live in normal-income communities. According to arithmetic mean in Table 5-6, residents in normal-income communities are exposed to 36% less localized mobile-source $PM_{2.5}$ than residents who live in extremely-low income area, or 29% less than that of very-low and low income communities. The race composition and exposure level can also be valuable in epidemiology studies. It will be very interesting to analyze the relationship between air-pollution-induced health effects, localized mobile-source $PM_{2.5}$ levels, race and other variables in the future.

5.4 Model Zone Aggregation

To apply the analysis results to LA-TRAN's geological units – model zones, we aggregate exposure and SES data of 10,577 block groups to 97 LA-TRAN model zones. Results show that Seal Beach - Los Alamitos, Compton and surroundings, Riverside, Tustin, and Anaheim areas are among the top 10 exposure list. For interactive map with more details, please access the reference link http://arcg.is/1GHsup1. One can click each model zone and view the relevant information, including exposure values, population by age, gender and race, as well as annual income distribution.

Table 5-8 The top 10 model zones with highest localized mobile-source $PM_{2.5}$ exposure

Model Zone Name	Normalized PM2.5 Exposure (µg/hour/capita)
Seal Beach - Los Alamitos	2.03
Cerritos	1.89
Compton	1.79
Placentia	1.69
Pico Rivera	1.46
Carson	1.46
Riverside	1.40
Tustin	1.40
West Compton	1.40
Anaheim	1.37

5.5 Conclusions and Discussions

This research estimates localized mobile-source $PM_{2.5}$ concentration in SCAG region, and explores the correlation between the local residents' $PM_{2.5}$ exposure and their SES.

$PM_{2.5}$ concentration is estimated at census block level, which is of high resolution compared with previous studies. According to historical $PM_{2.5}$ monitor records, estimated concentration values are at a reasonable magnitude. Further, $PM_{2.5}$ exposure assessment is aggregated to census block group level. Income analysis show that, Hispanic population makes higher percentage in the total low-income groups than all other races, while White population makes higher percentage in the normal low-income groups than all other races. In general, residents in normal-income communities are exposed to 36% less localized mobile-source $PM_{2.5}$ than residents who live in extremely-low income area, or 29% less than that of very-low and low income communities.

In this study, only primary out-of-tail-pipe $PM_{2.5}$ is considered. This model can be improved by incorporating other significant metrics, such as industrial, agriculture, and background sources. Also, vigorous concentration validation is required for real-world application.

With the aid of chemical models and computer simulation, secondary pollutants, such as ozone and secondary fine particles, could also be estimated. These different sources can be added as independent layers for the exposure model where the impacts of pollutants from various sources can be evaluated at more comprehensive levels.

In the era of big data, this framework can be enriched and realized from an array of data channels. For example, the public could contribute different sources that add to emission source inventory. The air resource management agency could input secondary pollutants' estimation and real-time monitor data to calibrate high-resolution concentration map of pollutants. The health care facilities could collect detailed information of patients' distribution, so that researchers have rich datasets to investigate into air-pollution-related health effects at a large scale and a detail level.

To reduce the health risks of residents who live in high-exposure areas, policy makers could take proactive measures to outreach to the communities and raise their awareness towards health problems induced by air pollution. For example, public health professionals could develop education programs to inform residents about health effects of air pollution and importance of healthy lifestyles. After survey and validation efforts, these programs can be applied to low-income and high-exposure neighborhoods, which could engage the local residents and bring them health benefits.

Currently, CARB conducts a series of research on air-pollution impacts on children's health and communities' health as a whole [*142*, *143*]. Our modeling framework is able to efficiently screen disadvantaged areas (high-exposure and low-income) for further health studies and mitigation measures at a low cost. Therefore, this research provides important implications for public health and policy studies.

5.6 Acknowledgement

The author would like to thank our laboratory colleagues, Alexander Vu, Haiyu Zhang, and Xuewei Qi, for their support in scripting and statistical analysis. Also, many thanks to GIS Academy instructors Colin Childs and Thomas Corrigan for their expertise in spatial analysis. The author would also thank Bill Strossman, who is from Computing Infrastructure & Security of UCR, to provide professional instructions to access cluster computers for our computation.

6 Conclusions and Future Directions

This dissertation proposes mitigation strategies from exposure standpoints, attempting to reduce exposure of clustered population undergoing daily activities, and en-route active travelers. Chapter Three develops a vehicle navigation method that minimizes local population's exposure to roadway emissions. First, a modeling suite is developed in order to assess human exposure to mobile-source pollutants. The exposure assessment provides critical inputs for routing cost evaluations. Experiments show that when informed with population distribution and local dispersion condition, this vehicle navigation method effectively reduces sensitive population's localized exposure to heavy-duty vehicles' emissions. For 10% of the cases studies, the low-exposure routes are also more fuel efficient than least-duration route.

Chapter Four introduces the unique digitization of sidewalk network. This study generates high-resolution vehicular emission maps and creates a pedestrian routing application. In a cast study carried in Riverside, California, pedestrian routing experiments demonstrate that the navigation tool is able to advise walking trips that significantly reduce pedestrians' localized $PM_{2.5}$ exposure up to 90%. As a result, pedestrians can be protected from excessive pollutant exposure. This method also applies to other active travelers, for example, cyclists and skateboarders.

Chapter Five develops modeling techniques for large-scale pollutant exposure assessment for Southern California Association of Governments (SCAG) residents, with spatial analysis resolution 58 times higher than previous research. The large-scale exposure assessment show that high-exposure residential blocks are usually within 400 meter of heavily travelled roadways. In addition, an interactive map is built so that one can select a street block and view relevant information within the block, including exposure values, adjacent traffic condition, population by age, gender, and race, as well as annual income distribution. In junction with socioeconomic parameter analysis, results reveal that in SCAG region, low-income and minority population are subject to high-level localized pollutant exposure. This study makes it possible for community outreach and mitigation planning targeted at disadvantaged residential communities. Hence, this research provides important implications for environmental justice and public health studies.

To summarize, the dissertation proposes mitigation strategies for human exposure from various standpoints, and the strategies can be integrated with and augmented by various smart applications for future improvements.

The future improvements include the following directions.

(1) In the advent of Big Data, it is possible to realize real-time collection of various datasets. For example, human activity is a key element in identifying exposure subjects in exposure mitigation strategies. Nowadays real-time population activity can be effectively predicted from Big Data applications (e.g. social media). Traffic activities and weather parameters can also be extracted from real-time data sources. What's more, air quality data collected from various platforms will greatly facilitate validation process.

(2) For vehicle road navigation, microscale emission should be simulated to account for real-world driving situations. more efficient navigation algorithm (e.g. A*, hybrid constrain method) can be applied. Eco-driving, Eco-routing can also be integrated into low exposure navigation and achieve both emission mass and emission exposure mitigation. These improvements will make the vehicle navigation method more practical and beneficial.

(3) For pedestrian navigation, there are strong interests to develop automatic extraction of sidewalk network on a large-scale from available map sets. Also, portable air quality instruments will be helpful in measuring surrogate pollutant concentration and validating the model results.

(4) The framework to assess large-scale and high-resolution pollutant exposure should be improved by incorporating other significant metrics, such as background concentration. Also, vigorous validation efforts are needed for concentration modeling. With validation it will be of great interests to apply it in air-pollution-induced health effect studies.

References

1 Ghio, A. J., C. Kim, and R. B. Devlin. Concentrated ambient air particles induce mild pulmonary inflammation in healthy human volunteers. *American journal of respiratory and critical care medicine,* Vol. 162, No. 3, 2000, pp. 981-988.

2 Brook, R. D., J. R. Brook, B. Urch, R. Vincent, S. Rajagopalan, and F. Silverman. Inhalation of fine particulate air pollution and ozone causes acute arterial vasoconstriction in healthy adults. *Circulation,* Vol. 105, No. 13, 2002, pp. 1534-1536.

3 Larsson, B.-M., M. Sehlstedt, J. Grunewald, C. M. Sköld, A. Lundin, A. Blomberg, T. Sandström, A. Eklund, and M. Svartengren. Road tunnel air pollution induces bronchoalveolar inflammation in healthy subjects. *European respiratory journal,* Vol. 29, No. 4, 2007, pp. 699-705.

4 Dvonch, J. T., S. Kannan, A. J. Schulz, G. J. Keeler, G. Mentz, J. House, A. Benjamin, P. Max, R. L. Bard, and R. D. Brook. Acute effects of ambient particulate matter on blood pressure differential effects across urban communities. *Hypertension,* Vol. 53, No. 5, 2009, pp. 853-859.

5 Hoek, G., B. Brunekreef, S. Goldbohm, P. Fischer, and P. A. van den Brandt. Association between mortality and indicators of traffic-related air pollution in the Netherlands: a cohort study. *The Lancet*, Vol. 360, No. 9341, 2002, pp. 1203-1209.

6 Beelen, R., G. Hoek, D. Houthuijs, P. A. van den Brandt, R. A. Goldbohm, P. Fischer, L. J. Schouten, B. Armstrong, and B. Brunekreef. The joint association of air pollution and noise from road traffic with cardiovascular mortality in a cohort study. *Occupational and environmental medicine,* Vol. 66, No. 4, 2009, pp. 243-250.

7 Woodcock, J., P. Edwards, C. Tonne, B. G. Armstrong, O. Ashiru, D. Banister, S. Beevers, Z. Chalabi, Z. Chowdhury, and A. Cohen. Public health benefits of strategies to reduce greenhouse-gas emissions: urban land transport. *The Lancet*, Vol. 374, No. 9705, 2009, pp. 1930-1943.

8 Beckerman, B., M. Jerrett, J. R. Brook, D. K. Verma, M. A. Arain, and M. M. Finkelstein. Correlation of nitrogen dioxide with other traffic pollutants near a major expressway. *Atmospheric Environment*, Vol. 42, No. 2, 2008, pp. 275-290.

9 Hu, S., S. Fruin, K. Kozawa, S. Mara, S. E. Paulson, and A. M. Winer. A wide area of air pollutant impact downwind of a freeway during pre-sunrise hours. *Atmospheric Environment,* Vol. 43, No. 16, 2009, pp. 2541-2549.

10 Committee to Review EPA's Mobile Source Emissions Factor (MOBILE) Model, Board on Environmental Studies and Toxicology, Transportation Research Board, National Research Council. Modeling Mobile-Source Emissions, National Academy Press, Washington D.C. http://www.nap.edu/catalog/9857/modeling-mobile-source-emissions. Accessed September 2015.

11 California Air Resources Board. Mobile Source Emission Inventory - Current Methods and Data. http://www.arb.ca.gov/msei/modeling.htm. Accessed July 2015.

12 U.S. EPA, Motor Vehicle Emission Simulator. http://www.epa.gov/oms/models/moves/. Accessed July 2015.

13 Barth, M., F. An, T. Younglove, C. Levine, G. Scora, M. Ross, and T. Wenzel. *Development of a comprehensive modal emissions model*. National Cooperative Highway Research Program, Transportation Research Board of the National Academies, 2000.

14 Barth, M., C. Malcolm, T. Younglove, and N. Hill. Recent validation efforts for a comprehensive modal emissions model. *Transportation Research Record: Journal of the Transportation Research Board,* Vol. 1750, No. 1, 2001, pp. 13-23.

15 Rakha, H., K. Ahn, and A. Trani. Development of VT-Micro model for estimating hot stabilized light duty vehicle and truck emissions. *Transportation Research Part D: Transport and Environment,* Vol. 9, No. 1, 2004, pp. 49-74.

16 Ntziachristos, L., D. Gkatzoflias, C. Kouridis, and Z. Samaras. COPERT–a European road transport emission inventory model. In *Information Technologies in Environmental Engineering,* Springer, 2009. pp. 491-504.

17 COPERT IV User Manual (Version 9.0). European Environment Agency, 2007, pp. 9-28.

18 Smit, R., R. Smokers, and E. Rabé. A new modelling approach for road traffic emissions: VERSIT+. Transportation Research Part D: Transport and Environment, Vol. 12, No. 6, 2007, pp. 414-422.

19 Nicole, D., J. Lents, M. Osses, N. Nikkila, and M. Barth. Development and application of an international vehicle emissions model. Transportation Research Record: J Transportation Res Board, Vol. 1939, 2005, pp. 1939-1918.

20 Kaur, S., M. Nieuwenhuijsen, and R. Colvile. Pedestrian exposure to air pollution along a major road in Central London, UK. *Atmospheric Environment,* Vol. 39, No. 38, 2005, pp. 7307-7320.

21 Zhu, Y., T. Kuhn, P. Mayo, and W. C. Hinds. Comparison of daytime and nighttime concentration profiles and size distributions of ultrafine particles near a major highway. *Environmental science & technology,* Vol. 40, No. 8, 2006, pp. 2531-2536.

22 Traffic-Related Air Pollution: A Critical Review of the Literature on Emissions, Exposure, and Health Effects. HEI Special Report 17. HEI Panel on the Health Effects of Traffic-Related Air Pollution, Health Effects Institute, 2010.

23 Cimorelli, A. J., S. G. Perry, A. Venkatram, J. C. Weil, R. J. Paine, R. B. Wilson, R. F. Lee, W. D. Peters, and R. W. Brode. AERMOD: A dispersion model for industrial source applications. Part I: General model formulation and boundary layer characterization. *Journal of Applied Meteorology,* Vol. 44, No. 5, 2005, pp. 682-693.

24 Perry, S. G., A. J. Cimorelli, R. J. Paine, R. W. Brode, J. C. Weil, A. Venkatram, R. B. Wilson, R. F. Lee, and W. D. Peters. AERMOD: A dispersion model for industrial source applications. Part II: Model performance against 17 field study databases. *Journal of Applied Meteorology,* Vol. 44, No. 5, 2005, pp. 694-708.

25 Snyder, M. G., A. Venkatram, D. K. Heist, S. G. Perry, W. B. Petersen, and V. Isakov. RLINE: A line source dispersion model for near-surface releases. *Atmospheric Environment,* Vol. 77, 2013, pp. 748-756.

26 Benson, P. E. CALINE3–A versatile dispersion model for predicting air pollutant levels near highways and arterial streets. Report No. FHWA/CA/TL-79/23. California Department of Transportation, Division of Construction, Office of Transportation Laboratory, November 1979.

http://www.epa.gov/ttn/scram/userg/regmod/caline3.pdf. Accessed July 2015.

27 Benson, P. E. CALINE4–A Dispersion Model for Predicting Air Pollutant Concentrations near Roadways. Report No. FHWA/CA/TL-84/15, California Department of Transportation, Division of New Technology and Research, November 1984. http://www.dot.ca.gov/hq/env/air/documents/C4manual_searchable.pdf. Accessed July 2015.

28 Community Modeling & Analysis System, R-LINE. https://www.cmascenter.org/r-line/. Accessed July 2015.

29 U.S. EPA, Support Center for Regulatory Atmospheric Modeling. http://www.epa.gov/scram001/dispersion_prefrec.htm. Accessed in July 2015.

30 Guidelines for exposure assessment. Risk Assessment Forum, Environmental Protection Agency, Washington, D.C., 1992.

31 Ott, W. R., A. C. Steinemann, and L. A. Wallace. *Exposure analysis*. CRC Press, 2006.

32 Özkaynak, H., T. Palma, J. S. Touma, and J. Thurman. Modeling population exposures to outdoor sources of hazardous air pollutants. *Journal of Exposure Science and Environmental Epidemiology*, Vol. 18, No. 1, 2007, pp. 45-58.

33 U.S. Census, 2010 Census Tallies of Census Tracts, Block Groups & Blocks. https://www.census.gov/geo/maps-data/data/tallies/tractblock.html. Accessed September 2015.

34 Quiros, D. C., E. S. Lee, R. Wang, and Y. Zhu. Ultrafine particle exposures while walking, cycling, and driving along an urban residential roadway. *Atmospheric Environment,* Vol. 73, 2013, pp. 185-194.

35 Rank, J., J. Folke, and P. Homann Jespersen. Differences in cyclists and car drivers exposure to air pollution from traffic in the city of Copenhagen. *Science of the Total Environment,* Vol. 279, No. 1, 2001, pp. 131-136.

36 Briggs, D. J. A framework for integrated environmental health impact assessment of systemic risks. *Environmental Health,* Vol. 7, No. 1, 2008, p. 61.

37 Integrated Environmental Health Impact Assessment System. http://www.integrated-assessment.eu/guidebook/exposure_intake_and_uptake. Accessed July 2015.

38 Barth, M., G. Wu, and K. Boriboonsomsin. Intelligent Transportation Systems and Greenhouse Gas Reductions. *Current Sustainable/Renewable Energy Reports*, 2015, pp. 1-8.

39 Barth, M., and K. Boriboonsomsin. ECO-ITS: Intelligent Transportation System Applications to Improve Environmental Performance. Publication FHWA-JPO-12-042. Center for Environmental Research & Technology, University of California, Riverside, 2012.

40 AERIS - Applications for the Environment: Real-Time Information Synthesis. Low Emissions Zones Operational Scenario Modeling Report. Publication Number: FHWA-JPO-14-187. http://ntl.bts.gov/lib/54000/54900/54931/Low_Emissions_Zones_Modeling_Report_-_Final_508_-_012715.pdf. Accessed July 2015.

41 Ellison, R. B., S. P. Greaves, and D. A. Hensher. Five years of London's low emission zone: Effects on vehicle fleet composition and air quality. *Transportation Research Part D: Transport and Environment*, Vol. 23, 2013, pp. 25-33.

42 Qadir, R., G. Abbaszade, J. Schnelle-Kreis, J. Chow, and R. Zimmermann. Concentrations and source contributions of particulate organic matter before and after implementation of a low emission zone in Munich, Germany. *Environmental Pollution,* Vol. 175, 2013, pp. 158-167.

43 Ferreira, F., P. Gomes, A. C. Carvalho, H. Tente, J. Monjardino, H. Brás, and P. Pereira. Evaluation of the implementation of a low emission zone in lisbon. *Journal of Environmental Protection,* Vol. 3, No. 09, 2012, p. 1188.

44 Boogaard, H., N. A. Janssen, P. H. Fischer, G. P. Kos, E. P. Weijers, F. R. Cassee, S. C. van der Zee, J. J. de Hartog, K. Meliefste, and M. Wang. Impact of low emission zones and local traffic policies on ambient air pollution concentrations. *Science of the total environment,* Vol. 435, 2012, pp. 132-140.

45 Panteliadis, P., M. Strak, G. Hoek, E. Weijers, S. van der Zee, and M. Dijkema. Implementation of a low emission zone and evaluation of effects on air quality by long-term monitoring. *Atmospheric Environment,* Vol. 86, 2014, pp. 113-119.

46 Widodo, A., and T. Hasegawa. A new inter-vehicle communication system for intelligent transport systems and an autonomous traffic flow simulator. In *Spread Spectrum Techniques and Applications, 1998. Proceedings, 1998 IEEE 5th International Symposium on, No. 1*, IEEE, 1998. pp. 82-86.

47 Widodo, A., T. Hasegawa, and S. Tsugawa. Vehicle fuel consumption and emission estimation in environment-adaptive driving with or without inter-vehicle communications. In Intelligent Vehicles Symposium, 2000. IV 2000. Proceedings of the IEEE, IEEE, 2000. pp. 382-386.

48 Barth, M., and K. Boriboonsomsin. Energy and emissions impacts of a freeway-based dynamic eco-driving system. Transportation Research Part D: Transport and Environment, Vol. 14, No. 6, 2009, pp. 400-410.

49 Barth, M., S. Mandava, K. Boriboonsomsin, and H. Xia. Dynamic ECO-driving for arterial corridors. In Integrated and Sustainable Transportation System (FISTS), 2011 IEEE Forum on, IEEE, 2011. pp. 182-188.

50 AERIS - Applications for the Environment: Real-Time Information Synthesis. Eco-Signal Operations: Operational Concept. Publication Number: FHWA-JPO-13-113. Oct, 2013. http://ntl.bts.gov/lib/51000/51400/51429/FINAL_Eco-Signal_Operations_ConOps_01-2014.pdf. Accessed July 2015.

51 Xia, H., G. Wu, K. Boriboonsomsin, and M. J. Barth. Development and evaluation of an enhanced eco-approach traffic signal application for Connected Vehicles. In Intelligent Transportation Systems-(ITSC), 2013 16th International IEEE Conference on, IEEE, 2013. pp. 296-301.

52 Kamalanathsharma, R. K., H. A. Rakha, and H. Yang. Network-wide impacts of vehicle eco-speed control in the vicinity of traffic signalized intersections. In Transportation Research Board 94th Annual Meeting, 2015.

53 Kari, D., G. Wu, and M. J. Barth. Eco-Friendly Freight Signal Priority using connected vehicle technology: A multi-agent systems approach. In *Intelligent Vehicles Symposium Proceedings, 2014 IEEE,* IEEE, 2014. pp. 1187-1192.

54 Wang, Y., Y. Zhu, R. Salinas, D. Ramirez, S. Karnae, and K. John. Roadside measurements of ultrafine particles at a busy urban intersection. Journal of the Air & Waste Management Association, Vol. 58, No. 11, 2008, pp. 1449-1457.

55 Barth, M., K. Boriboonsomsin, and A. Vu. Environmentally-friendly navigation. In *Intelligent Transportation Systems Conference, 2007. ITSC 2007. IEEE,* IEEE, 2007. pp. 684-689.

56 Boriboonsomsin, K., M. J. Barth, W. Zhu, and A. Vu. Eco-routing navigation system based on multisource historical and real-time traffic information. *Intelligent Transportation Systems, IEEE Transactions on,* Vol. 13, No. 4, 2012, pp. 1694-1704.

57 Ahn, K., and H. A. Rakha. Network-wide impacts of eco-routing strategies: A large-scale case study. *Transportation Research Part D: Transport and Environment,* Vol. 25, 2013, pp. 119-130.

58 Amirjamshidi, G., T. S. Mostafa, A. Misra, and M. J. Roorda. Integrated model for microsimulating vehicle emissions, pollutant dispersion and population exposure. *Transportation Research Part D: Transport and Environment,* Vol. 18, 2013, pp. 16-24.

59 An introduction to California Department of Transportation Performance Measurement System (PeMS). Caltrans, 2013. http://pems.dot.ca.gov/PeMS_Intro_User_Guide_v5.pdf. Accessed September 2015.

60 Quadstone, PARAMICS Microsimulation Software for the simulation and visualization of road traffic. http://www.paramics-online.com/. Accessed July 2015.

61 Esri, About StreetMap North America data. http://webhelp.esri.com/arcgisdesktop/9.3/index.cfm?TopicName=About_StreetMap_North_America_data. Accessed July 2015.

62 CARB, EMFAC Web Database. http://www.arb.ca.gov/emfac/. Accessed September 2015.

63 MathWorks, Matfile documentation. http://www.mathworks.com/help/matlab/ref/matfile.html. Accessed September 2015.

64 MathWorks, Matlab: The language of technical computing. http://www.mathworks.com/products/matlab/

65 ESRI, Shapefile Technical Description. http://www.esri.com/library/whitepapers/pdfs/shapefile.pdf. Accessed July 2015.

66 ESRI, ArcGIS for Desktop. http://www.esri.com/software/arcgis/arcgis-for-desktop. Accessed July 2015.

67 ArcMap Resource Center, Project. http://help.arcgis.com/EN/arcgisdesktop/10.0/help/index.html#//00170000007m000000. Accessed September 2015.

68 ArcMap Resource Center, Generalize. http://help.arcgis.com/en/arcgisdesktop/10.0/help/index.html#//001v00000006000000.htm. Accessed July 2015.

69 ArcMap Resource Center, Split line at vertices. http://help.arcgis.com/en/arcgisdesktop/10.0/help/index.html#//00170000003z000000. Accessed September 2015.

70 South Coast Air Quality Management District, Meteorological Data for AERMOD. http://www.aqmd.gov/home/library/air-quality-data-studies/meteorological-data/data-for-aermod. Accessed July 2015.

71 Snyder, M. and H. David. *User Guide for R-LINE Model 1.2*. USEPA/ORD/NERLMD-81. Atmospheric Exposure Research Branch, Atmospheric Modeling and Analysis Division, Research Triangle Park, NC, 2013.

72 Grodzevich, O., and O. Romanko. Normalization and other topics in multi-objective optimization. In Proceedings of the Fields MITACS Industrial Problems Workshop, Toronto, 2006. pp. 89-101.

73 Demir, E., T. Bektaş, and G. Laporte. The bi-objective pollution-routing problem. European Journal of Operational Research, Vol. 232, No. 3, 2014, pp. 464-478.

74 Mavrotas, G. Effective implementation of the ε-constraint method in multi-objective mathematical programming problems. Applied mathematics and computation, Vol. 213, No. 2, 2009, pp. 455-465.

75 Bektaş, T., and G. Laporte. The pollution-routing problem. Transportation Research Part B: Methodological, Vol. 45, No. 8, 2011, pp. 1232-1250.

76 Dijkstra, E. W. A note on two problems in connexion with graphs. *Numerische mathematik*, Vol. 1, No. 1, 1959, pp. 269-271.

77 Luo, J., A. Vu, and M. J. Barth. Vehicle road navigation to minimize pollutant exposure. In *Intelligent Vehicles Symposium (IV), 2013 IEEE*, IEEE, 2013. pp. 847-852.

78 Census 2010, Download Summary File 1.http://www2.census.gov/census_2010/04-Summary_File_1/. Accessed July 2015.

79 *Health assessment document for diesel engine exhaust*. EPA/600/8-90/057F. Prepared by the National Center for Environmental Assessment, Washington, D.C., for the Office of Transportation and Air Quality. U.S. EPA, 2002.

80 ArcGIS Resource Center, Add XY coordinates. http://help.arcgis.com/en/arcgisdesktop/10.0/help/index.html#//0017000000320000000. Accessed September 2015.

81 USGS, The National Map Viewer and Download Platform. http://nationalmap.gov/viewer.html. Accessed July 2015.

82 Adams, W. *Measurement of breathing rate and volume in routinely performed daily activities, Final report*. Prepared for the California Air Resources Board, Contract, No. A033-205. Human Performance Laboratory, Physical Education Department, University of California, Davis, 1993. http://www.arb.ca.gov/research/single-project.php?row_id=64931. Accessed July 2015.

83 ArcGIS Desktop 9.3 Help, What is new in Esri Data and Maps. http://webhelp.esri.com/arcgisdesktop/9.3/index.cfm?TopicName=What%27s_new_in_ESRI_Data_and_Maps. Accessed July 2015.

84 Census Geography, TIGER/Line Shapefiles. https://www.census.gov/geo/maps-data/data/tiger-line.html. Accessed July 2015.

---

85 Mesenbourg, T. L. *2010 Census Summary File 1 Technical Documentation*. U.S. Census Bureau, 2012. http://www.census.gov/prod/cen2010/doc/sf1.pdf. Accessed July 2015.

86 ArcGIS Resource Center, Spatial Join. http://help.arcgis.com/en/arcgisdesktop/10.0/help/index.html#//00080000000q000000. Accessed July 2015.

87 ArcGIS Resource Center, Summarize data in a table. http://resources.arcgis.com/en/help/main/10.1/index.html#//005s00000055000000. Accessed July 2015.

88 ArcGIS Resource Center, Performing calculations on feature geometry. http://help.arcgis.com/EN/arcgisdesktop/10.0/help/index.html#//005s00000025000000. Accessed September 2015.

89 ArcGIS Resource Center, Buffer. http://help.arcgis.com/en/arcgisdesktop/10.0/help/index.html#//000800000019000000http://help.arcgis.com/en/arcgisdesktop/10.0/help/index.html#//000800000019000000. Accessed July 2015.

90 Sælensminde, K. Cost–benefit analyses of walking and cycling track networks taking into account insecurity, health effects and external costs of motorized traffic. *Transportation Research Part A: Policy and Practice,* Vol. 38, No. 8, 2004, pp. 593-606.

91 Leyden, K. M. Social capital and the built environment: the importance of walkable neighborhoods. *American journal of public health,* Vol. 93, No. 9, 2003, pp. 1546-1551.

92 Litman, T. A. Economic value of walkability. *Transportation Research Record: Journal of the Transportation Research Board,* Vol. 1828, No. 1, 2003, pp. 3-11.

93 Pucher, J., and L. Dijkstra. Promoting safe walking and cycling to improve public health: lessons from the Netherlands and Germany. *American journal of public health,* Vol. 93, No. 9, 2003, pp. 1509-1516.

94 Bassett Jr, D. R., J. Pucher, R. Buehler, D. L. Thompson, and S. E. Crouter. Walking, cycling, and obesity rates in Europe, North America, and Australia. *Journal of Physical Activity and Health,* Vol. 5, No. 6, 2008, pp. 795-814.

95 O'Donoghue, R., L. Gill, R. McKevitt, and B. Broderick. Exposure to hydrocarbon concentrations while commuting or exercising in Dublin. *Environment international,* Vol. 33, No. 1, 2007, pp. 1-8.

96 Hankey, S., J. D. Marshall, and M. Brauer. Health impacts of the built environment: within-urban variability in physical inactivity, air pollution, and ischemic heart disease mortality. *Environmental health perspectives,* Vol. 120, No. 2, 2012, p. 247.

97 Kaur, S., M. J. Nieuwenhuijsen, and R. N. Colvile. Fine particulate matter and carbon monoxide exposure concentrations in urban street transport microenvironments. *Atmospheric Environment,* Vol. 41, No. 23, 2007, pp. 4781-4810.

98 Center for Sustainable Suburban Development, University of California Riverside. Creating walkability plans for Riverside neighborhoods. http://cssd.ucr.edu/NewUrbanism/About.html. Accessed July, 2015.

99 *Riverside County Transportation Analysis Model (RIVTAM): Model Development & Validation Report and Users Guide,* Iteris, Inc., May 2009.

100 California Air Resources Board. Meteorology Data Query Tool. http://www.arb.ca.gov/aqmis2/metselect.php. Accessed July, 2015.

101 De Nevers, N. *Air pollution control engineering*. Waveland Press, 2010.

102 ArcGIS Resource Center, Create fishnet. http://help.arcgis.com/EN/arcgisdesktop/10.0/help/index.html#//00170000002q000000. Accessed September 2015.

103 MathWorks, Execute DOS command and return outputs. http://www.mathworks.com/help/matlab/ref/dos.html. Accessed September 2015.
104 ArcMap Resource Center. Spline (Spatial Analysis). http://resources.arcgis.com/en/help/main/10.1/index.html#//009z0000006q000000. Accessed July, 2015.

105 Guidebook, Incorporating Pedestrians into Washington's Transportation System. Prepared for Washington State DOT, Otak Inc., 1997.

106 ESRI online publication, Sidewalk and pathway analysis: a walk around campus. http://downloads2.esri.com/campus/uploads/library/pdfs/58004.pdf. Accessed September 2015.

107 Goldschmidt, J. *Pedestrian delay and traffic management*. No. TRRL Suppl. Rpt. 356, Monograph. 1977.

108 Li, Q., Z. Wang, J. Yang, and J. Wang. Pedestrian delay estimation at signalized intersections in developing cities. Transportation Research Part A: Policy and Practice, Vol. 39, No. 1, 2005, pp. 61-73.

109 Knoblauch, R. L., M. T. Pietrucha, and M. Nitzburg. Field studies of pedestrian walking speed and start-up time. *Transportation Research Record: Journal of the Transportation Research Board,* Vol. 1538, No. 1, 1996, pp. 27-38.

110 Carr, L. J., S. I. Dunsiger, and B. H. Marcus. Walk Score (TM) As a Global Estimate of Neighborhood Walkability. *American Journal of Preventive Medicine,* Vol. 39, No. 5, 2010, pp. 460-463.

111 Sadd, J. L., M. Pastor, R. Morello-Frosch, J. Scoggins, and B. Jesdale. Playing it safe: Assessing cumulative impact and social vulnerability through an environmental justice screening method in the south coast air basin, California. *International Journal of Environmental Research and Public Health,* Vol. 8, No. 5, 2011, pp. 1441-1459.

112 Marshall, J. D., P. W. Granvold, A. S. Hoats, T. E. McKone, E. Deakin, and W. W. Nazaroff. Inhalation intake of ambient air pollution in California's South Coast Air Basin. *Atmospheric Environment,* Vol. 40, No. 23, 2006, pp. 4381-4392.

113 Marshall, J. D. Environmental inequality: air pollution exposures in California's South Coast Air Basin. *Atmospheric Environment,* Vol. 42, No. 21, 2008, pp. 5499-5503.

114 Su, J. G., R. Morello-Frosch, B. M. Jesdale, A. D. Kyle, B. Shamasunder, and M. Jerrett. An index for assessing demographic inequalities in cumulative environmental hazards with application to Los Angeles, California. *Environmental science & technology,* Vol. 43, No. 20, 2009, pp. 7626-7634.

115 Year 2003 Model Validation & Summary for SCAG Regional Transportation Model. SCAG, 2007.

116 Arterial Speed Study Final Report. Prepared for SCAG. Dowling Associates, Inc., 2005. http://www.scag.ca.gov/Documents/Arterial%20Speed%20Study_Phase%201_%20Final%20Report.pdf. Accessed July 2015.

117 TIGER Products: https://www.census.gov/geo/maps-data/data/tiger.html. Accessed July 2015.

118 U.S. Census 2000, SF1. https://www.census.gov/census2000/sumfile1.html. Accessed July 2015.

119 U.S. Census 2000, SF2. https://www.census.gov/census2000/sumfile2.html. Accessed July 2015.

120 U.S. Census 2000, SF3. https://www.census.gov/census2000/sumfile3.html. Accessed July 2015.

121 U.S. Census 2000, SF4. https://www.census.gov/census2000/SF4.html. Accessed July 2015.

122 TIGER FTP download for Census 2000. ftp://ftp2.census.gov/geo/tiger/tiger2k/ca/. Accessed July 2015.

123 Microsoft Office, Database Application Access. https://products.office.com/en-us/access. Accessed September 2015.

124 ArcGIS Resource Center, Mosaic. http://resources.arcgis.com/en/help/main/10.1/index.html#//001700000097000000. Accessed September 2015.

125 ArcGIS Resource Center, Extract Multi Values to Points. http://help.arcgis.com/en/arcgisdesktop/10.0/help/index.html#//009z0000002s000000.htm. Accessed September 2015.

126 Coe, D. L., D. S. Eisinger, J. D. Prouty, and T. Kear. *User's Guide for CL4: A User Friendly Interface for the CALINE4 Model for Transportation Project Impact Assessments*. Prepared for Caltrans-UC Davis Air Quality Project, STI-997480-1814-UG, 1998. http://www.dot.ca.gov/hq/env/air/documents/CL4Guide.pdf. Accessed September 2015.

127 U.S. Environmental Protection Agency. Guideline for Modeling Carbon Monoxide from Roadway Intersections. EPA Publication No. EPA-454/R-92-005, Office of Air Quality Planning and Standards, Research Triangle Park, North Carolina, November 1992

128 U.S. EPA, Meteorological Monitoring Guidance for Regulatory Modeling Applications, Feb, 2000, http://www.epa.gov/scram001/guidance/met/mmgrma.pdf. Accessed July 2015.

129 Allen, D. W. GIS tutorial 2: Spatial analysis workbook. Esri Press: 2010.

130 ArcGIS Resource Center, Feature vertices to point. http://help.arcgis.com/EN/arcgisdesktop/10.0/help/index.html#//00170000003p000000. Accessed September, 2015.

131 ArcGIS Resource Center, Add field. http://help.arcgis.com/EN/arcgisdesktop/10.0/help/index.html#//001700000047000000. Accessed September, 2015.

132 White, D. P., J. V. Weil, and C. W. Zwillich. Metabolic rate and breathing during sleep. *Journal of Applied Physiology,* Vol. 59, No. 2, 1985, pp. 384-391.

133 California Air Resource Board, Air quality data query tool. http://www.arb.ca.gov/aqmis2/aqdselect.php. Accessed July 2015.

134 U.S. EPA, National Ambient Air Quality Standards. http://www.epa.gov/air/criteria.html. Accessed July 2015.

135 Schauer, J. J., M. J. Kleeman, G. R. Cass, and B. R. Simoneit. Measurement of emissions from air pollution sources. 5. C1-C32 organic compounds from gasoline-powered motor vehicles. *Environmental science & technology*, Vol. 36, No. 6, 2002, pp. 1169-1180.

136 Zheng, M., G. R. Cass, J. J. Schauer, and E. S. Edgerton. Source apportionment of PM2. 5 in the southeastern United States using solvent-extractable organic compounds as tracers. *Environmental science & technology*, Vol. 36, No. 11, 2002, pp. 2361-2371.

137 Chen, L.-W. A., J. G. Watson, J. C. Chow, and K. L. Magliano. Quantifying PM2. 5 source contributions for the San Joaquin Valley with multivariate receptor models. *Environmental science & technology*, Vol. 41, No. 8, 2007, pp. 2818-2826.

138 AQI, a guide to air quality and your healthy. http://airnow.gov/index.cfm?action=aqibasics.aqi. Accessed July 2015.

139 AQI Calculator, AQI to Concentration. http://www.airnow.gov/index.cfm?action=resources.aqi_conc_calc. Accessed July 2015.

140 U.S. Department of Housing and Urban Development, Income limit. http://www.huduser.org/portal/datasets/il/fmr03/index.html. Accessed July 2015.

141 HUD, Income limit calculation. http://www.novoco.com/low_income_housing/resource_files/income_limits/sec8_IL_03.pdf. Accessed July 2015.

142 California Air Resource Board, children's health and exposure research: http://www.arb.ca.gov/research/children/children.htm. Accessed July 2015.

143 California Air Resource Board, community health program: http://www.arb.ca.gov/ch/ch.htm. Accessed July 2015.

Appendix A: An Example R-Line Input File

```
 User control file for RLINEv1_2
Source File Name
'ResedaSourceFacility175.txt'
Input Emission can be in AADT or g/m (see user guide)
---------------------------------------------------
Receptor File Name
'ResedaFacilityID175.txt'
-------------------------------------------------
Input Met File
'ResedaJday138Hr14sfc.txt'
---------------------------------------------------
Receptor Output File
'ResedaFacilityID175output.csv'
----------------------------------------------------
Error_Limit (suggested 1.0e-03)
1.0e-03
-----------------------------------------------------
Ratio of displacement height to roughness length (fac_dispht)
3.0
--------------------------------------------------
--- OUTPUT OPTION(S) BELOW: ----------------------
--------------------------------------------------
(1) Include concentrations from ['M'] Meander ONLY, ['P'] Plume ONLY, ['T'] Total = Plume+Meander
'T'
---------------------------------------------------
(2) Output daily 24-hour averages? ('Y'/'N')
'N'
---------------------------------------------------
(3) ['M'] Monthly Output Files, ['N'] No Hourly Files, ['A'] All hourly in one file
'A'
---------------------------------------------------
(4) Suppress source/receptor proximity warnings? ('Y'/'N')
'Y'
---------------------------------------------------
--- BETA OPTION(S) BELOW: ------------------------
---------------------------------------------------
(1) Use analytical solution ('Y'/'N'), speeds up run time, but less accurate
'N'
---------------------------------------------------
(2) Use barrier and depressed roadway algorithms? ('Y'/'N')
'N'
---------------------------------------------------
(3) Use non-zero road width? ('Y'/'N')Lane width [m]
'N' 5.0
---------------------------------------------------
```

Appendix B: An Example of CALINE4 Batch Run file

(Change Disk if needed)

```
Caline4_w32.exe <L828R1.txt>oAM-L828R1.txt
Caline4_w32.exe <L828R2.txt>oAM-L828R2.txt
Caline4_w32.exe <L828R3.txt>oAM-L828R3.txt
Caline4_w32.exe <L828R4.txt>oAM-L828R4.txt
Caline4_w32.exe <L828R5.txt>oAM-L828R5.txt
Caline4_w32.exe <L828R6.txt>oAM-L828R6.txt
Caline4_w32.exe <L828R7.txt>oAM-L828R7.txt
Caline4_w32.exe <L828R8.txt>oAM-L828R8.txt
Caline4_w32.exe <L828R9.txt>oAM-L828R9.txt
Caline4_w32.exe <L828R10.txt>oAM-L828R10.txt
Caline4_w32.exe <L828R11.txt>oAM-L828R11.txt
Caline4_w32.exe <L828R12.txt>oAM-L828R12.txt
Caline4_w32.exe <L828R13.txt>oAM-L828R13.txt
Caline4_w32.exe <L828R14.txt>oAM-L828R14.txt
Caline4_w32.exe <L828R15.txt>oAM-L828R15.txt
Caline4_w32.exe <L828R16.txt>oAM-L828R16.txt
Caline4_w32.exe <L828R17.txt>oAM-L828R17.txt
Caline4_w32.exe <L828R18.txt>oAM-L828R18.txt
Caline4_w32.exe <L828R19.txt>oAM-L828R19.txt
Caline4_w32.exe <L828R20.txt>oAM-L828R20.txt
Caline4_w32.exe <L828R21.txt>oAM-L828R21.txt
Caline4_w32.exe <L828R22.txt>oAM-L828R22.txt
```

Note: This file will process the receptor groups R1 to R22 for Link 828 with CALINE4_w32.exe in one batch run.

Appendix C: An Example of CALINE4 Input File

```
2003LA-PlanPM2.5
4Particulates
100 0 0 0 20 20 1 1 1 0
R1
R2
R3
R4
R5
R6
R7
R8
R9
R10
R11
R12
R13
R14
R15
R16
R17
R18
R19
R20
380455.15349      3763457.8862               1.6
380655.15349      3763457.8862               1.6
380855.15349      3763457.8862               1.6
381055.15349      3763457.8862               1.6
381255.15349      3763457.8862               1.6
381455.15349      3763457.8862               1.6
381655.15349      3763457.8862               1.6
381855.15349      3763457.8862               1.6
382055.15349      3763457.8862               1.6
382255.15349      3763457.8862               1.6
382455.15349      3763457.8862               1.6
382655.15349      3763457.8862               1.6
382855.15349      3763457.8862               1.6
383055.15349      3763457.8862               1.6
383255.15349      3763457.8862               1.6
383455.15349      3763457.8862               1.6
383655.15349      3763457.8862               1.6
383855.15349      3763457.8862               1.6
384055.15349      3763457.8862               1.6
384255.15349      3763457.8862               1.6
Link1
Link2
Link3
Link4
Link5
Link6
Link7
Link8
Link9
Link10
Link11
Link12
Link13
```

```
Link14
Link15
Link16
Link17
Link18
Link19
Link20
1   387899  3766046   387870  3766046        0       20        0        0
0
1   387870  3766046   387842  3766047        0       20        0        0
0
1   387842  3766047   387813  3766047        0       20        0        0
0
1   387813  3766047   387785  3766048        0       20        0        0
0
1   387785  3766048   387757  3766050        0       20        0        0
0
1   387757  3766050   387728  3766051        0       20        0        0
0
1   387728  3766051   387699  3766053        0       20        0        0
0
1   387699  3766053   387670  3766056        0       20        0        0
0
1   387670  3766056   387645  3766058        0       20        0        0
0
1   387645  3766058   387620  3766060        0       20        0        0
0
1   387620  3766060   387567  3766066        0       20        0        0
0
1   387567  3766066   387517  3766072        0       20        0        0
0
1   387517  3766072   387410  3766086        0       20        0        0
0
1   387410  3766086   387361  3766091        0       20        0        0
0
1   387361  3766091   387338  3766094        0       20        0        0
0
1   387338  3766094   387317  3766096        0       20        0        0
0
1   387317  3766096   387296  3766098        0       10        0        0
0
1   387296  3766098   387276  3766099        0       10        0        0
0
1   387276  3766099   387255  3766101        0       10        0        0
0
1   387255  3766101   387235  3766102        0       10        0        0
0
11101Hour 1
66384  66384  66384  66384  66384  66384  66384  66384  66384  66384
66384  66384  66384  66384  66384  66384  66384  66384  66384  66384
0.039178    0.039178    0.039178    0.039178    0.039178    0.039178
0.039178    0.039178    0.039178    0.039178
0.039178    0.039178    0.039178    0.039178    0.039178    0.039178
0.039178    0.039178    0.039178    0.039178
241.3188 0.82624 2 1300 104.0613 0 18.1039
```